Artificial Intelligence for Renewable Energy Systems

Gabriel Narvaez Morales

RÉPUBLIQUE FRANÇAISE
Liberté Égalité Fraternité

Université de Toulouse

Doctorat de l'Université de Toulouse

préparé à l'Université Toulouse III - Paul Sabatier

Intelligence artificielle pour les systèmes d'énergie renouvelable

---

Thèse présentée et soutenue, le 18 janvier 2024 par

Gabriel NARVAEZ MORALES

École doctorale
GEETS - Génie Electrique Electronique,Télécommunications et Santé : du système au nanosystème

Spécialité
Génie Electrique

Unité de recherche
LAAS - Laboratoire d'Analyse et d'Architecture des Systèmes

Thèse dirigée par
Corinne ALONSO et LUIS FELIPE GIRALDO TRUJILLO

Composition du jury
M. Nicanor QUIJANO, Président, Universidad de Los Andes
M. Philippe POGGI, Rapporteur, Université de Corse
M. Kodjo AGBOSSOU, Rapporteur, Université du Québec à Trois-Rivières
Mme Corinne ALONSO, Directrice de thèse, Université Toulouse III - Paul Sabatier
M. Luis Felipe GIRALDO TRUJILLO, Co-directeur de thèse, Universidad de Los Andes

Membres invités
M. Michael Bressan, Universidad de Los Andes

THÈSE

En vue de l'obtention du
DOCTORAT DE L'UNIVERSITÉ DE TOULOUSE

Délivré par l'Université Toulouse 3 - Paul Sabatier

Cotutelle internationale: Université des Andes

Présentée et soutenue par

Gabriel NARVAEZ MORALES

Le 18 janvier 2024

Intelligence artificielle pour les systèmes d'énergie renouvelable

---

Ecole doctorale : **GEETS - Génie Electrique Electronique,Télécommunications et Santé : du système au nanosystème**

Spécialité : **Génie Electrique**

Unité de recherche :
LAAS - Laboratoire d'Analyse et d'Architecture des Systèmes

Thèse dirigée par
Corinne ALONSO et LUIS FELIPE GIRALDO TRUJILLO

Jury

M. Philippe POGGI, Rapporteur
M. Kodjo AGBOSSOU, Rapporteur
M. Nicanor QUIJANO, Président
Mme Corinne ALONSO, Directrice de thèse
M. Luis Felipe GIRALDO TRUJILLO, Co-directeur de thèse

Université Toulouse III - Paul
Sabatier-LAAS-CNRS
Universidad de Los Andes

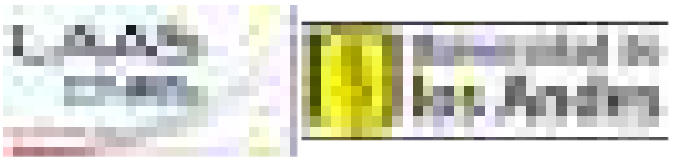

Thesis Manuscript

Artificial Intelligence for Renewable Energy Systems

Author:
Gabriel Esteban Narváez Morales

Advisors:
Luis Felipe Giraldo Trujillo
Michael Bressan
Bruno Jammes
Corinne Alonso

Submitted to the Ecole Doctorale GEET
and the School of Engineering of the Universidad de los Andes

January 2024

Acknowledgment

I couldn't have gone through this journey without my advisors, Luis Felipe Giraldo, Michael Bressan, Corinne Alonso, and Bruno Jammes. It's not just the knowledge and expertise you shared, but your patience and guidance outside of academia. I can't put into words how thankful I am for your support all these years. I would like to give special thanks to Fundación Ceiba, who financed my studies through the Bécate Nariño scholarship.

I want to express my deepest gratitude to the committee members: Nicanor Quijano, professor at Universidad de los Andes; Philippe Poggi, professor at Université de Corse; and Kodjo Agbossou, professor at Université du Québec à Trois-Rivières. I also want to thank my regional advisor, Andres Pantoja, professor at Universidad de Nariño.

I'm sincerely thankful to all my colleagues during these four years, especially those who made my time in France so enjoyable that I always felt at home. My biggest thanks go to the ISGE team at LAAS-CNRS in Toulouse.

I also want to thank my family. My parents Jorge, and Miriam, my brother David, and my sisters Gisella and Johanna, who supported, assisted, and motivated me. My nephew, Miguel Angel, and my nieces, Maria Cielo, and Maria Guadalupe, even in the distance their sweet smiles and playful jokes brighten my life. Last but not least, I would like to thank Wendy, my source of inspiration, and the person who encouraged me to begin this adventure and never give up.

Contents

List of Figures

List of Tables

List of abbreviations

Abbreviation	Definition
AI	Artificial intelligence
ANN	Artificial neural network
BESS	Battery energy storage system
CDF	Cumulative distribution function
CF	Capacity factor
CORDEX	Coordinated Regional Downscaling Experiment
CORE	Coordinated Output for Regional Evaluations
DHI	Diffuse horizontal irradiance
DNI	Direct normal irradiance
DoD	Depth of discharge
EMS	Energy management systems
ESS	Energy storage systems
FARMS	Fast All-sky Radiation Model for Solar applications
GCM	Global climate models
GHI	Global horizontal irradiance
GRU	Gated recurrent units
I_{sc}	Short circuit current
IDEAM	Institute of Hydrology, Meteorology, and Environmental Studies
LSTM	Long short term memory
MAE	Mean absolute error
MBD	Mean bias deviation
MBE	Mean bias error
MPPT	Maximum power point tracking
NREL	National Renewable Energy Laboratory
NSRDB	National Solar Radiation Database

Abbreviation	**Definition**
ρ	Pearson correlation coefficient
P_{DC}	Photovoltaic array power DC output
$P_{DC_{nom}}$	Nominal power
PR	Performance ratio
PSM	Physical solar model
PV	Photovoltaic
PV_{pot}	Photovoltaic power potential
QM	Quantile Mapping
RCM	Regional climate model
RCP	Representative concentration pathway
RES	Renewable energy sources
rMBE	Relative mean bias error
RMSE	Root mean squared error
RNN	Recurrent neural network
rRMSE	Relative root mean squared error
RSDS	Surface-downwelling shortwave radiation
SoC	State of charge
T_c	Solar cell temperature
T_p	Panel temperature
TAS	Surface air temperature
V_{mp}	Voltage at maximum power
V_{oc}	Open circuit voltage
WS	Surface wind speed
ZNI	Non-interconnected zones

Abstract

The worldwide expansion of alternative energy sources, particularly solar photovoltaic energy, is escalating. However, solar energy solutions present challenges due to the variable nature of the solar resource. To effectively address the uncertainty associated with solar photovoltaic production, the implementation of an optimal management system is essential. This management system must not only handle energy storage systems or alternate available sources in off-grid systems but also effectively manage the connection to the power grid in on-grid solutions. This is where the application of artificial intelligence techniques becomes crucial, enabling the construction of precise models for optimal management. Therefore, this thesis proposes the implementation of artificial intelligence techniques to address the challenges of renewable energy systems with a focus on solar photovoltaic energy, exploring current solutions, proposing new ones, and discussing future directions. In particular, we focus on three main problems: data analytics, data processing, and optimal management in renewable energy systems. Data analytics involves gathering meteorological data, integrating both in-situ and historical satellite data along with climate change scenarios. After cleaning and validating the collected data, an analysis of the photovoltaic potential is carried out. Data processing focuses on improving the historical data by combining the best of in-situ and satellite data through site-adaptation techniques. The improved database feeds a solar irradiance forecasting model. Finally, the irradiance forecasting model and optimal battery scheduling are combined to achieve the optimal management of renewable energy systems. The research presented in this thesis is the result of joint work between the Universidad de los Andes and the Laboratory for Analysis and Architecture of Systems (LAAS-CNRS), aiming to contribute to the development of a sustainable and clean energy future.

Résumé

L'expansion mondiale des sources d'énergie alternatives, en particulier de l'énergie solaire photovoltaïque, est en plein essor. Cependant, les solutions d'énergie solaire présentent des défis en raison de la nature variable de la ressource solaire. Pour répondre efficacement à l'incertitude associée à la production d'énergie solaire photovoltaïque, la mise en œuvre d'un système de gestion optimal est essentielle. Ce système de gestion doit non seulement gérer les systèmes de stockage d'énergie ou les sources alternatives disponibles dans les systèmes hors réseau, mais aussi gérer efficacement la connexion au réseau électrique dans les solutions en réseau. C'est là que l'application de techniques d'intelligence artificielle devient cruciale, permettant la construction de modèles précis pour une gestion optimale. Par conséquent, cette thèse propose la mise en œuvre de techniques d'intelligence artificielle pour relever les défis des systèmes d'énergie renouvelable en mettant l'accent sur l'énergie solaire photovoltaïque, en explorant les solutions actuelles, en proposant de nouvelles solutions et en discutant des orientations futures. En particulier, nous nous concentrons sur trois problèmes principaux : l'analyse des données, le traitement des données et la gestion optimale des systèmes d'énergie renouvelable. L'analyse des données implique la collecte de données météorologiques, l'intégration de données satellitaires in situ et historiques ainsi que des scénarios de changement climatique. Après avoir nettoyé et validé les données collectées, une analyse du potentiel photovoltaïque est effectuée. Le traitement des données se concentre sur l'amélioration des données historiques en combinant le meilleur des données in-situ et satellitaires grâce à des techniques d'adaptation au site. La base de données améliorée alimente un modèle de prévision de l'irradiation solaire. Enfin, le modèle de prévision de l'irradiation et la programmation optimale des batteries sont combinés pour parvenir à une gestion optimale des systèmes d'énergie renouvelable. La recherche présentée dans cette thèse est le résultat d'un travail conjoint entre l'Universidad de los Andes et le Laboratoire d'analyse et d'architecture des systèmes (LAAS-CNRS), visant à contribuer au développement d'un avenir énergétique durable et propre.

Chapter 1

Introduction

In a transition to a sustainable energy future, renewable energies are expected to predominate the energy market. This transition will be driven mainly by solar and wind power sources [10]. From these sources, solar photovoltaic (PV) energy is one of the most promising, and it has become the fastest-growing renewable energy technology, with an exponential increase in power generation per year [11]. Moreover, the cost of electricity from PV panels was reduced by almost 75% in the past decade [12].

Although renewable energy systems are a promising solution, the fluctuation of the resource poses a challenge [13]. The integration and management of renewable energies can be achieved through new electrical concepts named microgrids constituting in the same entity several functions as electrical production, loads, and eventually temporary storage able to work in total autonomy or be associated in graphs or other grids. A microgrid comprises the control and management of different energy sources, such as PV panels, wind turbines, and batteries [14]. The microgrid can operate connected to the power grid or disconnected in islanded mode [15]. Therefore, microgrids are a reliable energy solution because of their capacity to isolate and work independently of the main grid. Another significant benefit is their easy implementation in rural areas where it is difficult to bring electricity through the power grid [16–18].

However, the management of microgrids is still challenging, mainly due to the variable nature of the solar resource. To effectively address the uncertainty associated with solar photovoltaic production, the implementation of an optimal management system is essential [19]. This system should not only manage renewable energy sources and energy storage systems in off-grid systems but also efficiently handle the connection to the power grid in on-grid solutions [20].

In recent years, Artificial Intelligence (AI) methods have brought great benefits to the control and management of microgrids [21–23]. These AI applications allow for intelligent decision-making leading to smart energy systems. AI techniques can be applied in different fields of renewable energy systems, such as power economic dispatch, intelligent optimal design and sizing, forecasting of energy production, optimization of distributed energy resources, and supply-demand management [8, 24]. By optimizing the use of resources through AI, savings are also generated in equipment, taking into account life cycles, aging, and maintenance costs [25]. Control methods based on AI have outperformed classical control techniques for microgrid management [26–32].

Despite advances in AI applications in renewable energy, there are still significant opportunities for advancement, especially in microgrids with solar PV systems [33]. The performance of solar PV systems fluctuates according to meteorological conditions [34, 35]. Variations in solar irradiance and other weather working conditions can decrease power generation [36]. Cloud cover can cause potential problems such as hot spots [37]. Also, one or more energy storage systems (ESS) are necessary when the PV solution is off-grid [38]. The most common ESS in PV solutions are lead-acid or lithium-ion batteries [39]. Therefore, an intelligent system is needed to control the energy generated by the PV system, regulate the charging and discharging of the batteries, and control the dispatch of energy.

In this thesis, we propose the implementation of AI techniques to address the challenges of renewable energy systems with a focus on solar PV energy and batteries as energy storage systems, exploring current solutions, proposing new ones, and discussing future directions. We address three main problems: data analytics, data processing, and optimal management in renewable energy systems. A graphical abstract of the thesis proposal is presented in Figure 1.1. The first stage is to collect data on meteorological variables (solar irradiance, temperature, and wind speed), including historical data from in-situ stations and satellite-based data, as well as projections related to climate change scenarios. These databases allow us to estimate the potential of PV systems, involving both historical patterns and climate change scenarios. In the data processing stage, our goal is to improve the historical data by taking advantage of the best aspects of both in-situ and satellite data, by using site-adaptation techniques. The improved database subsequently provides the input for a solar irradiance forecasting model. Finally, the optimal management stage utilizes the solar irradiance forecasting model along with optimal battery scheduling to achieve effective management of renewable energy systems.

To achieve these objectives, Chapter 3 introduces the importance of data collection and analysis in the assessment of solar PV potential. The chapter presents the Colombian Solar Atlas, an innovative tool designed to assess the PV potential in Colombia. The Atlas incorporates historical meteorological data from in-situ measurements [40] and satellite data [41] for the period from 1998 to 2019. In addition, future climate change projections for 2070–2099 are analyzed [42]. The Atlas provides users with a user-friendly interface and two PV generation models, basic and advanced, to estimate the performance of PV systems at specific locations, improving the accessibility and reliability of PV potential data. This innovative tool addresses the lack of robust and easily accessible meteorological information in Colombia, promoting renewable energy solutions and supporting sustainable energy policies, while ensuring broad accessibility for users from the scientific community to the general public. The chapter also provides a comprehensive analysis of the possible impact of climate change on solar PV potential in South America, a region rich in renewable energy potential. We examine the influence of changes in solar irradiance, air temperature, and wind speed by the end of the century under two climate scenarios, one optimistic (RCP2.6) and one pessimistic (RCP8.5) [43, 44]. The chapter provides valuable information on the possible effects of climate change on PV potential in South America, serving as a fundamental resource for the selection of optimal areas for solar energy projects.

Chapter 4 introduces a new methodology to improve the spatio-temporal resolution of solar irradiance databases through site-adaptation techniques and obtain more accurate prediction models. The chapter addresses the challenges related to data quality and spatio-temporal resolution by proposing a machine learning-based approach that combines the best of satellite and in situ measurements. This improved database is then used to develop solar irradiance prediction models using deep learning techniques. The chapter demonstrates the effectiveness of this approach, showing how machine learning models for site-adaptation can outperform traditional statistical methods, resulting in databases with superior data quality. These improved databases serve as the basis for the development of highly accurate solar irradiance prediction models.

Finally, Chapter 5 introduces an advanced approach to the energy management of DC microgrids, focusing on the integration of solar irradiance forecasting with optimal scheduling techniques to address the challenges presented by renewable energy variability and battery degradation. The chapter emphasizes the importance of accurate forecasts of solar PV production. The main objective is to reduce the energy costs of grid consumption, considering also the costs of battery degradation. By incorporating meteorological data

into the forecasting model, the chapter highlights the critical role of meteorological data in providing information on future renewable energy generation, allowing more accurate scheduling decisions in microgrid systems.

The research presented in this thesis represents a collaborative effort between the Universidad of los Andes and the Laboratory for Analysis and Architecture of Systems (LAAS-CNRS) through a cotutelle between the Andes University in Bogota and the Paul Sabatier University in Toulouse. Our objective through this work is to contribute to the advancement of a sustainable and clean energy future, by confronting the challenges and uncertainties inherent in renewable energy systems while facilitating their effective integration. As a result of this thesis, the following papers have been published: "Machine learning for site-adaptation and solar radiation forecasting" [45], "The impact of climate change on photovoltaic power potential in Southwestern Colombia" [46], "Climate change impact on photovoltaic power potential in South America" [47], and "An interactive tool for visualization and prediction of solar radiation and photovoltaic generation in Colombia" [48]. It is important to mention that this thesis, in collaboration with master's and undergraduate students from the Universidad de los Andes, has resulted in the publication of three papers. These papers have been published in the journals Renewable Energy [8], Heilyon [35], and a conference paper at the 22nd Workshop on Control and Modelling of Power Electronics (COMPEL) [34]. These papers add up to over 130 citations. Furthermore, as a product of this thesis, a summer course focusing on the applications of artificial intelligence in photovoltaic systems was offered "Aplicaciones de machine learning en sistemas fotovoltaicos".

1.1 General objective

Develop and implement artificial intelligence (AI) techniques for effectively managing renewable energy systems, focusing on solar photovoltaic (PV) energy and batteries as energy storage systems.

1.2 Specific objectives

- Collect, validate, and analyze meteorological data, including in-situ measurements, satellite data, and climate change scenarios, to accurately assess photovoltaic potential.

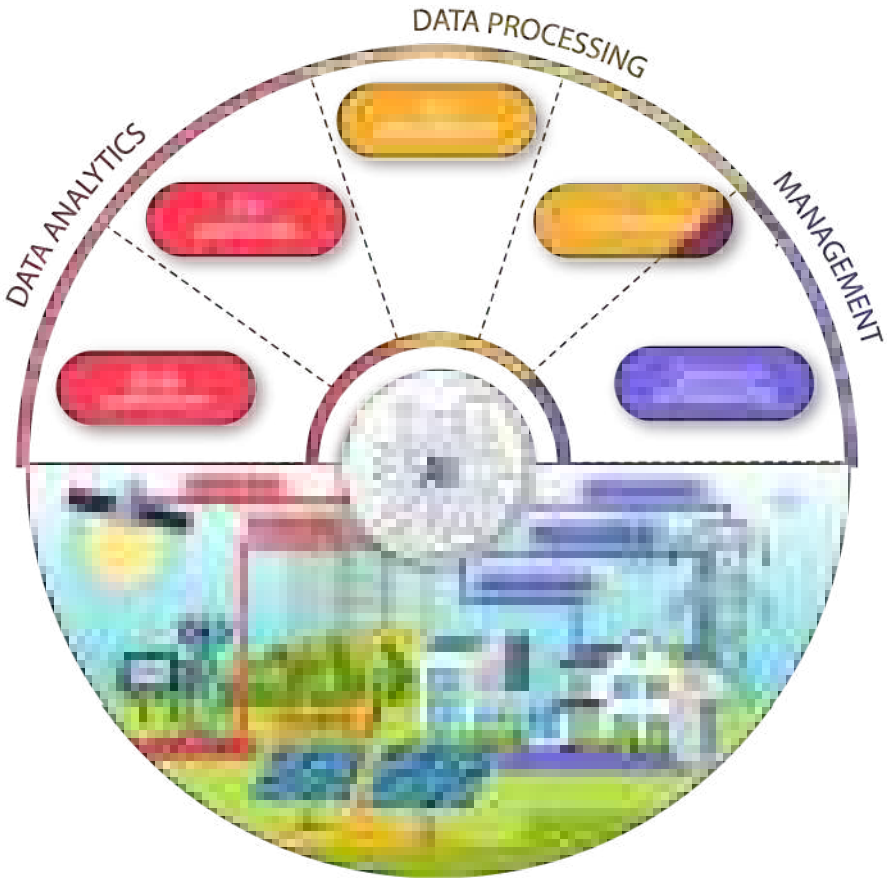

FIGURE 1.1: **Graphical Abstract:** The first step involves data collection from various meteorological databases to evaluate the photovoltaic power potential. These databases are then enhanced to provide more precise spatio-temporal data, allowing accurate solar irradiance forecasting models. These forecasting models, along with optimal scheduling, are subsequently integrated to achieve efficient microgrid management.

- Improve historical data quality by combining in-situ and satellite data using site-adaptation techniques for an improved solar irradiance forecasting model with AI techniques.
- Integrate the solar irradiance forecasting model with optimized battery scheduling to reduce energy costs while avoiding battery degradation.

Chapter 2

Context and background

Table of Contents

2.1 Introduction

Global interest in renewable energy, with a particular focus on solar PV systems, has emerged as a sustainable response to growing energy demand and concerns about climate change [49]. However, the widespread deployment of PV systems is coupled with a series of complex challenges that require thorough examination [50]. One of the main complications of PV systems is their inherent intermittency and susceptibility to weather variations, particularly fluctuations in solar irradiance. These variations can result in irregular patterns of power generation, making it difficult to maintain a constant power supply [45]. Addressing this challenge requires the application of advanced forecasting and management techniques to ensure a quality power supply. Meanwhile, the integration of energy storage systems (ESS) is becoming increasingly important to store surplus energy during peak generation periods and discharge it during off-peak periods, thus optimizing solar energy utilization and reducing costs [51].

Another fundamental challenge is geographical analysis of solar resources, as some regions enjoy abundant sunlight while others experience less favorable conditions. Analyzing photovoltaic potential can help to identify precisely those regions with the greatest potential. Likewise, PV systems can help supply energy in remote areas, mainly in developing countries [52].

Artificial Intelligence (AI) has emerged as a disruptive tool in the renewable energy sector, providing solutions to complex challenges and improving the efficiency and sustainability of renewable energy systems. The main AI techniques used in renewable energy include machine learning, deep learning, and reinforcement learning [53]. Machine learning, characterized by algorithms that allow systems to learn from data and make predictions or decisions, is widely used in renewable energy forecasting. This involves developing models to predict solar irradiance, wind speed, and energy demand, which are crucial for optimizing energy production and storage in renewable energy systems. Deep learning, a subset of machine learning, is particularly suited to handle complex, high-dimensional data. In renewable energy applications, deep neural networks are used for tasks such as image recognition in solar panel maintenance and optimization of energy storage systems. Reinforcement learning, which focuses on training agents to make sequential decisions through trial and error, is used for grid management and power distribution, optimizing the operation of microgrids and seamlessly integrating renewable energy sources into the overall power grid [54, 55].

However, the application of AI to renewable energy is not without its difficulties. One of the main challenges is the need for large amounts of high-quality data to train AI models [56]. Reliable data on weather patterns, energy consumption, and system performance are essential, and gaps or inaccuracies in the data can cause AI performance to be sub-optimal [57]. Furthermore, the interpretability of AI models remains a challenge, as complex neural networks often operate as black boxes, making it difficult to understand the logic behind their decisions. Ethical issues, especially in autonomous energy systems, require careful consideration to ensure that AI-based solutions prioritize sustainability, equity, and safety. Integrating AI into existing energy infrastructures and regulatory frameworks can pose logistical and political challenges [58]. Despite these obstacles, AI holds great promise for advancing renewable energy systems, making them more efficient, reliable, and sustainable [59].

Government policies and incentives have promoted investments in renewable energies, reinforcing them as a key element of climate action programs. Collaborative efforts between government support measures and private sector investments have driven the expansion of renewable energies [60]. In particular, Colombia is increasingly recognizing the potential of renewable energy sources to diversify its energy matrix, improve energy security, reduce greenhouse gas emissions, foster economic growth, and supply remote and non-interconnected zones [61].

As the global transition to renewable energy continues to accelerate, research and innovation continue to drive advances in this field. PV systems are emerging as one of the most promising renewable sources. However, their variable and intermittent nature, their integration into the grid, and the efficient management of energy storage systems remain central issues for researchers, underscoring the need for further research and innovation in the field of renewable energy.

2.2 Renewable energy

2.2.1 Types of renewable energy sources

Renewable energy is defined as energy derived from natural sources that is replenished faster than it is consumed. Among these sources, solar energy stands out as one of the most accessible and widely adopted [62]. Solar panels convert sunlight into electricity, making it an excellent option for decentralized energy generation. Wind power, on the

other hand, is based on the kinetic energy of moving air masses captured by wind turbines. This technology is often used in large wind farms, contributing significantly to grid-scale electricity generation. Hydropower harnesses the energy of flowing water, typically through dams and turbines, and remains a steady and reliable source of renewable electricity. Biomass energy uses organic materials such as wood, agricultural residues, and waste to produce heat and electricity [63]. Geothermal energy harnesses the Earth's internal heat, providing geographically specific opportunities for heating and electricity production [64].

Solar energy, derived from the radiant light and heat emitted by the sun, is one of the most abundant and accessible forms of renewable energy [65]. PV systems, composed of solar panels, convert sunlight directly into electricity [66]. Solar thermal systems, on the other hand, capture solar energy to generate heat, often used for heating water or spaces [67]. The adaptability and versatility of solar energy make it an attractive option for both centralized and decentralized power generation. It is a clean and sustainable source that can significantly reduce greenhouse gas emissions and dependence on fossil fuels. With continuous advancements in PV technology and energy storage solutions, solar energy is poised to play an increasingly vital role in the global energy landscape [68]. It is necessary to consider that solar energy presents intermittent generation due to weather and daylight variations, energy storage solutions may be necessary for continuous power supply, and energy production efficiency can be influenced by shading and soiling [69].

Wind energy harnesses the kinetic energy of moving air masses to generate electricity. Large wind turbines, often grouped together in wind farms, capture the energy from the movement of wind, converting it into electrical power [70]. Wind energy is a versatile and scalable source that can range from small-scale, distributed wind turbines to massive offshore wind farms [71]. It has gained widespread adoption due to its capacity to generate substantial amounts of electricity with minimal environmental impact once the infrastructure is in place. While wind energy is highly dependent on geographic location and local wind patterns, advancements in turbine design and improved grid integration continue to make it an attractive option for clean energy production [72]. However, as in the case of solar energy, wind energy is also intermittent due to weather conditions, and it is important to mention that land use permits are a challenge for large wind farms [73–75].

Hydropower harnesses the energy of flowing water, typically through the construction of dams and the use of turbines. This renewable energy source is reliable and efficient, providing a continuous supply of electricity as long as there is a constant flow of water

[76]. Large hydropower plants are often integrated into centralized power grids, making a significant contribution to electricity generation [77]. In addition, small-scale hydropower systems can be installed in remote areas to provide decentralized power [78]. Although hydropower offers numerous advantages, such as minimal greenhouse gas emissions and the ability to store energy in reservoirs, it also poses environmental challenges related to dam construction and disruption of the river ecosystem, and is vulnerable to droughts and changing precipitation patterns [79].

Biomass energy utilizes organic materials, such as wood, agricultural residues, and even waste, to produce heat, electricity, or biofuel. This source of renewable energy is versatile and can be utilized in various applications, from heating homes to powering vehicles [80]. Biomass energy is particularly beneficial in the context of waste management, as it can convert organic waste into valuable energy resources [81]. However, the sustainability of biomass energy depends on responsible sourcing and management of biomass feedstocks to avoid adverse environmental impacts, such as deforestation or excessive land use for biofuel crops [82].

Geothermal energy harnesses the Earth's internal heat, making use of the natural flow of heat from the Earth's core to its surface. Geothermal resources are concentrated in regions of high geological activity, such as volcanic areas [83]. Geothermal power plants typically drill wells to access deposits of hot water or steam deep within the earth. Once harnessed, this thermal energy can be converted into electricity or used directly for heating. Geothermal energy is considered highly sustainable, as it provides a continuous and reliable source of energy with minimal environmental impact. It is an excellent example of localized and decentralized energy production, especially in areas with abundant geothermal resources [84]. However, geothermal is local-dependent and concentrated in specific regions, there is also a risk of geothermal resource depletion over time [85].

2.2.2 Global renewable energy trends

In 2022, investments in renewable energy reached a historic high of US$495.42 billion, accompanied by a remarkable growth in installed capacity of distributed renewable for electricity access. Sales of solar PV products increased by 24%. However, projections indicated that the global population without access to electricity would increase by 20 million in that year. During the decade from 2010 to 2020, 45 countries achieved universal access to electricity. Nevertheless, by the end of 2022, 113 countries still lacked universal

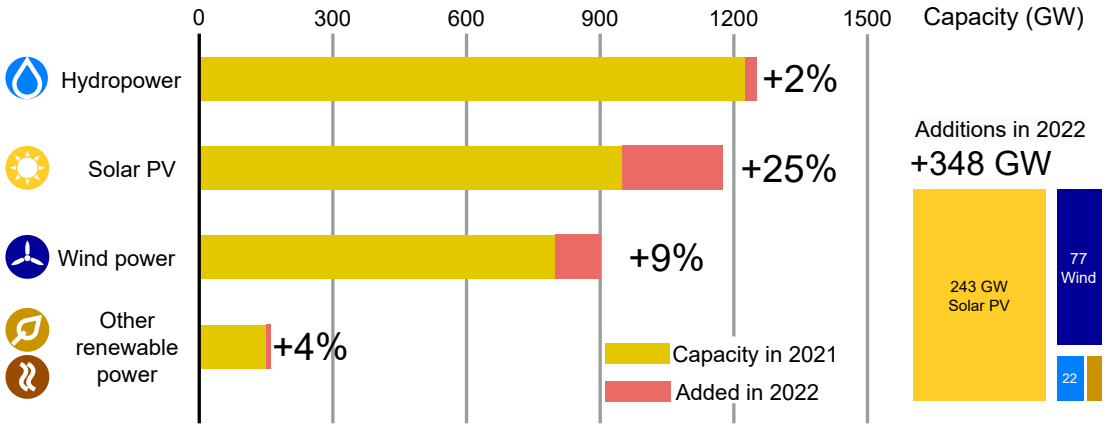

FIGURE 2.1: Global installed renewable power capacity and annual additions, by technology, 2022. Adapted from [1].

access. Among these countries, 25 had set targets to achieve universal access to electricity by 2030 or earlier, while 29 had targets to improve access. In contrast, 59 countries lacked defined targets for improving access to electricity [86, 87].

As a solution, renewable energies with particular emphasis on solar PV systems, have attracted significant interest as a sustainable solution to address growing global energy demand and mitigate climate change [49]. According to the Renewables 2023 Global Status Report, the renewable energy source with the highest percentage increase in installed capacity was PV systems, with a remarkable 25 percent growth in 2022 [1], as shown in Figure 2.1.

Furthermore, over the past ten years, the worldwide PV capacity has shown exponential growth, expanding from 100 GW to 1185 GW, an increase of more than 1000%, as can be seen in Figure 2.2.

Despite these high growth rates, the integration and deployment of PV systems pose multiple challenges that deserve careful consideration [50]. One of the most widespread challenges of PV systems is their inherent intermittency and variability due to weather factors, particularly solar irradiance. These fluctuations can lead to irregular power generation patterns, making it difficult to ensure a constant power supply [88]. To solve this problem, advanced forecasting and predictive modeling techniques are needed to improve grid stability and reliability [45]. Moreover, energy storage systems are increasingly crucial for storing excess energy during peak generation periods and discharging it during low generation periods, thus optimizing the utilization of solar energy [51].

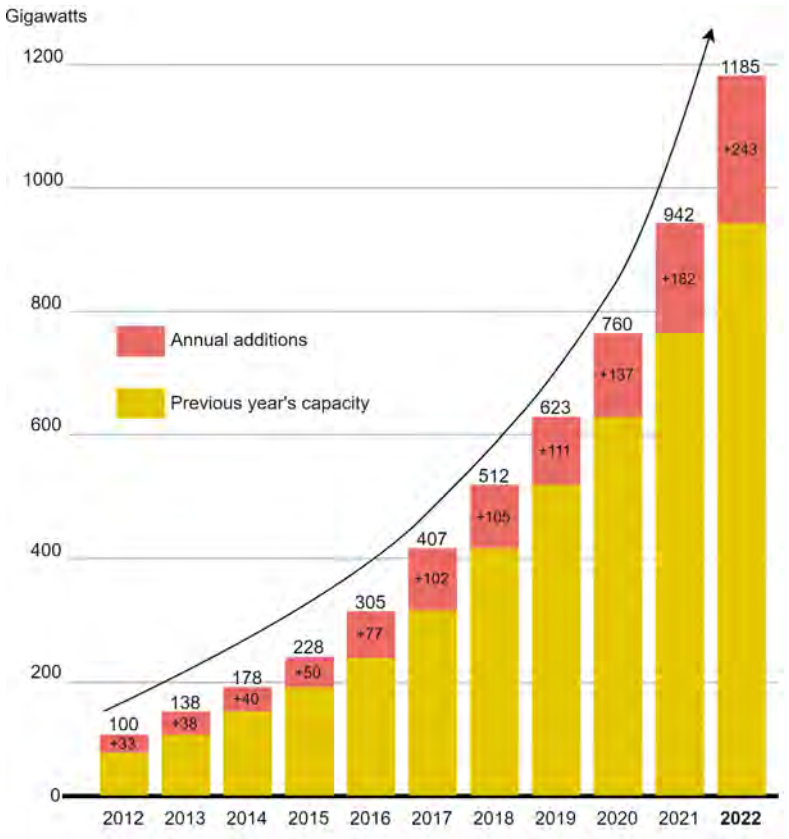

FIGURE 2.2: Global installed PV capacity and annual additions, 2012-2022. Adapted from [1].

Another key challenge is the geographic variability of solar resources [89]. While some regions benefit from abundant sunlight, others experience less favorable conditions [90]. This spatial disparity necessitates the development of efficient power transmission and distribution infrastructures to transport surplus energy from resource-rich areas to regions with lower solar potential [91]. Furthermore, incorporating PV systems into existing grid structures often requires significant infrastructure upgrades, including smart grids and microgrids, to accommodate bi-directional power flows and ensure grid resilience [92].

The economic viability of PV systems remains a pertinent concern. Despite significant cost reductions in PV technology, the initial capital investment for large-scale installations can still be substantial, especially for developing countries [93]. Comprehensive financial mechanisms, such as subsidies, tax incentives, and favorable regulatory frameworks, are needed to encourage widespread adoption [94]. Additionally, extending the lifetime of PV panels and optimizing their efficiency are ongoing research tasks, as premature degradation can hinder the economic viability of these systems [95].

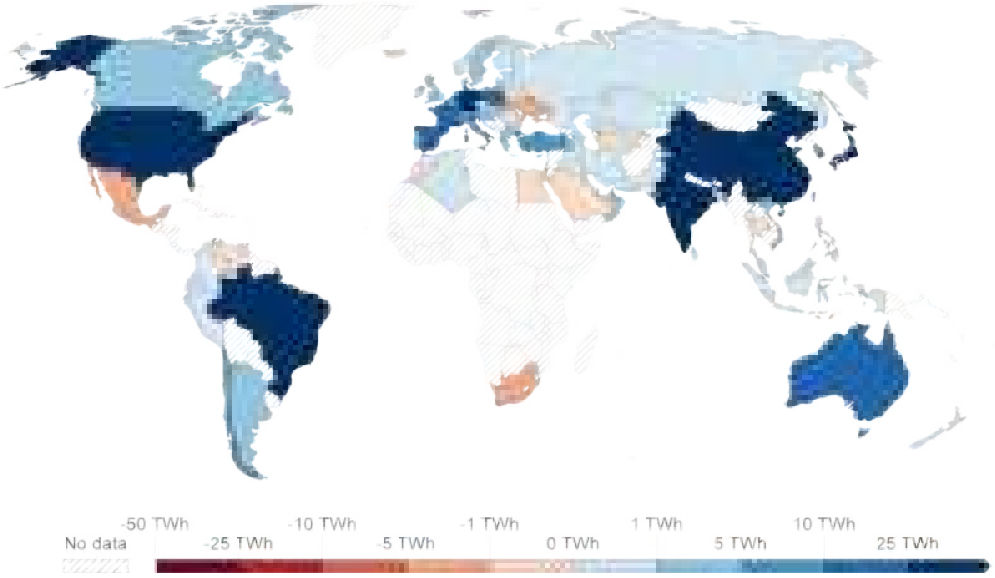

FIGURE 2.3: Global change in solar power generation in 2022 compared to 2021. Source: Energy Institute Statistical Review of World Energy (2023) [2]. Adapted from Our World in Data.

Government policies and incentives have boosted investments in renewable energy. These include tax incentives, renewable energy targets, and carbon pricing mechanisms [96]. Cooperation between government support measures and private sector investments has driven the expansion of renewable energies [97]. Figure 2.3 shows the global change in solar power generation in the year 2022 compared to the previous year [2, 98].

2.2.3 Challenges in renewable energy

Renewable energy sources, such as solar and wind power, are inherently intermittent. Their energy generation depends on weather conditions and time of day. This intermittency poses challenges in ensuring a consistent power supply. For instance, during periods of low sunlight or wind, solar and wind farms may produce significantly less energy, causing potential energy shortfalls [13, 99–101].

Energy storage is critical for mitigating the intermittency of renewable sources and ensuring a continuous power supply. However, challenges in energy storage technologies persist. For example, lithium-ion batteries, commonly used for energy storage, have limitations such as high costs and limited lifespan [102, 103].

The integration of renewable energy sources into existing grids poses challenges that require advances in grid infrastructure and energy storage solutions [104]. The widespread

use of energy storage technologies, particularly batteries, is critical not only to ensure energy supply but also to mitigate intermittency issues [105].

Despite these challenges, the global transition to renewable energy has accelerated, with many countries setting ambitious targets to diversify their energy mix [60]. The Paris Agreement's commitment to climate action has catalyzed international collaboration, reinforcing renewable energies as a foothold for mitigating climate change [106].

2.2.4 Renewable energy in Colombia

Colombia is increasingly recognizing the potential of renewable energy sources to diversify its energy matrix, improve energy security, reduce greenhouse gas emissions, and drive economic growth [107]. While historically reliant on hydropower, Colombia is now positioned to take advantage of a broader spectrum of renewable resources, presenting a promising outlook for renewable energy in the country [61].

One of the main renewable energy sources with great unexploited potential in Colombia is solar energy. The country has significant levels of solar irradiation, especially in regions such as La Guajira [108]. The Colombian government has implemented policies and incentives to promote solar photovoltaic installations [109]. These efforts aim to harness solar energy to meet the growing electricity demand, especially in non-interconnected zones (ZNI by its Spanish acronym). The ZNI is the geographic area where public electricity service is not provided through the National Interconnected System (SIN), and represents 52% of the national territory, as shown in Figure 2.4. The ZNI generally has diesel plants for electricity supply. However, this supply, besides being highly polluting, is not provided on a continuous basis, which translates into a very poor quality service [110, 111].

With advances in PV technology and decreasing installation costs, solar energy is set to play a key role in the energy transition of Colombia [112]. Furthermore, according to [4], although solar energy represents about 3% of the total energy mix, solar PV stands out among non-conventional renewable energies due to its significant growth. In 2022, solar PV experienced an impressive 183% increase compared to the previous year, as depicted in Figure 2.5.

As renewable energies advance, research and innovation continue to play a key role in driving progress in this field. Photovoltaic systems appear to be one of the most promising renewable sources. However, their variable and intermittent nature, integration with

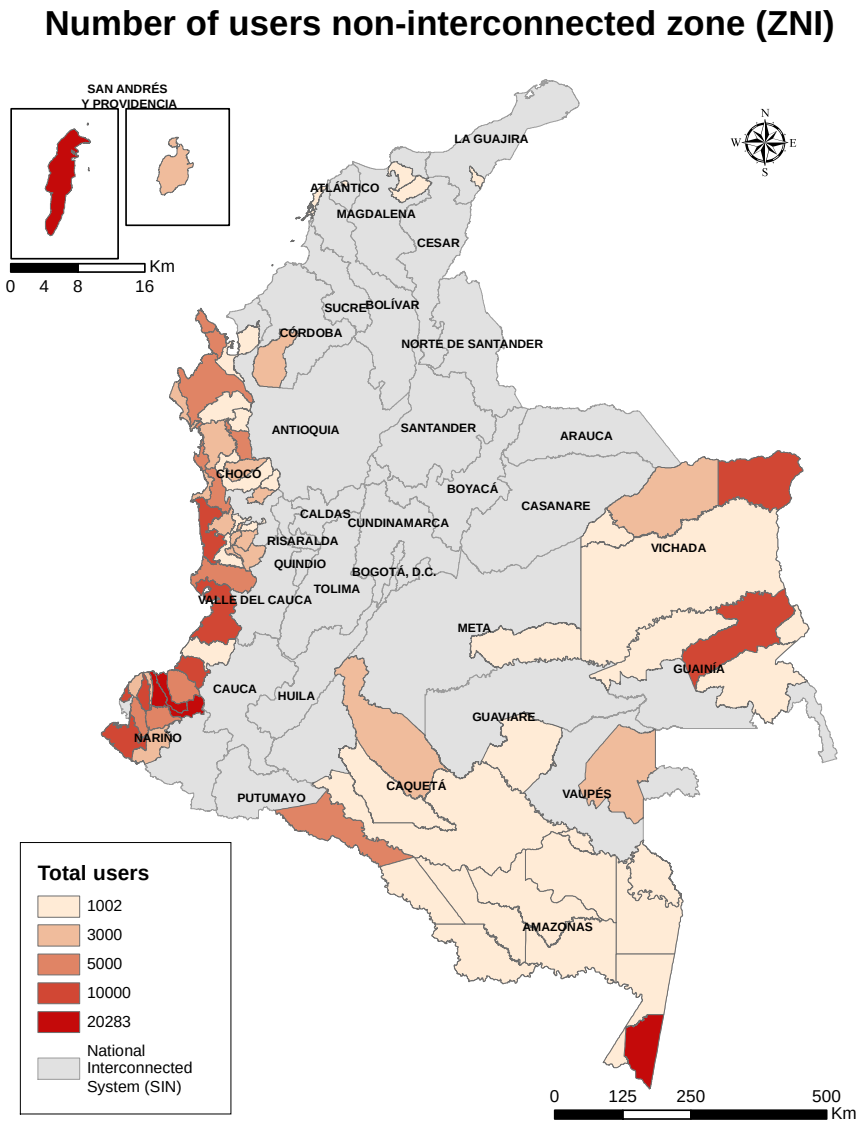

FIGURE 2.4: Total number of users per municipality belonging to the ZNI. Adapted from [3].

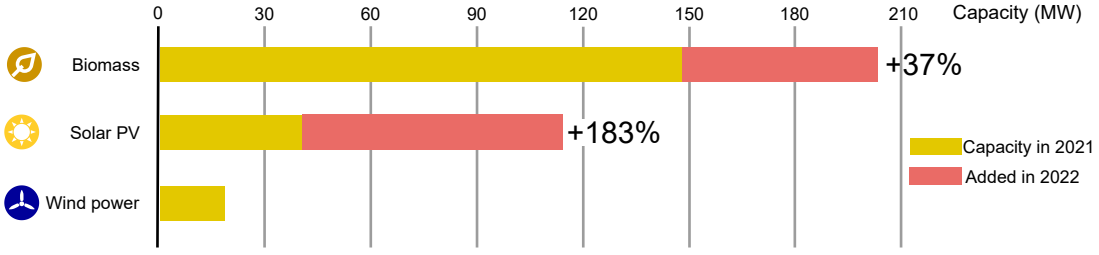

FIGURE 2.5: Colombian installed renewable power capacity and annual additions, by technology, 2022. Adapted from [4].

the grid, and management of energy storage systems remain points of interest for researchers [113]. An alternative to address this problem is through the use of microgrids, as described in the following section.

2.3 Microgrids

Microgrids are smaller-scale versions of the larger electrical grid, capable of generating, storing, and distributing electricity independently or in conjunction with the main grid. Microgrids are gaining prominence as a solution to enhance energy resilience, reduce carbon emissions, and improve the reliability of power supply [20]. However, microgrids face several challenges that require innovative approaches for effective integration into existing electrical grids [19] for on-grid solutions, and to address intermittency issues in off-grid solutions. Two key technologies, solar irradiance forecasting, and energy storage system (ESS) management, play a pivotal role in overcoming these challenges and realizing the full potential of microgrids [114].

2.3.1 Types of microgrids

Microgrids can be categorized by size into three main groups: small-scale, medium-scale, and large-scale. Small-scale microgrids typically serve single buildings or small communities, such as residential areas or small businesses. They are characterized by relatively low power generation and storage capacities, making them suitable for localized energy needs [115]. Medium-scale microgrids serve larger communities or industrial facilities, offering a balance between scalability and energy capacity [116]. Large-scale microgrids are designed to provide power to entire cities or regions. These microgrids incorporate extensive generation, storage, and control systems, often involving multiple energy sources and complex infrastructure [117].

Based on their operation mode microgrids are categorized into grid-connected and islanded each type possesses distinct characteristics that influence their functionality and applicability [118].

Grid-connected microgrids are primarily connected to the main utility grid. They operate in tandem with the central grid, allowing the exchange of electricity in both directions. Grid-connected microgrids are characterized by their ability to draw power from the central grid during periods of high demand or when local renewable generation falls short

[119]. Conversely, they can feed excess electricity back into the grid when generation exceeds local demand. This two-way power flow ensures grid stability and reliability. Grid-connected microgrids are typically employed in urban or suburban areas and are ideal for maximizing the use of renewable energy sources while maintaining a strong connection to the central grid. Usually, grid-connected microgrids can switch between grid-connected and islanded modes based on specific conditions or requirements [120]. Grid-connected microgrids face the challenge of coordinating power flow with the main grid and adhering to grid regulations, which may limit their independence during grid outages [121].

Islanded microgrids, as the name suggests, operate independently and autonomously from the central grid. They disconnect from the main grid during grid failures or as a deliberate strategy [122]. Islanded microgrids rely primarily on local generation sources, such as solar panels, wind turbines, or diesel generators. They are characterized by their ability to provide reliable power to critical loads even when the central grid is down. These microgrids are commonly used in remote or off-grid areas, providing energy access and ensuring essential services like healthcare, education, and telecommunications [123]. However, ensuring a balanced supply-demand relationship can be challenging. Managing power quality and load sharing among distributed resources are key concerns [124].

Microgrids can also be classified based on the type of electricity they use, alternating current (AC) or direct current (DC) [125]. AC microgrids primarily rely on AC power for generation, distribution, and consumption, aligning with the traditional grid system [126]. Key characteristics of AC microgrids include compatibility with existing AC infrastructure, ease of integration with the main grid, and the ability to support a wide range of loads [127]. However, they face challenges related to power conversion, as many distributed energy resources, such as solar panels and batteries, generate DC power, requiring multiple power conversion stages, potentially leading to energy losses [128].

DC microgrids utilize DC power for generation and distribution, eliminating the need for multiple conversions. This results in higher energy efficiency and reduced infrastructure complexity [129]. DC microgrids are well-suited for specific applications like data centers and electric vehicle charging stations, where DC loads are prevalent [130]. However, their key challenge lies in limited compatibility with the existing AC infrastructure, requiring dedicated DC lines. Furthermore, DC microgrids may face voltage stability issues when integrating fluctuating renewable energy sources [131].

The choice between AC and DC microgrids depends on the specific application, existing infrastructure, and energy resource availability [132]. Hybrid microgrids that combine both AC and DC components are also emerging to capitalize on the strengths of each type while mitigating their respective challenges [133]. The selection of AC or DC microgrids should be made based on careful consideration of technical requirements and cost-effectiveness for the intended purpose [125].

2.3.2 Control approaches for microgrids

Control systems play a key role in the operation of microgrids, underscoring their importance in ensuring efficient and reliable energy management within these decentralized systems. Advanced control technologies are essential for microgrids, especially due to their dynamic and multifaceted nature. These control systems facilitate real-time monitoring and management of various components, such as generation sources, ESS, and loads. By continuously assessing the status of the microgrid and its components, advanced controls enable rapid response to fluctuations in generation or energy consumption [6, 134].

Furthermore, advanced microgrid control systems enable grid operators to implement demand response strategies, load shedding, and smooth transitions between grid-connected and islanded modes [20]. These capabilities are critical to optimize energy use, improve grid resiliency, and ensure uninterrupted power supply during unforeseen events or grid disturbances [135]. Moreover, these control technologies facilitate the integration of microgrids into the overall power grid, enabling bi-directional power flow, which can be especially beneficial for balancing supply and demand [136].

The management and control of microgrids, both on-grid and off-grid, taking into account available energy sources such as PV panels, wind turbines, diesel plants, and energy storage systems, can be classified as centralized, decentralized, and distributed control [5, 137]. A microgrid central controller is used to coordinate and manage the available energy sources, as shown in Figure 2.6.

In a centralized control scheme, a single central controller is responsible for making decisions regarding energy generation, distribution, and consumption. This central controller monitors all aspects of the microgrid operation, including energy production from the different sources, energy demand, and the state of energy storage systems [138]. Based on real-time data and predefined algorithms, the central controller determines how to allocate energy resources optimally. For example, it can decide when to charge or discharge batteries, how much power should be supplied by renewable sources, and when

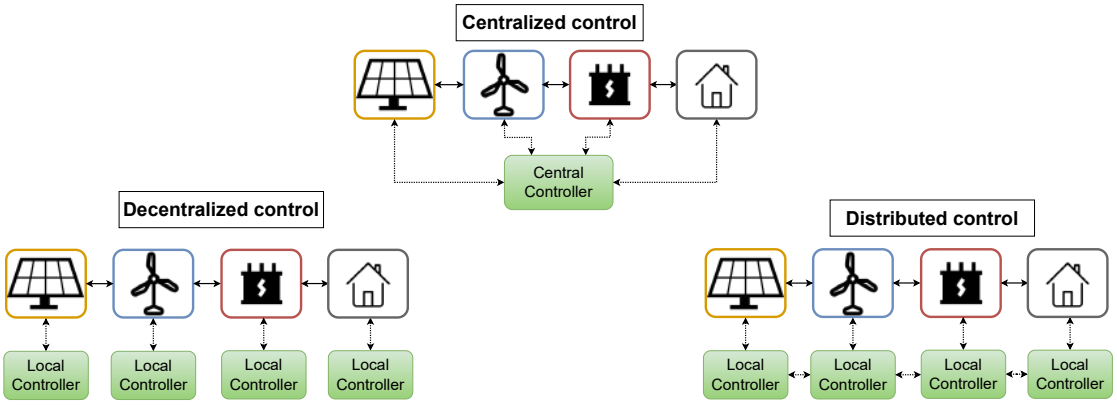

FIGURE 2.6: Centralized, decentralized, and distributed control schemes. Adapted from [5]

to import or export electricity to the main grid in on-grid microgrids [139]. Centralized control offers a high degree of coordination and optimization, ensuring efficient energy management. However, it can be vulnerable to a single point of failure, and communication delays or system malfunctions at the central controller can disrupt microgrid operations [140].

Decentralized control in microgrids distributes decision-making authority across multiple local controllers. Each component within the microgrid, such as solar panels, wind turbines, batteries, and loads, has its own controller capable of making autonomous decisions [141]. Decentralized control enhances the resilience and robustness of the microgrid, by adapting to component failures or communication disruptions without affecting the entire system operation. For example, if a solar panel controller detects a malfunction, it can autonomously adjust its operation to mitigate the issue [142]. Decentralized control also enables rapid response to changes in energy supply or demand, improving the ability of microgrids to handle fluctuations [143]. However, coordinating decentralized control can be challenging, and multiple distributed energy resources might make conflicting decisions without a central authority to coordinate [144].

Distributed control is a hybrid approach that combines elements of both centralized and decentralized control [145]. In this approach, the microgrid is divided into smaller clusters or zones, each with its own local controller. These local controllers can make decisions independently, optimizing the operation of individual distributed energy resources [146]. Distributed control can adapt to local conditions and disturbances while still benefiting from global coordination when needed. This approach is often used in medium-sized microgrids where both scalability and reliability are essential [147]. However, distributed

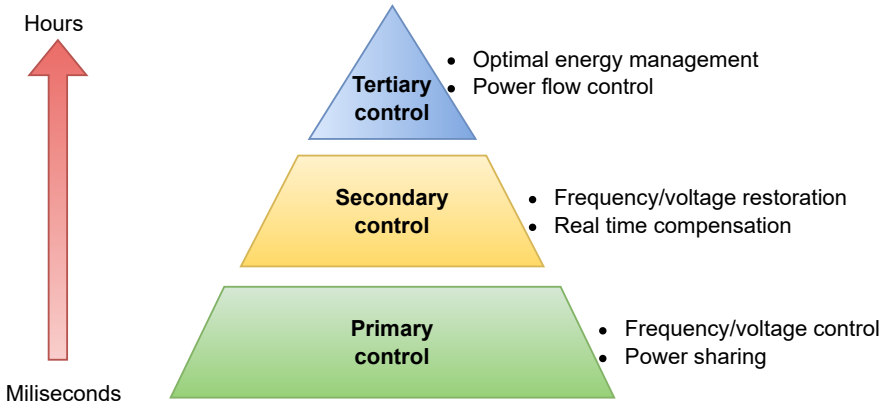

FIGURE 2.7: Hierarchical control structure of a microgrid. Adapted from [6]

schemes are more complex to implement and manage compared to pure centralized or decentralized control strategies, requiring reliable communication between local controllers and the central controller, and depending on the implementation, distributed control may involve higher costs [148].

The multiple control objectives of a microgrid are generally achieved through a hierarchical structure. This hierarchical control structure consists of primary, secondary, and tertiary levels. Primary control focuses on rapid frequency and voltage regulation, secondary control optimizes long-term system balance and economic efficiency, and tertiary control addresses macro-level optimization and integration with external grids and markets [6, 32, 143], as shown in Figure 2.7.

The primary control is the first line of defense against disturbances and deviations in the system. It operates at a high-speed level and is responsible for maintaining the balance between generation and consumption. Key characteristics of primary control include rapid response times, typically in the order of milliseconds to seconds, and ensuring that the microgrid operates within its nominal frequency and voltage limits [149]. Primary control mainly relies on local controllers embedded within distributed energy resources, such as inverters and generators. Primary control challenges include managing rapid load changes and sudden power fluctuations, which can lead to frequency and voltage deviations [122].

The secondary control takes a more comprehensive approach to system management. It operates at a slower timescale, typically in the order of seconds to minutes. Secondary control adjusts the set points for different distributed energy resources to restore the system to its desired state, ensuring a long-term balance between generation and consumption. Key characteristics include economic optimization, load scheduling, and power

sharing among distributed energy resources [126]. Challenges associated with secondary control involve the need for advanced algorithms to manage the diverse distributed energy resources within the microgrid efficiently. It must also consider forecasting errors, which can impact decision-making for load scheduling and energy distribution. Additionally, secondary control may need to address uncertainties related to renewable energy sources like solar and wind, as these sources are inherently variable [150].

The tertiary control operates at a slower timescale, typically in the order of minutes to hours, and focuses on optimizing the overall performance and economics of the microgrid. It makes decisions regarding energy trading, demand response, and coordination with the main grid [151]. Key characteristics include demand forecasting, market participation, and grid integration. Tertiary control often involves aggregating microgrids or coordinating with the main grid operator to ensure grid stability and reliability [152]. The challenges associated with tertiary control include complex decision-making processes, data exchange with external entities, such as utility companies, and adherence to regulatory frameworks for energy markets. It also requires advanced communication and coordination among multiple microgrids if they are part of a larger grid network. Ensuring cybersecurity is another challenge, as tertiary control involves external interactions that could potentially be vulnerable to cyber threats [152].

2.3.3 Energy storage system in microgrids

The integration of energy storage systems (ESSs) into microgrids has attracted increasing interest due to their ability to store energy during off-peak hours and discharge it during peak demand periods. Energy storage systems offer several advantages, such as improving power quality, mitigating the intermittency of renewable sources, and facilitating ancillary services such as frequency and voltage regulation in microgrid operation [153]. However, despite the substantial advantages offered by ESSs, their integration presents several challenges, including issues related to control, protection, state-of-charge (SoC), state-of-discharge (SoD), safety, lifetime, capacity, reliability, and cost. Therefore, addressing these challenges is crucial to improve the effective implementation of ESSs in microgrids [154].

The configuration of an ESS for microgrid applications generally falls into two categories: aggregated and distributed [7]. In the aggregated ESS setup, power consistently flows from distributed energy resources to the point of common coupling bus, allowing the entire ESS capacity to effectively dampen fluctuations in the power system. While this

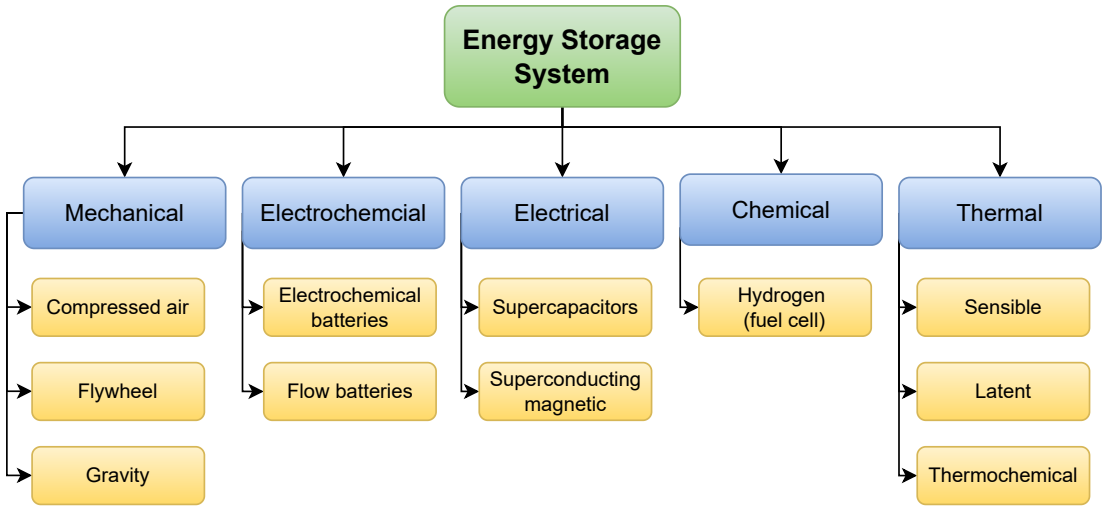

FIGURE 2.8: Classification of energy storage systems by technology. Adapted from [7]

configuration enhances the capability of ESSs, it does come with increased costs and the inherent challenges of manufacturing, controlling, and protecting large-scale ESSs. On the other hand, the distributed approach employs small-scale ESS units integrated directly with appropriate sources through various power electronic interfaces. This setup is favored for its potential to deliver reliable and efficient power regulation. However, the utilization of power electronic interfaces introduces harmonics into the system, imposing complex control mechanisms within the power network. Furthermore, the storage process results in losses attributable to power electronic interfaces applied to distributed energy resources and ESS units [155].

Depending on the technology, ESS can be classified into five major mechanical categories: electrochemical, electrical, chemical, and thermal, as shown in Figure 2.8 [7, 153, 156].

A mechanical energy storage system stores energy in the form of mechanical work, typically using the motion of masses or compressed air. Common technologies include compressed air, flywheel, and gravity. These systems have the advantage of high round-trip efficiency and fast response times, making them suitable for applications requiring rapid energy dispatch. However, they often face challenges related to material stress and cost, limiting their scalability and widespread adoption in comparison to other energy storage technologies [157].

An electrochemical energy storage system is a technology that stores electrical energy in the form of chemical energy, which can be converted back to electricity as needed. It typically consists of one or more electrochemical cells or batteries that use chemical

reactions to store and release energy. The two main categories are electrochemical batteries and flow batteries [158]. Their advantages lie in their high energy density, rapid response times, and ability to discharge electricity on demand, ensuring a stable power supply [159]. However, challenges such as limited lifespan, environmental concerns related to materials sourcing and disposal, and the potential for thermal runaway incidents underscore the need for ongoing research and development to optimize their performance and mitigate associated drawbacks [160].

An electrical energy storage system is a technology that stores electrical energy during periods of surplus and releases it when needed, serving as a critical component in managing and optimizing power supply and demand. Two main types of electrical energy storage are supercapacitors and superconducting magnetic [161]. Supercapacitors are increasingly gaining attention in the context of microgrids. These devices differ from traditional batteries in their energy storage mechanism. While batteries store energy through chemical reactions, supercapacitors store energy electrostatically, achieving high power density, long cycle life, fast response time, and low maintenance. However, supercapacitors have limited energy storage capacity, voltage limitations, and self-discharge [162]. On the other hand, superconducting magnetic stores energy in a magnetic field. These devices have a compact design and high power density, but they require extremely low temperatures to maintain their superconducting properties, and materials costs are a limiting factor [163].

Fuel cells are electrochemical devices that convert chemical energy from a fuel source, typically hydrogen or natural gas, directly into electricity. Fuel cells have high energy density, long cycle life, and fast response. However, the initial cost can be relatively high, along with limited energy storage capacity, environmental concerns, and degradation over time [164].

A thermal energy storage system is a technology used to store and manage thermal energy, typically in the form of heat or cold, for later use [165]. Thermal energy typically involves a medium, such as a liquid or solid, that can absorb and retain heat. The main technologies include sensible heat storage, latent heat storage, and thermochemical storage [166]. These storage systems allow for cost savings, grid stability, and environmental benefits. However, this technology faces high initial costs, energy losses, significant space requirements, and regular maintenance [167].

From these technologies, electrochemical batteries are the most common energy storage system in microgrids [154]. These batteries offer several significant advantages that

contribute to the reliability and efficiency of microgrid systems [153]. They enable the efficient storage of surplus energy generated during periods of high renewable energy production, such as sunny days for PV systems or windy conditions for wind turbines. This stored energy can then be discharged during periods of high demand or low renewable energy generation, ensuring a consistent and reliable power supply within the microgrid. Moreover, electrochemical batteries facilitate the integration of intermittent renewable energy sources, smoothing fluctuations and improving the stability of the microgrid. This integration is especially important in remote or off-grid areas, where a constant power supply is crucial [168].

Despite their advantages, electrochemical batteries are not without limitations. One notable drawback is their finite energy storage capacity, which necessitates careful consideration of system design and sizing to meet the energy demands of the microgrid effectively [169]. Additionally, batteries degrade over time with each charge and discharge cycle, which can lead to reduced energy storage capacity and lifespan. Mitigating this degradation is a key challenge in microgrid management [170]. Furthermore, the cost of acquiring and maintaining high-capacity batteries can be a significant investment for microgrid operators. Balancing the initial costs with long-term benefits is crucial in the economic feasibility of battery integration within microgrids. While these batteries have near-zero greenhouse gas emissions during operation, battery disposal, and resource extraction are open environmental issues to be addressed [171].

2.3.4 Benefits of microgrids

Microgrids offer a multitude of advantages that make them an increasingly appealing choice for energy generation, distribution, and management. First, microgrids significantly contribute to improved energy efficiency. By localizing energy production and distribution, they reduce transmission losses, which often occur when electricity is transmitted over long distances through conventional grids [20]. This enhanced efficiency translates into more economical use of energy resources and decreased energy wastage [118].

Reliability is another key advantage of microgrids. Traditional centralized grids are susceptible to large-scale failures due to natural disasters, equipment malfunctions, or cyberattacks. Microgrids, on the other hand, operate on a decentralized basis, making them more resilient to such disruptions. In the event of grid failures, microgrids can seamlessly transition into islanded mode, ensuring a consistent power supply to critical

facilities like hospitals or emergency services. This reliability enhances overall energy security [148, 172].

One of the most notable advantages of microgrids is their positive impact on the environment. Microgrids are often designed to incorporate renewable energy sources like solar panels and wind turbines. By utilizing clean, renewable energy, microgrids significantly reduce greenhouse gas emissions. This reduction contributes to mitigating climate change and promoting environmental sustainability. Moreover, microgrids can also incorporate advanced energy storage systems, further enhancing their ability to manage energy efficiently and reduce carbon footprints. In essence, microgrids are at the forefront of fostering both energy sustainability and environmental preservation [19, 64].

Microgrids have been widely adopted worldwide. In the particular case of Colombia, microgrids are presented as a solution for remote areas, such as non-interconnected zones, and regions that do not have quality energy supply. Therefore, the study of the feasibility and implementation of microgrids in Colombia has a social and economic impact that is worth addressing [16, 173–175].

2.3.5 Challenges of microgrids

One of the primary challenges faced by on-grid microgrids is their perfect integration with the main electrical grid [176]. In the particular case of photovoltaic sources, microgrids often rely on intermittent renewable energy sources, which can introduce variability and uncertainty into the energy supply. To address this challenge, accurate solar irradiance forecasting is indispensable. Short-term and long-term forecasting models provide microgrid operators with vital information about solar energy generation patterns. This knowledge enables proactive decision-making and grid coordination, ensuring a smooth transition between grid-connected and islanded modes. By minimizing disruptions during grid transitions, solar irradiance forecasting enhances grid integration and fosters grid stability [177].

According to [177], weather forecast errors are responsible for a relevant part of the uncertainty in microgrid operation. This is because meteorological conditions determine renewable energy source generation, and to a lesser extent, the system load. The difficulties in accurately modeling atmospheric processes lead to forecast errors, which can result in deviations from plans and affect the scheduling process of microgrids. Therefore, it is important to consider possible deviations resulting from forecasting errors in the proposed energy management strategies. The authors in [177] also provide a list of

recommendations for future implementations of weather forecasts in microgrid energy management systems. These recommendations include the need for standardized data sources, methodologies, and uncertainty approaches for weather forecasting. The authors also suggest the use of probabilistic forecasting methods to account for forecast errors and the need for a comprehensive analysis of the impact of weather information on microgrid scheduling. Additionally, the authors recommend the development of new optimization models that incorporate weather information and the need for further research on the integration of weather forecasts with other energy forecast applications.

Energy storage is a key enabler for off-grid microgrids. It allows excess energy generated during favorable conditions to be stored for use when energy generation is low. However, challenges in energy storage technologies, such as cost, efficiency, and environmental impact, need to be overcome. Advancements in battery technologies, grid-scale energy storage solutions, and innovative materials are essential for optimizing energy storage systems [155, 178].

Microgrids play a key role in the energy transition and the reduction of carbon emissions with several possibilities named LVDC (Low voltage Direct current), LVAC (Low voltage Alternative current), or recently hybrid microgrids are able to supply different types of AC and DC voltages. However, microgrids face significant challenges in integrating intermittent renewable energy sources. Efficient integration of these renewable sources is essential and requires innovative solutions [179]. Most notably, solar irradiance forecasting provides vital information on solar power generation patterns. Accurate forecasting of potential PV production facilitates proactive decision-making [45]. Furthermore, energy storage technologies play a key role in optimal microgrid management by storing excess energy for periods of low generation and mitigating the variability and uncertainty of renewable energies. [180].

One of the most widely used renewable sources in microgrids is photovoltaic solar energy. To integrate PV systems into microgrids, the first step is to assess the PV potential. To evaluate the PV potential a georeferenced study of photovoltaic potential is required. This approach allows us to identify regions with the highest PV potential and facilitate energy solutions in non-interconnected zones, as described in the following section. An experimental point of view of a simple LVDC microgrid was studied in LAAS-CNRS. This part will be explained in the fifth chapter of this manuscript.

2.4 Photovoltaic systems

Due to the growing need for sustainable and clean energy sources, PV systems have gained significant attention as a viable solution for generating electricity from solar energy. A PV system is a renewable energy technology that converts sunlight into electrical energy using PV cells [181]. These cells are typically made from semiconductor materials, such as silicon, that exhibit the photovoltaic effect. The main components of a PV system include the PV panels, also known as modules, which consist of multiple interconnected PV cells. These panels are responsible for absorbing sunlight and converting it into direct current electricity. In addition to the panels, a PV system also consists of a solar inverter, which plays a crucial role in converting the direct current generated by the panels into alternating current, which is suitable for use in electrical devices and for grid connection [182]. Another important component of a PV system is the battery bank, which is used to store excess electricity generated during periods of high sunlight for later use or during times when sunlight is not available [103]. Furthermore, a charge controller is included in the system to regulate the voltage of the battery bank and prevent overcharging or discharging [181].

Furthermore, the modeling of PV systems involves creating mathematical models that represent the behavior and performance of these systems. These models are used to simulate and analyze the operation of PV systems under different conditions [183]. One aspect of PV system modeling is the characterization of PV modules. This includes modeling the electrical characteristics of PV cells, such as the current-voltage (I-V) curve, which describes the relationship between the current and voltage output of a PV cell under varying conditions [184]. Another aspect of PV system modeling is the consideration of various factors that can affect system performance, such as shading, aging of modules, and other defects [37]. By incorporating these factors into the models, researchers can analyze the impact of these issues on the overall performance of PV systems. Moreover, the modeling of PV systems is essential for understanding their behavior, optimizing their performance, and identifying potential issues or improvements, allowing researchers and engineers to evaluate the efficiency, reliability, and economic viability of PV systems in different scenarios [185].

Several models have been developed at LAAS-CNRS to analyze the behavior of PV systems, detect failures, and improve their integration into microgrids, as presented in the thesis [186–189].

However, PV systems also face several challenges. One of the foremost issues is their intermittent nature due to sunlight availability, which necessitates the integration of energy storage solutions like batteries to ensure a consistent power supply [99]. Grid integration poses another challenge, as PV energy must be seamlessly integrated into existing electrical grids, requiring advanced control and management systems. Furthermore, the manufacturing and disposal of PV panels can have environmental implications, necessitating responsible end-of-life recycling practices [13]. Economic factors, such as initial installation costs and fluctuations in solar panel prices, can affect the affordability and widespread adoption of PV systems [100].

To support the adaptation and integration of PV systems, it is necessary to know the PV potential of the area of interest. This PV potential analysis provides an overview of the expected PV production according to the local environmental conditions and the technical characteristics of the PV installation. The following subsections explain in detail the importance of the PV potential analysis [52].

2.4.1 Photovoltaic power potential

Photovoltaic power potential refers to the amount of electrical energy that PV panels can generate when converting solar radiation energy into electricity [190]. Understanding PV power potential is critical for energy transition, resource assessment, grid integration, and investment decisions [191].

PV systems play a key role in the energy transition. As societies worldwide transition toward cleaner and sustainable energy sources, solar PV systems offer a renewable and environmentally friendly solution [192]. PV power potential is critical for estimating the contribution of solar energy to the energy mix, reducing reliance on fossil fuels, and mitigating climate change [193]. An accurate assessment of the PV potential helps to identify regions with high solar energy potential. This information guides the optimal siting of solar installations, ensuring efficient energy generation and reducing transmission losses [194]. Grid operators use PV power potential data to plan and manage the integration of solar energy into existing energy grids. Understanding the fluctuations in solar irradiance helps maintain grid stability and reliability [92]. Investors and policymakers rely on PV power potential assessments to make informed decisions regarding solar energy projects [195].

Evaluating PV power potential involves a comprehensive analysis of solar irradiance, which is the electromagnetic energy received from the sun per unit area, and other meteorological variables that affect its performance, such as temperature, and wind speed. Realizing the full potential of PV power generation comes with its own set of challenges. Variability in solar radiation due to weather patterns and time of day poses a challenge to grid integration and stable power supply [52]. Seasonal variations and the intermittent nature of sunlight require efficient energy storage solutions, such as batteries, to ensure continuous electricity generation. Moreover, the geographical distribution of PV potential may not always align with energy demand centers, necessitating grid infrastructure improvements and energy management strategies. The process of estimating PV power potential includes data collection, data validation, solar resource assessment, capacity factor calculation, and mapping and visualization [196].

Data collection involves gathering meteorological data from various sources, including in-situ weather stations, satellites, and climate models. This data includes solar radiation levels, temperature, wind speed, and geographical coordinates. The data validation process includes quality control procedures to ensure data accuracy and consistency. This step includes filtering out erroneous or missing data points. For the solar resource assessment, using the collected data, solar resource assessment models estimate the solar irradiance at specific locations over various time scales (hourly, daily, monthly, and yearly) [197]. Then, the capacity factor, representing the ratio of actual energy generated to the maximum possible energy generation, is calculated. The capacity factor provides insights into the reliability and efficiency of a PV system [198]. Finally, in mapping and visualization, PV power potential maps are generated to represent the solar energy potential across a geographical area [199].

2.4.2 Impact of climate change on PV systems

Understanding the impact of climate change on PV systems is crucial due to its potential implications for renewable energy production and sustainability [47]. As the effects of climate change become increasingly pronounced, they pose both challenges and opportunities for PV technology [46].

PV systems rely on consistent solar radiation patterns [200]. Climate change can alter these patterns, affecting the reliability of energy production [201]. An accurate assessment of the impact of climate change helps investors and policymakers make informed decisions about PV infrastructure [202]. Climate change adaptation and mitigation

strategies often include expanding renewable energy capacity. Therefore, a thorough understanding of how climate change affects PV systems is essential for achieving environmental goals [49].

Assessing the impact of climate change on PV systems involves a multidisciplinary approach combining climatology, meteorology, and PV technology analysis [203]. To assess the impact of climate change on PV systems, climate change models are used. These models project future climate scenarios based on various greenhouse gas emissions scenarios, simulating changes in temperature, precipitation, cloud cover, wind speed, and solar radiation patterns. Historical meteorological data is analyzed to identify trends and changes in local climate variables. This historical context is essential for understanding how local conditions have evolved [204].

Climate change models include global models that offer a broad perspective on climate change trends. Regional climate models, on the other hand, refine global models to regional or local levels, providing more accurate data for the assessment of PV systems [205]. These models are used to assess how changes in solar radiation, temperature, and other meteorological factors affect PV system performance [47]. Based on the assessment, adaptation strategies can be developed. These strategies may include changes in PV system design, energy storage capacity, or grid infrastructure [206].

2.5 Artificial Intelligence in PV systems

Artificial Intelligence (AI) is of great importance in the context of PV systems, contributing to the transformation of the renewable energy landscape. AI represents a key enabler to address some of the fundamental challenges faced by PV systems. One of the primary challenges is the variable and intermittent nature of solar power generation [23]. The output of PV panels is highly dependent on weather conditions, so accurate predictions are crucial for optimal operation. AI techniques, in particular machine learning and deep learning, enable accurate prediction of solar irradiance, offering a solution to mitigate the impact of unpredictability. These AI-based forecasts not only improve the efficiency of PV systems but also facilitate their integration into the energy grid [58, 197].

Furthermore, AI plays a key role in the efficient management of energy storage systems in PV installations [207]. Energy storage is vital for balancing energy supply and demand, especially during periods of low solar power generation. AI algorithms enable intelligent control of ESSs, by determining when to charge or discharge batteries, considering factors

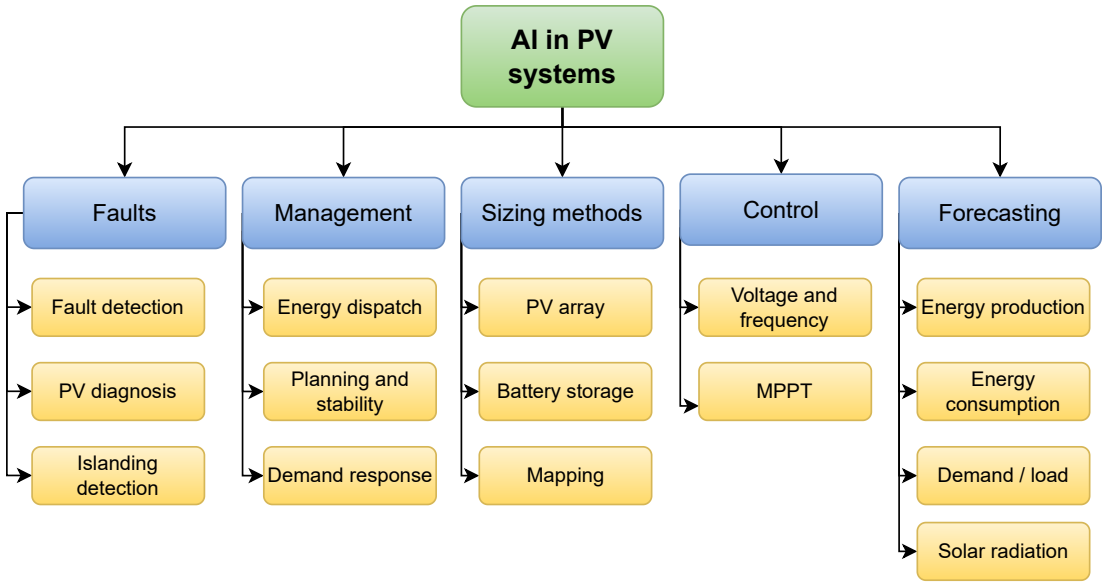

FIGURE 2.9: Main applications of AI in PV systems. Adapted from [8]

such as energy cost, grid conditions, and battery degradation. The result is greater energy self-sufficiency, less dependence on external power sources, and longer battery life [54]. As the world's energy systems evolve toward greater reliance on renewable energy, the role of AI in improving the stability, reliability, and sustainability of PV systems becomes increasingly evident, underscoring its importance in the PV field [25, 208].

The main applications of AI in PV systems include fault detection, management, sizing methods, control, and forecasting, as depicted in Figure 2.9

2.5.1 AI in fault detection

PV systems are susceptible to malfunctions due to severe environmental conditions, impacting energy conversion efficiency and system lifespan. AI assists in detecting and diagnosing these issues, classified into fault detection, fault diagnosis, and islanding detection [209]. Various types of faults, such as incipient, abrupt, intermittent, line-to-line, line-to-ground, hot spot, open circuit, and arc faults, are addressed using AI techniques [210–213]. Random Forest classifiers, LSTMs, and convolutional neural networks are commonly employed for fault classification and location detection [214, 215]. These techniques enhance fault detection accuracy, ensuring PV system reliability.

2.5.2 AI in energy management systems

In the context of energy management systems (EMS) aimed at improving efficiency and reducing electricity costs, AI, particularly reinforcement learning, has emerged as a significant solution [216]. Algorithms like Q-learning and Deep Q-Networks optimize energy consumption in various scenarios, leading to substantial cost savings of up to 45% [217]. Open environments like CityLearn facilitate standardization and better comparability among research developments, promoting experimentation in real EMS scenarios [218]. These solutions consider diverse state-spaces, reward functions, and objectives, thus improving EMS efficiency [219, 220].

2.5.3 AI in sizing methods

AI techniques optimize different aspects of PV systems, determining the ideal number of panels, battery capacity, and panel tilt and azimuth angles [221]. Artificial Neural Networks (ANNs), Recurrent Neural Networks (RNNs), and Convolutional Neural Networks (CNNs) size PV arrays and batteries, improving load loss estimation and geographic assessment [222, 223]. These techniques ensure PV system components are accurately sized for enhanced performance.

2.5.4 AI in control

AI techniques find application in microgrid control, specifically for Maximum Power Point Tracking (MPPT), and voltage and frequency control. They enhance power generation efficiency, particularly in partial shading conditions, when compared to traditional methods [224, 225]. Reinforcement learning, including Q-Learning and SARSA, demonstrates efficient voltage control in high-penetration PV distribution systems [226, 227]. However, the real-world applicability of these methods requires further investigation [228].

2.5.5 AI in forecasting

AI addresses solar irradiance and temperature variability, vital factors affecting PV energy production [35]. Techniques like ANNs, RNNs, LSTMs, and convolutional neural networks predict solar power output accurately [45, 229]. While considerable progress has been made, future research should focus on real-time model deployment for practical PV energy sector applications [8, 230, 231].

2.5.6 Challenges of AI in PV systems

In the context of PV system implementation and analysis, AI presents considerable potential but faces challenges, particularly in acquiring sufficient data for effective pattern recognition and automated learning [8]. Addressing these challenges necessitates the sharing of open datasets containing authentic PV system data, which would be of immense value to the research community [21]. Future research directions in this domain cover a range of promising avenues. Conducting more experimental tests using real-world testbeds, comparing various agent-critic reinforcement learning methods for MPPT. Exploring reinforcement learning techniques for both MPPT and voltage/frequency control simultaneously. Evaluating emerging techniques such as attention-based transformers for improved forecasting. Performing physical trials to assess newly proposed models for islanding detection. Studying the behavior of RL-based MPPT algorithms in the presence of faults to enhance fault detection and classification. Examining image recognition algorithms like vision transformers. Finally, advancing the deployment of ML models for real-time processing by integrating them into pipelines that leverage TinyML or EdgeAI, addressing the current research gap in real-time processing and decision-making [22, 232–237].

2.6 Problem statement

In recent years, significant advances have been made in the application of artificial intelligence to microgrid management. However, numerous challenges persist in the realm of alternative energy implementation and management [238]. Challenges such as the intricate issues of renewable energy variability, effective energy storage system management, and cost reduction [239, 240]. The persistence of these challenges has prompted the formulation of our central research question: **"How can artificial intelligence techniques be effectively employed to optimize the management of renewable energy systems, with a specific focus on solar photovoltaic energy and energy storage systems?"**

This thesis aims to provide a robust and innovative solution to address these pressing challenges, with a particular focus on photovoltaic systems. The proposed approach utilizes artificial intelligence techniques to introduce a pioneering dimension in renewable energy management. By applying artificial intelligence, we can predict future energy parameters with remarkable accuracy. For example, using historical data to predict solar

radiation patterns in specific regions allows informed decisions to be made for electricity management in microgrids. Moreover, artificial intelligence enables accurate control of energy flows and real-time monitoring of supply and demand dynamics, resulting in substantial energy savings. Beyond these benefits, the optimization of resource utilization in microgrids allows for reducing equipment costs, accounting for considerations such as equipment lifetime, aging, and maintenance costs.

The exploration and application of artificial intelligence techniques in this context promise to deliver an innovative analysis with far-reaching environmental and socio-economic implications. Notably, it holds the potential to provide sustainable energy solutions to remote communities, such as the non-interconnected zones prevalent in Colombia. Furthermore, this research contributes significantly to the body of knowledge concerning alternative energy management within microgrids, thereby paving the way for future research endeavors and energy solution projects, both in rural and urban settings.

As stated in the Introduction section, the overall objective of this thesis is to advance the field of renewable energy management through the development and application of AI techniques. Specifically, with a focus on improving the management of solar PV energy systems and optimizing the operation of batteries as energy storage systems. The specific objectives to achieve this general objective were also set out in the Introduction. The importance of each of these objectives is explained in detail below.

The first specific objective centers on the collection, validation, and comprehensive analysis of meteorological data to accurately assess photovoltaic potential. The data collection includes the incorporation of in-situ measurements, satellite-derived data, and climate change scenarios. We aim to establish a robust foundation for accurately assessing the photovoltaic potential in target regions. This objective is fundamental to harnessing the full potential of solar PV and the efficient use of resources within microgrids.

The second specific objective addresses the refinement of historical data quality. We intend to achieve this by implementing advanced site-adaptation techniques, harmonizing both in-situ and satellite-derived data. This process serves to bolster the accuracy of our solar irradiance forecasting models, enhanced through the integration of AI techniques. The success of this objective will allow early decisions in the management of microgrids.

The third specific objective addresses the integration of the improved solar irradiance forecasting model with optimized battery scheduling. This integration is the core of our research, as it addresses the dual challenge of reducing costs and avoiding battery

degradation. Our artificial intelligence-based approach aims to achieve an optimal balance between efficiently harnessing renewable energy and safeguarding the longevity of energy storage systems. By successfully achieving this goal, we not only promote economic viability within microgrids but also contribute to the sustainability and reliability of renewable energy solutions.

2.7 Conclusion

In this chapter, we have contextualized the environmental concerns that motivate our exploration of alternative methods for generating, managing, and consuming electrical energy. These methods hold the potential to significantly alleviate the strain on our ecosystems and mitigate the depletion of finite fossil resources. Our discussion began with a comprehensive overview of global renewable energy sources, with a particular focus on Colombia. Within this landscape, we introduced the concept of microgrids and elucidated their pivotal role in tackling the challenges posed by renewable energy integration. Of these renewable sources, we focused on PV energy, acknowledging its status as one of the most promising and rapidly expanding alternatives in recent years. Furthermore, we delved into the realm of AI techniques, analyzing their applicability to PV systems. Through a detailed examination, we uncovered the distinct advantages and obstacles associated with each element of our exploration, conducting a thorough analysis of their current status and identifying the research gaps that culminated in the formulation of our central research problem for this thesis.

The analysis of PV power potential, the impact of climate change on PV systems, and how to address these challenges through solar irradiance forecasting and microgrid management are challenges that need to be addressed. Assessing the potential of PV is critical for transitioning to sustainable energy sources, reducing dependence on fossil fuels, and mitigating climate change. Understanding the geographic distribution of solar energy resources and forecasting solar irradiation patterns are essential for optimizing PV system deployments and grid integration. A tool to analyze the PV potential of Colombia can help address these challenges. Climate change, with its potential to alter solar irradiance patterns, requires climate modeling and adaptation strategies to ensure the continued reliability of PV systems in a changing environment.

Incorporating PV systems into microgrids offers a robust solution for improving energy resilience and reducing carbon emissions. However, this integration poses challenges,

mainly related to the intermittency of solar power. Accurate forecasting of solar irradiance is emerging as a key tool to mitigate these challenges. In addition, ESSs play a key role in optimizing microgrids. ESSs make it possible to store surplus energy generated under favorable conditions and use it during periods of low generation, maximizing the use of renewable energies.

Chapter 3

Solar photovoltaic power potential

Abstract

Data collection is the heart of a solid analysis of solar photovoltaic power potential and for the application of artificial intelligence. To ensure accurate assessments of the reliability and feasibility of photovoltaic installations, it is necessary to analyze the historical patterns of solar irradiance and other meteorological variables. This analysis allows the need to identify trends, seasonal variations, and any irregularities that might affect energy production. Moreover, data collection is crucial for forecasting future solar energy potential. By gathering meteorological data, including in-situ measurements and satellite information, we gain insights into the prevailing weather conditions. These different types of data constitute the base of knowledge for developing artificial intelligence predictive models able to estimate solar irradiance for different time frames, ranging from hours to decades ahead. These forecast models are essential for optimizing energy management systems and grid integration. This chapter introduces the process of collecting and analyzing meteorological data to assess the photovoltaic potential. In this context, we present the Colombian Solar Atlas which is an interactive tool designed to help users estimate potential photovoltaic production in any location of the country. The Colombian Solar Atlas is designed to accommodate users of all levels, from beginners to advanced. This tool is the first open interactive online tool particularly adapted to study the photovoltaic power potential in Colombia, considering the needs of the country and native language. Together with a team composed of my advisors, master's and undergraduate students, I led the design and implementation of this tool. The chapter also introduces an analysis of the possible impact of climate change on the photovoltaic

power potential in South America. The outcomes regarding photovoltaic potential in Colombia have been published in the international journal Big Earth Data, in the article "An interactive tool for visualization and prediction of solar radiation and photovoltaic generation in Colombia"[48]. Part of the work of the Colombian Solar Atlas has been carried out within the framework of the *"Cooperación Triangular: Estudio de concepto de exploradores de potencial energético solar y de biomasa"* project. The findings of the impact of climate change on the photovoltaic power potential have been published in the international journal Environmental Research Communications, in the paper "Climate change impact on photovoltaic power potential in South America" [47], and in the international journal Heliyon, under the paper "The impact of climate change on photovoltaic power potential in Southwestern Colombia" [46].

Table of Contents

3.1 Introduction

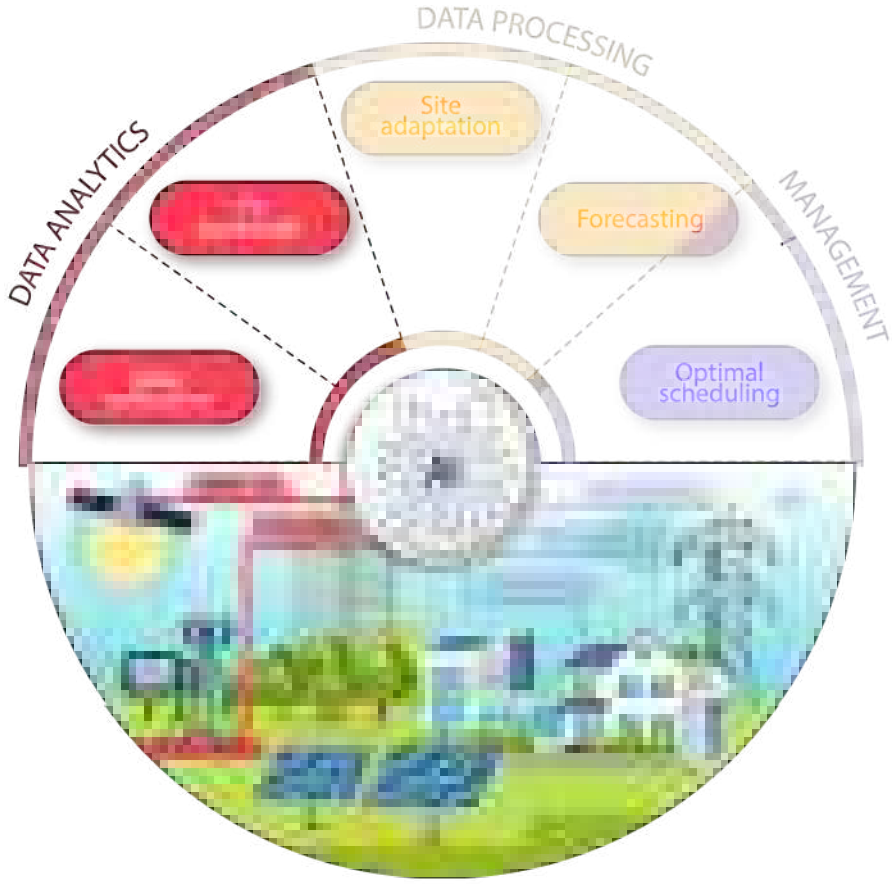

FIGURE 3.1: **Graphical Abstract of Chapter 3:** The first step involves data collection from various meteorological databases to evaluate the photovoltaic power potential.

Quality of data collection is crucial in the analysis of PV power potential. Accurate data sets including solar radiation, temperature, wind speed, and geographic data are essential to estimate PV generation with good precision. During system design, the data collected is used to make critical decisions such as panel orientation and sizing, ensuring both energy efficiency and cost-effectiveness [241]. Furthermore, the data supports the assessment of solar resource potential in specific regions, helping to make investment decisions. This assessment can be used by governments and institutions to develop policies and incentives that promote renewable energy adoption [242]. An accurate database is therefore required for precise analysis of PV power potential. This analysis is critical in the global shift towards renewable energy, as it contributes to greenhouse gas reduction, climate change mitigation, and sustainability efforts [91]. PV power potential also plays a critical role in optimizing system design, ensuring reliable grid integration, facilitating

effective policy development, and promoting environmentally responsible clean energy management [243].

Historical meteorological data is usually acquired from in-situ weather stations and satellite data. In-situ weather stations provide accurate and location-specific meteorological data but can have missing data, and they may not be available in remote areas. On the other hand, satellite data offers global coverage and historical records but may have limited spatial resolution and can be affected by cloud cover [244]. Therefore, satellite data are widely used to gain an overview of the PV potential [245]. However, for more detailed analysis, in-situ data is usually utilized, or a combination of the two databases can be combined using site-adaptation techniques [45].

Even though renewable energies are critical in the fight against climate change, some studies have found that climate change can have an impact on the performance of renewable energies, particularly PV, which is directly dependent on solar radiation. Therefore, determining the potential impact of climate change on PV performance is critical. To assess this impact, it is necessary to collect databases of different climate scenarios, providing insights into potential future PV outcomes [46, 47, 201].

Furthermore, the quantity and quality of databases form the foundation for artificial intelligence models [246], which have seen widespread application in recent years for enhancing the efficiency of renewable energy systems [247]. AI technologies enable the prediction of various scenarios, including PV production across different time frames, ensuring reliable energy supply for consumers, and establishing optimal conditions for energy storage systems [8].

This chapter presents the collection and cleaning of the databases used in this thesis, including in-situ measurements, satellite data, and climate change scenarios. Then, the PV power potential is formulated, and an interactive tool for assessing PV power in Colombia is introduced. Additionally, the chapter explores the potential influence of climate change on PV power potential in South America, as shown in Figure 3.1. The databases presented here are subsequently used in Chapters 4 and 5 for the application of artificial intelligence techniques to optimize microgrid management.

3.2 Data collection

In this section, we present the collected databases needed for our model. The origins include in-situ measurements from the Colombian Institute of Hydrology, Meteorology, and

Environmental Studies (IDEAM) [248] and satellite data from the National Solar Radiation Database (NSRDB) [41]. To take into account climate change, we used two climate change models from the Coordinated Regional Downscaling Experiment (CORDEX) [42].

3.2.1 In-situ data

The in-situ database for Colombia corresponds to IDEAM weather stations. [248]. This is an open-access database. The variables collected are GHI, temperature, and wind speed from a total of 116 (Figure 3.2 (a)), 256 (Figure 3.2 (b)), and 152 (Figure 3.2 (c)) stations respectively, between the years 1998–2019. During that time interval, some stations suspended measurements while others started them, so not all the stations had the full data at the complete time interval. The GHI and wind speed variables are measured every hour, while temperature is measured three times a day (7 a.m., 1 p.m., 7 p.m.).

3.2.2 Satellite data

We use historical data from the National Solar Radiation Database (NSRDB) [41]. This database includes meteorological data such as global horizontal irradiance (GHI), direct normal irradiance (DNI), diffuse horizontal irradiance (DHI), temperature, and wind speed. The latest version of the database offers gridded data from 1998 to 2019, with a spatial resolution of 4 Km $\times$ 4 Km and a temporal resolution of 30 minutes, generated using a physical solar model (PSM). This model computes solar irradiance from different satellite data sources, specifically by measuring aerosol, water vapor, and other meteorological properties, combined with satellite-derived cloud properties in the Fast All-sky Radiation Model for Solar applications (FARMS) [249].

Since NSRDB uses a two-step physical model, different satellites are required to extract data. Figure 3.3 shows a flowchart of the two-step PSM employed to calculate solar irradiance from satellite data. NSRDB utilizes data from the Geostationary Operational Environmental Satellite (GEOES) and Advanced Very High-Resolution Radiometer (AVHRR), both developed by the National Oceanic and Atmospheric Administration (NOAA), which retrieve cloud products at 4 Km $\times$ 4 Km resolution every 30 minutes. The PSM has used this information to produce cloud-sky solar irradiance since 1998.

Based on monthly data from the Moderate Resolution Imaging Spectroradiometer (MODIS) and the Modern-Era Retrospective Analysis for Research and Applications version 2

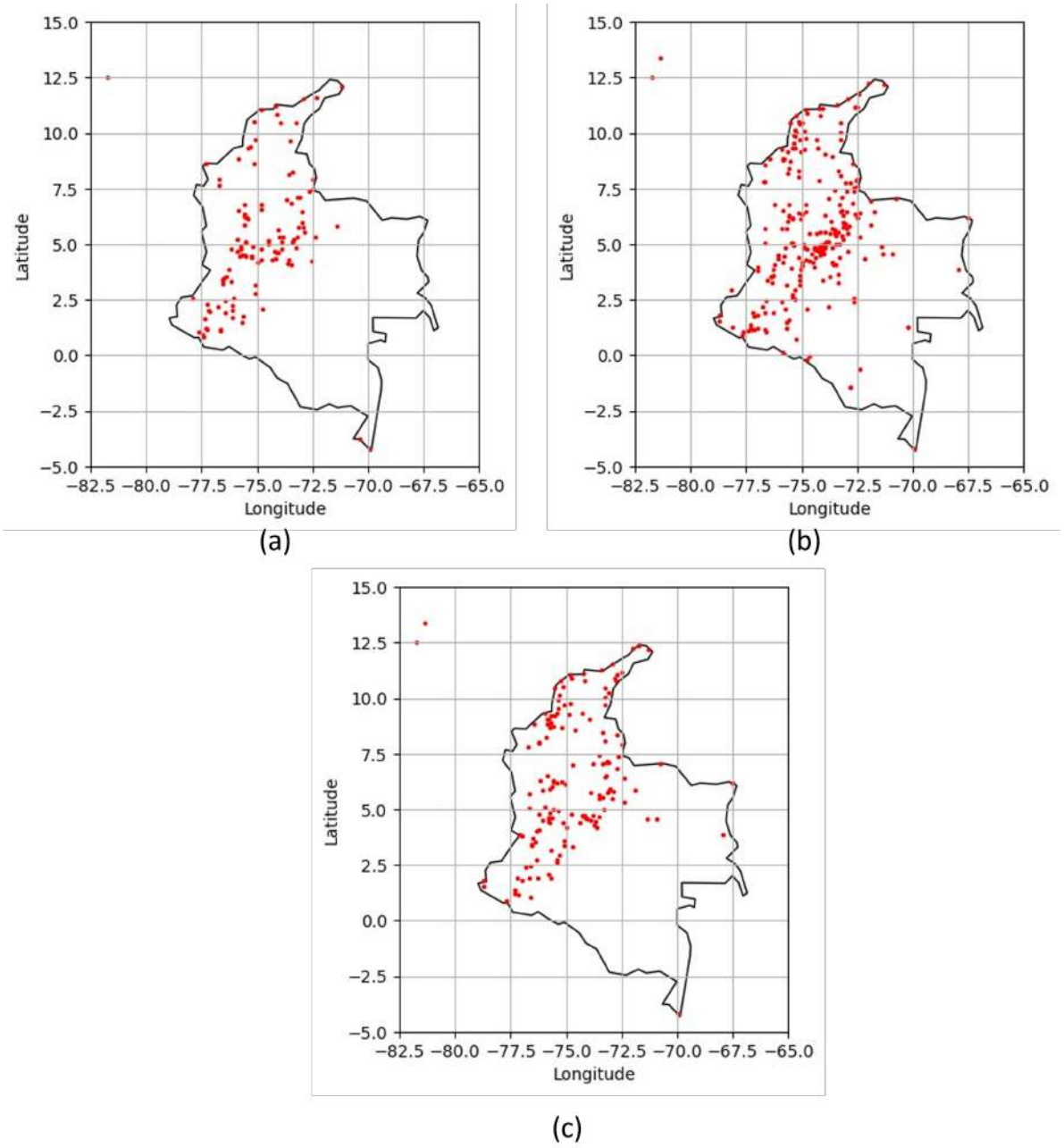

FIGURE 3.2: IDEAM in-situ stations spatially located along the Colombian territory collecting data for (a) GHI, (b) temperature, and (c) wind speed variables.

(MERRA-2) aerosol dataset, the PSM uses aerosol optical depth (AOD) information. In arid areas, such as the southern and western United States and northern Mexico, AOD is obtained through an optimal linear combination of data from the MERRA-2 and MODIS satellites. When MODIS data is unavailable, only MERRA-2 data is used. On the other hand, in vegetation or urban areas like the eastern and northern United States, Canada, southern Mexico, and Central America, AOD is determined exclusively using MERRA-2

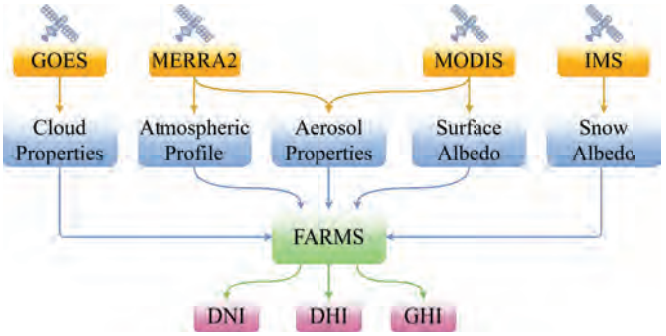

FIGURE 3.3: Flowchart of the NSRDB Physical Solar Model (PSM)

data. This choice is made because MERRA-2 has similar accuracy to MODIS, which occasionally presents unavailable data [41].

NSRDB provides the atmospheric and land properties, such as the atmospheric profile, wind direction and speed, snow depth, surface temperature, and pressure. These properties are based on data from the MERRA-2 dataset. Meanwhile, MODIS provides the surface albedo, and the snow albedo is provided by the Interactive Multisensor Snow and Ice Mapping System (IMS). FARMS collects all of this data and uses it to calculate GHI, DNI, and DHI. The solar irradiance data with other meteorological properties such as temperature, wind speed, and solar zenith angle are utilized to implement the Colombian Solar Atlas.

Particularly for Colombia, NSRDB defined 62,187 coordinates using the same spatial resolution provided by the NSRDB, obtaining half-hourly data from 1998 to 2019 for GHI, DNI, DHI, wind speed, surface temperature, and solar zenith angle. It is important to note that, even if the NSRDB database was validated using surface observations in several sites in the United States, validation has been very limited in Colombia, with similar work done only at a single coordinate, as shown in [8, 45]. Because of this lack of validation, the Colombian Solar Atlas is explicitly presented as an initial estimate of solar irradiance in the country. Therefore, users are advised to be cautious regarding possible inaccuracies in the values.

3.2.3 Climate change models

CORDEX-Coordinated Output for Regional Evaluations (CORE), offers detailed regional climate model (RCM) projections [204]. It may be useful to discuss about different results of our model if it takes into account a series of scenarios for the future to determine the pertinence of our forecasting tool. For South America, the CORE project

TABLE 3.1: Overview of the analyzed CORDEX-CORE experiments. Each experiment has one historical and two scenarios (RCP2.6 and RCP8.5), spanning the periods 1970-2005 and 2070-2099 respectively. The horizontal resolution of all simulations is 0.22º in both latitude and longitude.

	RCM	
Forcing GCM run	GERICS-REMO2015	ICTP-RegCM4-7
MOHC-HadGEM2-ES	✓	✓
MPI-M-MPI-ESM-LR	✓	
MPI-M-MPI-ESM-MR		✓
NCC-NorESM1-M	✓	✓

utilized two RCMs to downscale four global climate models (GCMs) under two distinct climate scenarios. The available GCM and RCM models for the region are listed in Table 3.1 [250].

Several studies have assessed the accuracy of CORDEX-CORE models [251–253]. These models are designed based on representative concentration pathways (RCPs), which estimate various greenhouse gas emission scenarios. The RCP2.6 scenario portrays an optimistic outlook, aiming to limit the global mean temperature increase to a maximum of 2° by the end of the century. Achieving this goal requires a substantial adoption of renewable energy sources and a significant reduction in fossil fuel usage. Conversely, the RCP8.5 scenario represents a worst-case scenario, anticipating a maximum global mean temperature rise of 4.3° by the end of the century. This pessimistic scenario assumes a continuous increase in greenhouse gas emissions, low adoption of renewable energy sources, and extensive reliance on fossil fuels and coal.

Table 3.2 provides an overview of the model-specific schemes utilized for the physical parameterization of each RCM model, along with the corresponding references.

3.3 Photovoltaic power potential

This section introduces the Colombian Solar Atlas, which is an interactive tool we had designed for analyzing the PV potential in the country. The formulation of the PV generation models is fully explained in the Appendix, Section .1.

Over the last few years, several tools have been developed with the aim of collecting data and enabling users to analyze the PV power potential. One of the main tools is provided by NSRDB, which includes a data viewer tool offering worldwide meteorological data, multiple base maps, and accessible spatial layers through a website [284].

Table 3.2: Model-specific schemes for the physical parameterization of the RCP models.

GERICS-REMO2015	**ICTP-RegCM4-7**
Radiation [254, 255]	Radiation [256, 257]
Snow-free land surface albedo [258]	Land surface [259, 260]
Vertical diffusion and surface fluxes [261]	Pressure gradient [262]
Soil processes heat transfer [263]	Convective precipitation [264–267]
Cumulus convection [268, 269]	Large-scale precipitation [270]
Fractional surface cover [271]	Prognostic sea surface skin temperature [272]
Stratiform clouds [273, 274]	Aerosols and dust [275, 276]
Monthly variation of vegetation parameters [258]	Cloud microphysics [277–279]
Freezing and thawing of soil water [271]	Planetary boundary layer [280, 281]
	Lake model [282]
	Ocean flux [283]

On a continent-scale, different organizations have created different solar atlases. PVGIS was developed by the European Commission Joint Research Centre. The PVGIS Atlas [285] uses different datasets, such as SARAH, which has been calculated by The Satellite Application Facility on Climate Monitoring (CM SAF), NSRDB, in collaboration with National Renewable Energy Laboratory (NREL), and ERA5, a new reanalysis product from the European Centre for Medium-Range Weather Forecasts (ECMWF). SARAH data covers Europe, Africa, and most of Asia, NSRDB covers North and Central America, and ERA5 is available only for Europe. The data provided by this atlas corresponds to the years 2005 to 2015 [286]. PVGIS atlas calculates the performance of a custom PV system, allowing users to enter different values regarding the solar panel for various panel configurations. Even though it allows users to obtain the monthly average for GHI, DNI, DHI, temperature, and hourly solar irradiance [245], the heat map only shows the average solar irradiance.

Another atlas on a continent-scale is the Global Solar Atlas, developed by The World Bank and the International Finance Corporation to support the scale-up of solar power in different countries. The main purpose of this atlas is to provide quick access to potential PV data, and global solar resources [287], allowing countries and communities to transform their energy infrastructure and accelerate their transition to low-carbon energy sources [288]. This atlas uses information obtained through SOLARGIS, a paid platform that provides meteorological data for solar energy investments. SOLARGIS is specially focused on project development and operational projects. Unfortunately, this dataset does not contain information for all parts of the world [289].

The Global Solar Atlas has different functions related to the visualization of solar variables and the estimation of PV power potential through interactive maps. It provides annual average values for PV power output, DNI, GHI, DHI, global tilted irradiance at an optimum angle, an optimum tilt of PV modules, air temperature, and terrain elevation. Users can select a point on the map or search for a specific location. The atlas also has a PV energy yield calculator, allowing users to calculate the long-term energy yield for a customized PV system. The atlas shows daily and annual averages of estimated PV production. Users have the option to download an image of a heat map for a specific region or country, depicting the GHI, DNI, and PV power potential [290]. However, it is not possible to select a particular year for data display.

On a country scale, the University of Chile, in partnership with the Chilean government, has developed one of the most complete databases and tools [52]. The Chilean Ministry of Energy developed several tools in an effort to provide an accessible and free way of analyzing Chile's renewable resources. In particular, The Solar Explorer [291] is a website that provides an interactive map in which a user can select a specific point and visualize data such as solar irradiance, cloudiness, ambient temperature, wind speed, and elevation. This tool also includes a photovoltaic generation simulator, which allows the user to calculate the electricity generation of a photovoltaic system as if it were installed at a specific point. All data can be visualized in graphs that display the daily and annual averages of photovoltaic generation and other meteorological variables. The user can compare two graphs from different points simultaneously. The database provides hourly data from 2004 to 2016 at a spatial resolution of 90 meters. It uses cloud detection and characterization methods based on data from the GOES EAST satellite, as well as transfer models such as NASA's CLIRAD-SW, to estimate the clear sky solar irradiance.

Finally, the IDEAM developed the Solar, Ultraviolet, and Ozone Radiation Atlas. This tool provides a set of maps representing the monthly and yearly distribution of global horizontal irradiance, sunshine duration, number of days without sunshine, ultraviolet radiation, total ozone, and regional analysis of the annual average behavior for each variable in the year 2015. The data is measured from 230 global irradiance sensors, and 497 sunshine sensors [292]. This tool only has information for some of the main cities in Colombia in 2015 and does not include data for other meteorological variables such as wind speed or ambient temperature.

Our Colombian Solar Atlas, created during this PhD, attempts to combine the best elements of the other atlases presented in the literature to obtain a robust tool to assess the PV power potential throughout the entire Colombian territory. Table 3.3 compares

	PVGIS	Global Solar Atlas	Chilean Atlas	IDEAM Atlas	**Proposed Colombian Solar Atlas**
Datasets used	ERA5, NSRDB, SARAH	SOLAR-GIS	GOES EAST	In-situ data	NSRDB and CORDEX
Analyzed time period	2005–2015	1994–2020	2004–2016	2015	1998–2019 and 2070–2099
Visualize different heat maps		✓		✓	✓
Allows to download information	✓	✓	✓	✓	✓
Allows to calculate PV potential for different models	✓		✓		✓
Shows meteorological variables	✓	✓	✓		✓
Allows the user to choose different years	✓				✓
Shows maps for climate change scenarios					✓

TABLE 3.3: Comparison between other atlases and the Colombian Solar Atlas.

the different atlases found in the literature with our proposed interactive tool. Our proposed Solar Atlas is the only atlas in Colombia that contains all the features listed in Table 3.3. Details on our interactive tool design will be provided in the following sections

3.3.1 Validation Methodology

In the following subsections, we describe our Colombian Solar Atlas with historical data. This Colombian Solar Atlas also includes the same functionalities for assessing PV potential based on climate change scenarios. The Atlas with climate change scenarios is presented in the Appendix section .2. As previously mentioned, the data obtained from NSRDB consist of six variables with a temporal resolution of 30 minutes for the period 1998 to 2019, and cover 62,187 points defined in a 4 Km $\times$ 4 Km grid in Colombia [35]. To validate the satellite data, we compare the NSRDB database against the available in-situ data from the IDEAM. The time resolution differs between the two databases. For the in-situ database, GHI and wind speed were collected hourly, while three measurements per day were available for temperature stations. The data validation process involved a pre-processing stage to clean the in-situ data, an adjustment of time-spatial resolution, and a bias correction process, as described below.

3.3.1.1 Clean In-Situ Data

This process consists of removing not-a-number (NaN) values, negative values, and constant values that persist throughout the day [293]. After that, we used an outlier detection process to identify incorrect measurements that could have been missed during the data-cleaning process. Due to the potential drastic changes in climate conditions at each station, we conducted data analysis on a yearly basis for each station within the Colombian territory. We used the Local Outlier Factor method, which estimates the

local deviation of the density of a given sample for its neighbors [294]. We considered a total of 30 neighboring samples for the analysis of each meteorological variable.

3.3.1.2 Time-spatial resolution adjustment

The spatial resolution for the satellite data is 4 Km × 4 Km along the Colombian territory [41]. In most cases, the spatial location of in-situ data does not match the spatial location of a satellite measurement. Hence, to make satellite and in-situ data comparable, we estimated the variable from satellite, denoted by $\hat{y}_i$, for every in-situ station i. The sample $\hat{y}_i$ is computed as the weighted sum of the four nearest satellite measurements y_j as

$$\hat{y}_i = \sum_j w_{ij} y_j, \quad \sum_j w_{ij} = 1, \quad w_{ij} > 0. \tag{3.1}$$

The constant w_{ij} scales measurement y_j to compute $\hat{y}_i$ and it is defined as

$$w_{ij} = \frac{1/d_{ij}}{\sum_k 1/d_{ik}}, \tag{3.2}$$

where d_{ij} is the Euclidean distance between locations i and j. Thus, the weighted average of the measurement will be closer to the measurement of the closest locations. Satellite data are reported in a half-hourly time resolution for all meteorological variables. Therefore, for the in-situ data, we take only the satellite measures in their corresponding time resolution. Nevertheless, some additional pretreatments are needed to obtain equivalent satellite databases.

3.3.1.3 Bias Correction

We used Quantile Mapping (QM) to correct the bias in the satellite data using in-situ data. This technique is widely used to transform the distribution function of a modeled variable to match the distribution function of an observed one [295–297], which can be mathematically expressed as

$$\hat{x}_m = f_o^{-1}[f_m(x_m)], \tag{3.3}$$

where $\hat{x}_m$ is the corrected variable, x_m represents the modeled variable, f_o^{-1} is the inverse of the cumulative distribution function (CDF) of the observed variable, and f_m is the CDF of the modeled variable.

3.3.1.4 Validation Metrics

The metrics used in the validation process include the root mean squared error (RMSE), the mean bias error (MBE), and the Pearson correlation coefficient (ρ) as shown in the following equations (3.4), (3.5), and (3.6):

$$RMSE = \sqrt{\frac{1}{N}\sum_{i=1}^{N}(x_i - \hat{y}_i)^2}, \tag{3.4}$$

$$MBE = \frac{1}{N}\sum_{i=1}^{N}(x_i - \hat{y}_i), \tag{3.5}$$

$$\rho = \frac{cov(x_i,\ \hat{y}_i)}{\sigma_{x_i}\sigma_{\hat{y}_i}}, \tag{3.6}$$

where x_i and $\hat{y}_i$ are the in-situ and (pre-processed) satellite measurements. $cov()$ and σ refer to the covariance and standard deviation. The RMSE and the MBE allow us to quantify the difference between the satellite and the in-situ data, and ρ allows us to validate the presence of a linear correlation between the satellite and the in-situ data. Additionally, we computed the relative RMSE (rRMSE).

$$rRMSE = \sqrt{\frac{\frac{1}{N}\sum_{i=1}^{N}(x_i - \hat{y}_i)^2}{\sum_{i=1}^{N}(\hat{y}_i)^2}}, \tag{3.7}$$

and the relative MBE (rMBE)

$$rMBE = \frac{\frac{1}{N}\sum_{i=1}^{N}(x_i - \hat{y}_i)}{\sum_{i=1}^{N}(\hat{y}_i)^2}, \tag{3.8}$$

by normalizing the error values with the in-situ data [293]. All these indicators are used to evaluate progressively our model.

3.3.1.5 Validation results

Tables 3.4 and 3.5 show the indicators calculated for three meteorological variables GHI, temperature, and wind speed, before and after the bias correction, respectively. We observe that the Pearson correlation coefficient ρ is still the same after the bias correction. This result ensures that QC only corrects the bias and does not affect the linear distribution of the data. Moreover, in Figures 3.4(b), 3.4(d), and 3.4(f) we can observe how

	GHI [W/m²]	Temperature [°C]	Wind Speed [m/s]
RMSE	116.43 ± 11.92	2.61 ± 0.84	1.85 ± 0.52
%rRMSE	12.07 ± 1.69	24.01 ± 14.15	31.95 ± 15.46
MBE	-25.50 ± 14.37	0.54 ± 1.42	0.75 ± 0.74
%rMBE	-2.72 ± 1.66	5.72 ± 17.26	11.93 ± 19.24
ρ	0.91 ± 0.01	0.75 ± 0.09	0.31 ± 0.17

TABLE 3.4: Results of the satellite data validation with IDEAM in-situ data before bias correction.

	GHI [W/m²]	Temperature [°C]	Wind Speed [m/s]
RMSE	105.28 ± 12.05	2.02 ± 0.46	1.43 ± 0.38
%rRMSE	10.84 ± 1.19	17.96 ± 6.33	24.08 ± 6.03
MBE	-0.60 ± 1.11	-0.02 ± 0.41	0.21 ± 0.19
%rMBE	-0.06 ± 0.12	-0.31 ± 5.26	2.94 ± 3.46
ρ	0.91 ± 0.02	0.75 ± 0.10	0.31 ± 0.17

TABLE 3.5: Results of the satellite data validation with IDEAM in-situ data after bias correction.

QC corrects the bias of the satellite data and its relationship with the results presented in Table 3.4 and Table 3.5. After the bias correction, the MBE and rMBE values for the climate variables drop drastically.

The results for ρ show a high linear correlation between GHI and Temperature, with 0.912, and 0.748, respectively. Additionally, it is evident via the rRMSE values respectively for GHI, temperature, and wind speed, that the satellite data do not differ by more than 11%, 18%, and 24%, compared to the in-situ data. These results are summarized in Table 3.5.

3.3.2 Data visualization

The interactive tool contains three main components: interactive maps, variable graphs, and a photovoltaic generation calculator. In general, users can select a specific point on the map to explore, which visualizes summary averages for each variable and provides several graphs describing their behavior from 1998 to 2019. Additionally, users have the option to calculate the PV generation of a system by providing technical information about it. In this subsection, we explain the interactive maps. Each map represents data for a single year and one of five meteorological variables. The photovoltaic generation calculator is explained in the next section named Section 3.3.3. In addition, the Appendix section .1 gives more details with various types of graphs that can be displayed in the

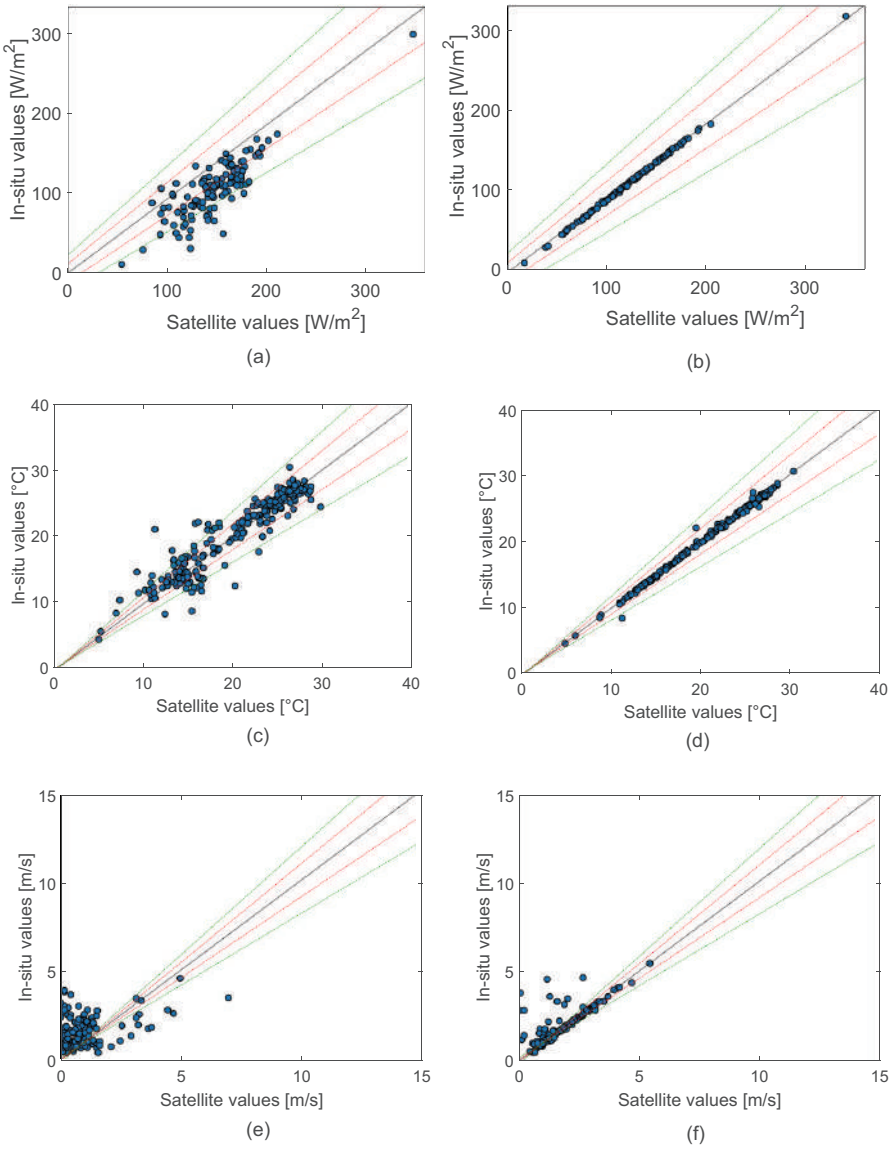

FIGURE 3.4: Satellite (x-axis) vs. in-situ (y-axis) averages for GHI (a)(b), temperature (c)(d), and (e)(f) wind speed variables before (left column) and after (right column) bias correction from the period between 1998–2019. Red and green lines represent the 10% and 20% of difference, respectively.

Colombian Solar Atlas. Each graph can be generated for GHI, DHI, DNI, temperature, and wind speed. For each meteorological variable, different averages can be selected, including hourly, daily, monthly, and annual averages.

The Colombian Solar Atlas has a map for GHI, DHI, DNI, wind speed, and temperature available for each year in the period 1998 to 2019. Each map contains the yearly averages of all points, representing the value of the selected variable with a color scale (dark blue

for the lowest value and red for the highest). The available maps are shown in Figure 3.5.

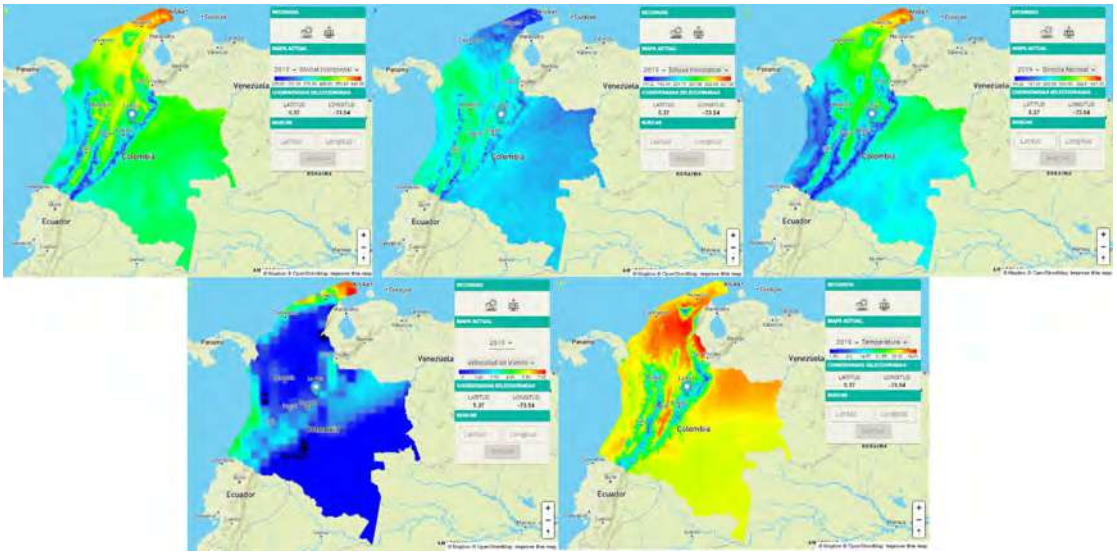

FIGURE 3.5: Available maps (from left to right and top to bottom): GHI, DHI, DNI, wind Speed, and temperature.

On the left side of the map, there is a summary of latitude, longitude, elevation, and yearly averages of the meteorological variables. Within this panel, users can access to historical graphs and download the chosen averages for the selected coordinates. Users can also change the current map and access to the photovoltaic generation calculator on the right side.

3.3.3 Photovoltaic generation models

Different models have been developed to estimate PV power production. The most commonly used methods for estimating PV production are the empirical correlation method, the analytical accounting method, and the detailed simulation method [298].

Empirical correlation methods for estimating solar PV potential are based on a comparison of the project in question with similar existing plants in nearby locations. This approach lacks precision, as it does not consider the unique characteristics of each individual plant. Some studies have even revealed substantial differences in energy production between PV installations in proximity. However, this method can be valuable for large-scale assessments, as it provides rough but reliable estimates of the average solar PV potential, especially when a detailed description of the technology and site-specific factors is not required [299].

Analytical accounting methods use mathematical equations to assess plant performance. The core formula calculates electric energy generated, considering performance ratio (PR), nominal power, total solar irradiation, and solar irradiance in standard test conditions. It can be shown that PR is a sensitive criteria, summarizing deviations from standard conditions, equipment losses, and external factors. The empirical coefficients to be set in these methods, depending on the different PV technologies, influence the accuracy of the model [300].

Various computer simulation models have been created to assess the potential and efficiency of PV systems. The choice of model determines its pertinence on a precise objective with different degrees of complexity. Indeed, the level of physical detail and description available is the main criteria of choice but also it is important to know if it includes system output, peak and annual efficiencies, the cost of electricity over time, capital investment, and operating and maintenance expenses. These models vary from freely available software to licensed versions, catering to both advanced users and non-specialists [301, 302].

In our case, we aim to offer a tool that is free accessible to everyone, and requires no specific expertise. However, it also caters to experts in the field, enabling them to conduct more in-depth studies of PV potential according to different technologies. Therefore, we use a basic generation model and an advanced generation model. These are analytical models based on references [303–307]. These models are described in detail in the Appendix section .1.

3.4 Impact of climate change on PV potential

To assess the impact of climate change on PV potential in South America, we compare the difference in PV power potential between the reference period (1970-1999) and the estimated PV power potential at the end of the century (2070-2099), following the formulation presented in [46, 201, 308, 309]. We considered the periods 1970-1999 and 2070-2099 to align with the 30-year life cycle of the Si crystalline PV modules [310]. The formulation of the PV power potential is fully described in the Appendix section .3.

3.4.1 Change in solar irradiance and its influence on PV power potential

Surface-downwelling shortwave radiation (RSDS) represents the amount of energy that reaches the Earth's surface from the sun in watts per square meter. Fig. 3.6(a) and Fig. 3.6(b) show changes in RSDS between the historical reference period (1970-1999) and the projected end of the century period (2070-2099) according to the RCP2.6 scenario, and their effect on PV power potential in South America, respectively. The southern part of the sub-continent shows no significant changes. In contrast, the northern part experiences a general increase of approximately $30W/m^2$ in most areas, with a maximum increase of $64W/m^2$ in northern Colombia. However, some regions, particularly western Ecuador, experience a decrease in solar irradiance of around $30W/m^2$. The most substantial decrease is observed in southern Peru, with a value of $112W/m^2$. This decrease is much larger than the next largest decrease (Bolivia with $42W/m^2$) and the average decrease for each country ($36W/m^2$). Such large changes in irradiance levels should be treated with caution, as they seem to be outliers. Therefore, combining the accuracy of historical data with current in-situ measurements, as well as improving this database with the site-adaptation techniques proposed in [8, 45], would be of great value. These variations in solar irradiance may cause a maximum decrease in PV potential of 12% in southern Peru, western Ecuador, and some coastal regions of northeastern Brazil (as shown in blue on the map). However, an increase of up to 6% is observed in the northern region (as shown in red on the map), and on average, the sub-continent shows an increase of $8W/m^2$, resulting in an expected increase of 0.6% on PV_{pot} across the sub-continent.

The effects on RSDS and PV power potential in South America, according to the RCP8.5 scenario, are shown in Fig. 3.6(c) and Fig. 3.6(d), respectively. Solar irradiance generally increases by over $30W/m^2$ in the northern region of the sub-continent, with a maximum increase of $74W/m^2$ in northern Colombia. Some coastal areas, especially in Ecuador, present a reduction in solar irradiance of around $30W/m^2$. Similar to the previous scenario, the greatest decrease is observed in southern Peru, with a reduction of $130W/m^2$. On average, the sub-continent shows an increase of $11W/m^2$ in solar irradiance. According to this scenario, variations in solar irradiance could lead to a maximum decrease of 15% on PV power potential (indicated by blue regions on the map), while an increase of up to 7% is observed in the northern region (indicated by red regions on the map). On average, there is an expected increase of 1% in PV_{pot} across the sub-continent due to an average increase of $11.3W/m^2$ in solar irradiance.

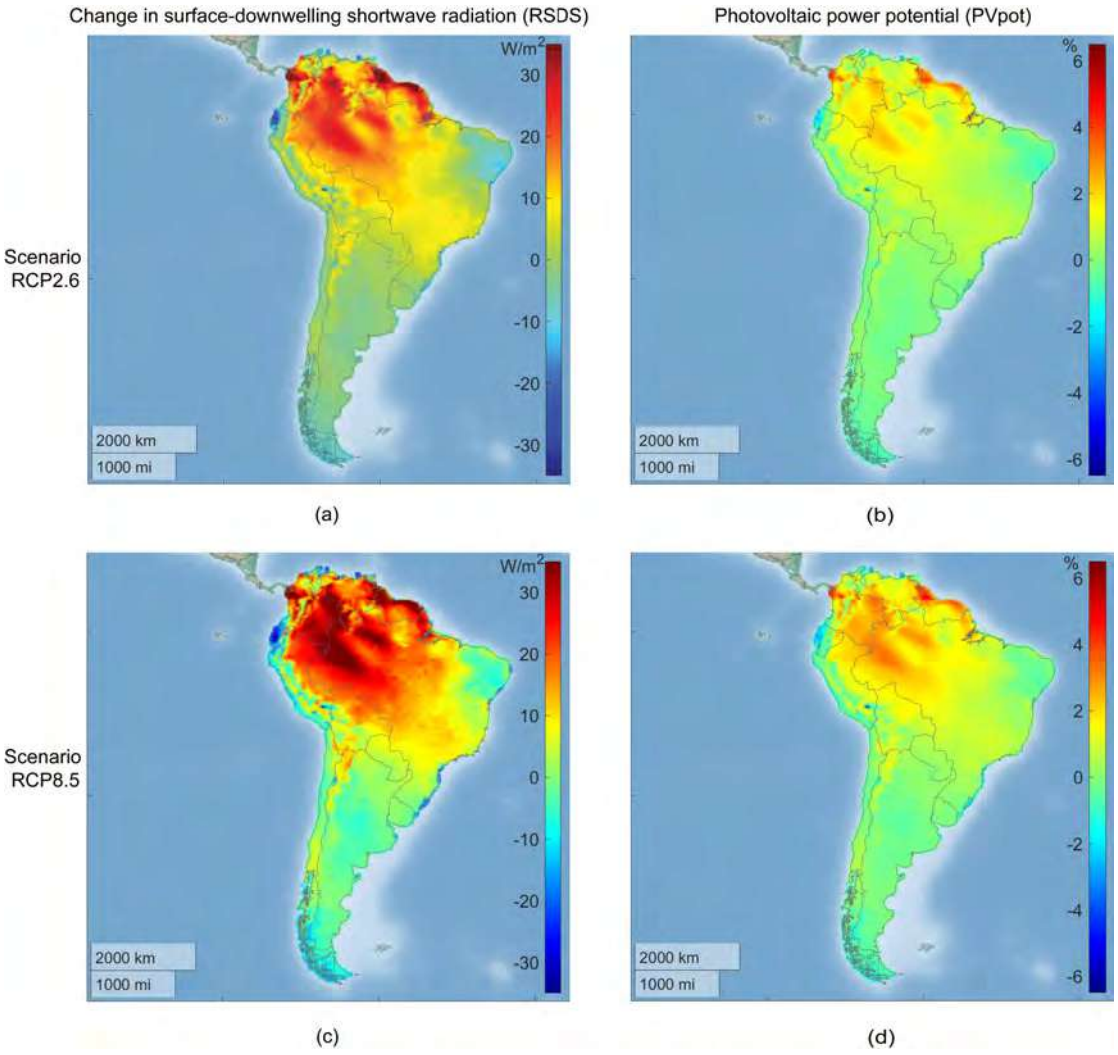

FIGURE 3.6: **Solar irradiance change analysis.** The left column compares the change in solar irradiance, in Watts per square meter, between the end of the century (2070-2099) and the reference period (1970-1999). The right column represents the respective change in PV power potential as a percentage. In particular, it shows (a) changes in RSDS with RCP2.6, (b) PV_{pot} with RCP2.6, (c) changes in RSDS with RCP8.5, and (d) PV_{pot} with RCP8.5. The plots were generated in Matlab.

3.4.2 Change in temperature and its influence on PV power potential

The effects on surface air temperature (TAS) and PV power potential in South America, according to the RCP2.6 scenario, are shown in Fig. 3.7(a) and Fig. 3.7(b), respectively. There is a general increase in air temperature, especially in the northern part of the sub-continent, with a rise of approximately 2° and a maximum increase of 7° on the border between Bolivia, Chile, and Argentina. In the southern part of the sub-continent, the temperature increase is around 1°. However, the results indicate a decrease of 4° in a small area on the northern coast of Chile. The average temperature rise for the

entire sub-continent is 1.4°. These changes can affect PV power potential, resulting in a 1% decrease in PV cell performance in warmer locations and an average reduction of 0.15% across the sub-continent. It is worth remembering that according to the RCP 2.6 scenario, a global temperature increase of about 2° is expected by the end of 2100.

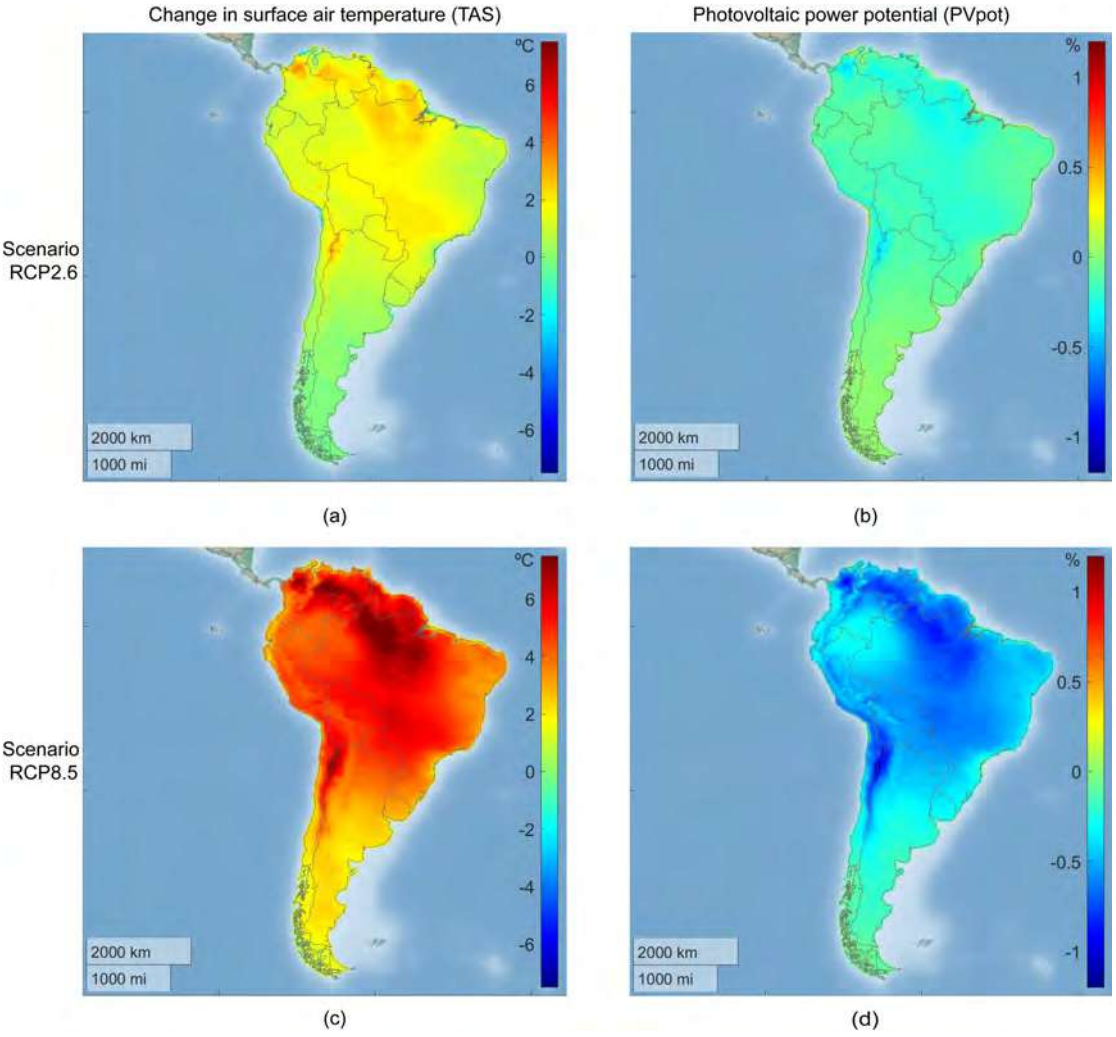

FIGURE 3.7: **Temperature change analysis.** The left column compares the change in temperature (in Celsius) between the end of the century (2070-2099) and the reference period (1970-1999). The right column represents the respective change in PV power potential as a percentage. In particular, changes in (a) TAS with RCP2.6, (b) PV_{pot} with RCP2.6, (c) TAS with RCP8.5, and (d) PV_{pot} with RCP8.5. The plots were generated in Matlab.

Fig. 3.7(c) and Fig. 3.7(d) present the effects of changes in air temperature and PV power potential based on the RCP8.5 scenario. In this scenario, the changes are more notable than in the case of RCP2.6, with a maximum temperature increase of 11.3° and a maximum temperature decrease of 1.9°. The region most affected by these changes is the northwest of South America, where a decrease in PV power potential of up to 1.8%

is observed. On average, the temperature across the entire sub-continent rises by 4.6°, resulting in an average decrease of 0.5% in PV power potential.

3.4.3 Change in wind speed and its influence on PV power potential

Fig. 3.8(a) and Fig. 3.8(b) show, according to the RCP2.6 scenario, the projected changes in wind speed and their effects on PV potential, respectively. In general, wind speed changes range from $-1.5m/s$ to $1.3m/s$. These changes have a practically negligible impact on PV power potential, with variations between -0.28% and 0.26%.

For the RCP8.5 scenario, the results are presented in Fig. 3.8(c) and Fig. 3.8(d). In this scenario, changes in wind speed range from $-1.3m/s$ to $1.95m/s$, which may affect the PV power potential between -0.28% and 0.43%. These results demonstrate the slight impact of wind speed on the PV power potential and are in accordance with other results presented in the literature [201, 309, 311–313].

3.4.4 Analysis of time variability

Figure 3.9 shows the daily, monthly, and annual variability of PV power potential for each country by the end of the century (2070–2099), relative to the reference period (1970–1999) for both RCP2.6 and RCP8.5 scenarios. The box plot displays the median, quartiles, and outliers for each scenario. It is worth noting the major differences between the two scenarios in the case of Peru. Specifically, while the RCP2.6 scenario exhibits an increase in PV potential, the RCP8.5 scenario, on the other hand, shows a decrease.

3.4.5 Analysis of the impact of climate change on PV potential in South America.

South America has great potential for renewable energy solutions, mainly due to high levels of solar irradiance. It is important to note that countries such as Colombia, Venezuela, Ecuador, Peru, Brazil, Bolivia, and Uruguay have tropical or subtropical climates. This condition causes temperature and irradiance values to remain relatively constant throughout the year, making it ideal for the use of solar energy through fixed-tilt PV systems. In particular, Chile, Bolivia, and Argentina are among the top ten countries in the world with the highest levels of solar irradiance [314]. Despite the great potential of solar and wind energy solutions, South America's energy supply depends

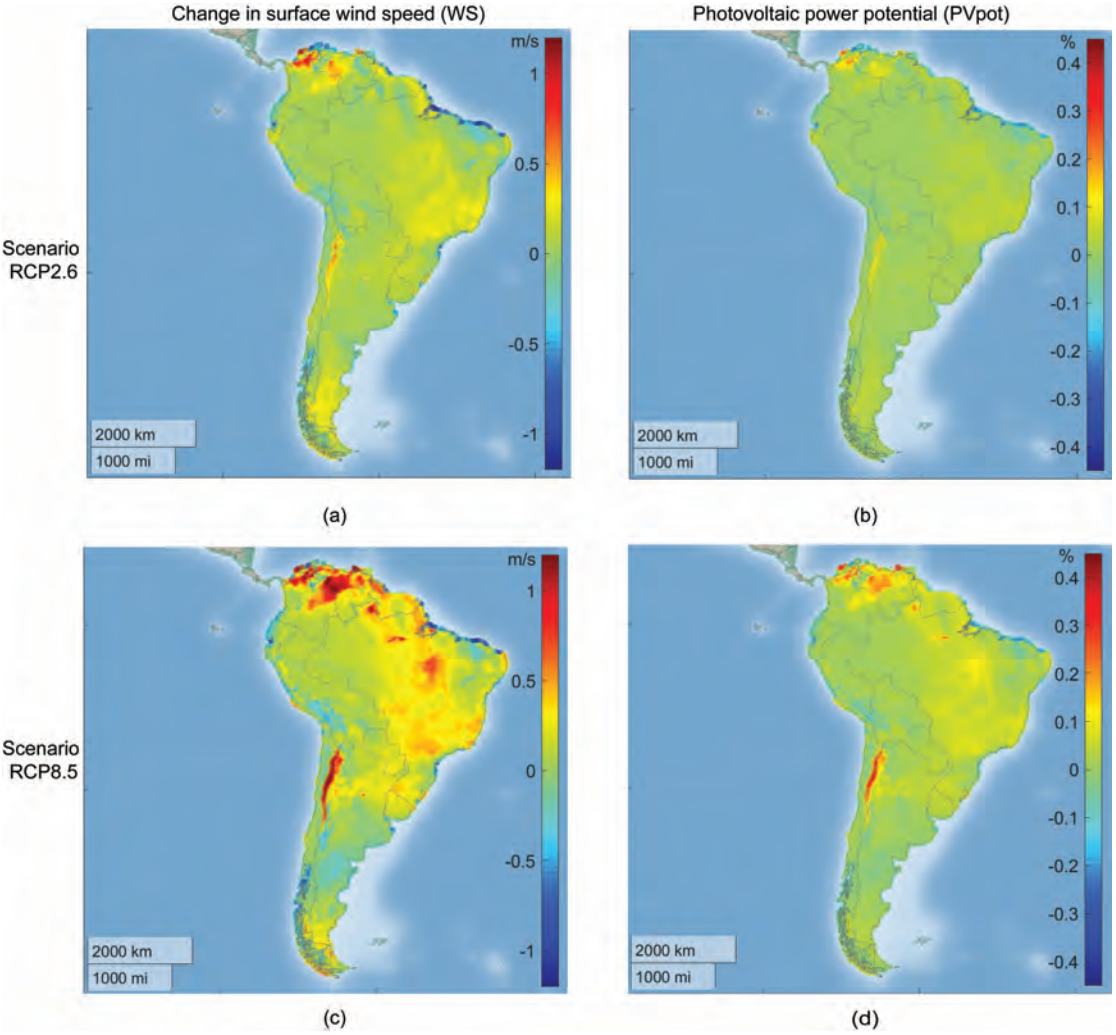

FIGURE 3.8: **Wind change analysis.** The left column compares the change in wind speed (in meters per second) between the end of the century (2070-2099) and the reference period (1970-1999). The right column represents the respective change in PV power potential as a percentage. In particular, changes in: (a) Changes in WS with RCP2.6, (b) PV_{pot} with RCP2.6, (c) WS with RCP8.5, and (d) PV_{pot} with RCP8.5. The plots were generated in Matlab.

primarily on hydropower. This over-reliance on hydropower has caused supply problems during periods of drought, leading to power failures. However, solar and wind power are taking a significant share of the electricity portfolio, with exponential growth in the last decade. This growth is expected to continue in the medium and long term due to the policies established by most South American countries [251, 315].

According to [316], solar energy is expected to be the primary renewable energy source in South America in the upcoming decades. Therefore, it is crucial to evaluate both, the photovoltaic power potential and its susceptibility to climate change. The following is a

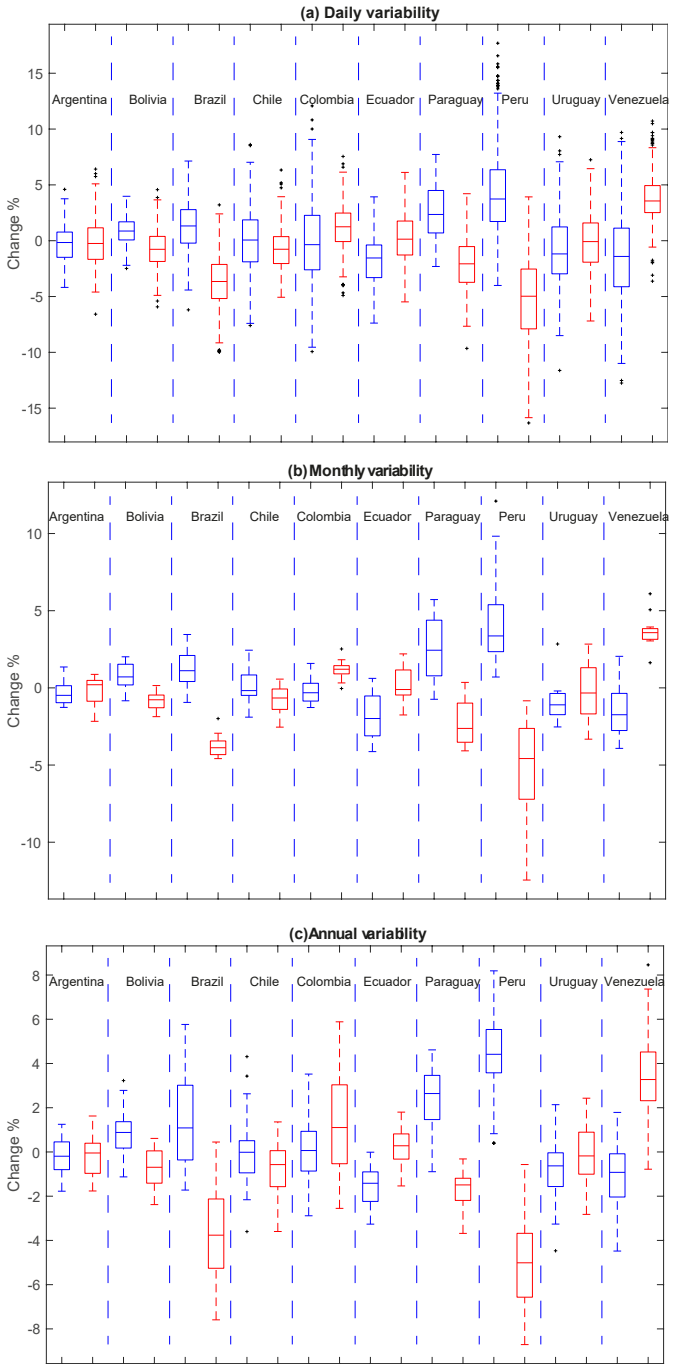

FIGURE 3.9: Projected differences in (a) daily variability, (b) monthly variability, and (c) annual variability of PV power potential for each country by the end of the century (2070–2099), relative to the reference period (1970–1999). The changes are illustrated for both RCP2.6 (blue) and RCP8.5 (red) scenarios.

comprehensive analysis of the potential impact of climate change on photovoltaic energy throughout the entire South American region.

As expected, our analysis reveals that solar irradiance is the most influential factor impacting PV potential in South America by the end of the century. It can lead to a maximum decrease of 15% and a maximum increase of 7% in PV_{pot} based on the RCP8.5 scenario, and 12% and 6% under the RCP2.6 scenario. Notably, the northeastern region, including southeastern Colombia, southwestern Venezuela, eastern Ecuador, northeastern Peru, and western Brazil, stands to benefit from increased PV potential due to higher solar irradiance. Conversely, regions like southwestern Colombia, western Ecuador, southern Peru, and southeastern Brazil might experience a slight reduction in PV potential due to decreased solar irradiance. Nonetheless, this decrease is limited to small areas, making it a minor concern for the future of PV solutions in South America.

The air temperature is the second most important variable affecting PV potential. The differences between the RCP2.6 and RCP8.5 scenarios are remarkable. While the RCP2.6 scenario estimates a less dramatic temperature increase, the RCP8.5 scenario predicts a more intense one. According to these air temperature changes, PV_{pot} would decrease by a maximum of 1% to 1.8% under RCP2.6 and RCP8.5 scenarios, respectively.

The northern region of the continent would experience the most critical increase in air temperature, especially in northeastern Colombia, western Venezuela, northwestern Brazil, northern and southern Bolivia, northern Paraguay, northeastern Chile, and northwestern Argentina. Although temperature changes are expected to decrease the PV_{pot} in these areas, this decrease would be less than 2%. In addition, an increase in solar irradiance is expected in some of these regions, which could offset the losses caused by the increase in air temperature. Therefore, the photovoltaic potential for this region is still positive. However, it is important to note that an increase above 4° would exceed the upper limit of 2° by the end of the century [317], causing possibly irreversible changes to nature. Consequently, a joint effort among all nations is necessary to achieve a transition to clean energy sources and thus reduce global warming, as suggested in the latest Intergovernmental Panel on Climate Change (IPCC) report [318]. South America can be a leader in this transition for a 100% renewable energy supply as proposed in [315].

It is worth noting that areas of projected air temperature increases (which cause decreases in photovoltaic potential) are somewhat compensated for by increases in solar irradiance.

The projected changes in wind speed for South America do not represent a significant threat. In literature, other authors report similar results regarding the influence of

wind speed on PV potential [201, 309, 311–313]. However, it would be worth examining whether changes in wind speed affect other renewable energy sources such as wind energy. These changes are most notable in the RCP8.5 scenario. Northern and eastern Colombia, western Venezuela, northern and central Brazil, and the northern part of Chile on the Argentinean border could see increases of up to $1m/s$.

Regarding RCMs, it is crucial to recognize their restrictions due to factors such as the quality of the models, data from GCMs with potential biases, and challenges in capturing the scale and nature of point data from weather stations. Biases in RCMs are present in variables such as temperature, precipitation, and atmospheric circulation patterns. These biases can lead to errors in simulating regional climate characteristics, including temperature extremes, precipitation patterns, and weather event timing and intensity [319–321]. It is also important to note that the use of projections with multiple GCMs and RCMs requires a thorough analysis of the associated uncertainties. An in-depth study of CORDEX simulations across South America is presented in [322], focusing on assessing the added value of RCMs in this context. These RCMs, sourced from CORDEX and driven by CMIP5 GCMs, demonstrate multi-model ensembles capturing key features of seasonal climatologies.

While climate models have been proven to be reliable tools for projecting many aspects of climate change, modeling the impacts water bodies have on climate models remains an active area of research [323, 324]. The climate change models used in this study have shown significant changes in solar irradiance and temperature in places where there are rivers, lakes, and coastlines, such as the extreme change in solar irradiance observed in southeastern Peru. Therefore, it is essential to validate the accuracy of climate change models in areas with bodies of water [205, 325]. Efforts should be made to improve the representation of water bodies in climate models, such as incorporating more detailed observations and advanced modeling techniques. Additionally, this study did not consider the orientation and tilt of the PV panels, which is also a significant factor affecting their performance. Moreover, when deciding on the best locations for implementing PV systems, land-use restrictions, such as nature reserves, should be taken into account.

In the Appendix section .4, we provided a detailed analysis of the impact of climate change in the most populated South American countries.

3.5 Conclusion

This chapter introduced the importance of collecting and analyzing meteorological data to accurately assess the PV power potential. Today, data collection primarily involves in-situ weather stations and satellite sources, each with distinct advantages and limitations to be used for predictive models. The potential impact of climate change was studied on PV systems via different scenarios. These studies require the collection of different climate scenarios to assess future PV performance to have an average ideathe solar production in several years.

To analyze the PV potential at a local scale, we introduced the Colombian Solar Atlas. This Atlas includes both historical meteorological data and climate change data. The historical dataset was sourced from the NSRDB, featuring a collection of meteorological variables with a spatial resolution of 4 km x 4 km and a temporal resolution of 30 minutes, comprising 62,187 data points spanning across Colombia. The meteorological database was validated with in-situ weather stations from IDEAM. Additionally, the Atlas provides two PV generation models: a basic model and an advanced model. Users can employ these models to simulate the performance of a solar panel installation at specific coordinates, providing an estimate of the capacity factor. The Colombian Solar Atlas was developed to offer interactive and user-friendly access to both current and future PV potential in Colombia. Moreover, it allows users to visualize and download meteorological variables, which can be valuable for various fields of study.

To assess the possible impact of climate change on PV power potential, we used meteorological data from the CORDEX framework. Based on this dataset, we studied the potential impact of climate change on PV power potential in South America, a region rich in renewable energy potential, particularly solar energy. We focused on analyzing the influence of solar irradiance, air temperature, and wind speed changes on PV potential by the end of the century under two climate scenarios, RCP2.6 and RCP8. Our findings highlight the significance of solar irradiance as the most influential factor affecting PV potential in South America. The analysis indicates that solar irradiance fluctuations could lead to a maximum decrease of approximately 15% and a maximum increase of about 7% in PV potential under the RCP8.5 scenario. Notably, regions in the northeastern part of South America stand to benefit from increased solar irradiance, while some areas may experience slight reductions in PV potential due to decreased solar irradiance. However, these reductions are limited to small areas, having minimal implications for PV solutions in South America. Air temperature emerged as the second significant factor,

with potential decreases ranging from 1% to 1.8%. Changes in wind speed were found to have a relatively insignificant impact on PV potential in South America, consistent with previous research.

The collected databases allow for the development of artificial intelligence techniques that can be applied to renewable energy systems, as shown in Chapters 4 and 5.

Chapter 4

Machine learning for site-adaptation and solar radiation forecasting

Abstract

Optimal management for solar energy systems requires quality data to build accurate models for predicting the behavior of solar irradiance. As shown in the preview chapter, satellite and in-situ measurements are commonly used to obtain solar irradiance and environmental data. Satellite measurements offer high temporal resolution but limited spatial resolution, and are more adapted to global studies for different countries. While in-situ measurements provide higher accuracy in a dedicated geographic site but may have significant missing data. To address an improvement of both challenges with less new equipment and low costs, a novel methodology based on machine learning algorithms is proposed. This approach combines the strengths of both data sources to enhance the spatio-temporal resolution, known as site-adaptation. The improved database is then utilized to develop precise solar irradiance forecasting models using deep learning techniques. Through a study case, we demonstrate the advantages of our proposed methodology based on machine and deep learning techniques to integrate data from different sources and to construct precise solar irradiance forecasting models. Our findings show that machine learning models for site-adaptation performed up to 38% better than traditional methods. The results presented in this chapter have been published in the international journal Renewable Energy, in the paper "Machine learning for site-adaptation and solar radiation forecasting" [45].

Table of Contents

4.1 Introduction

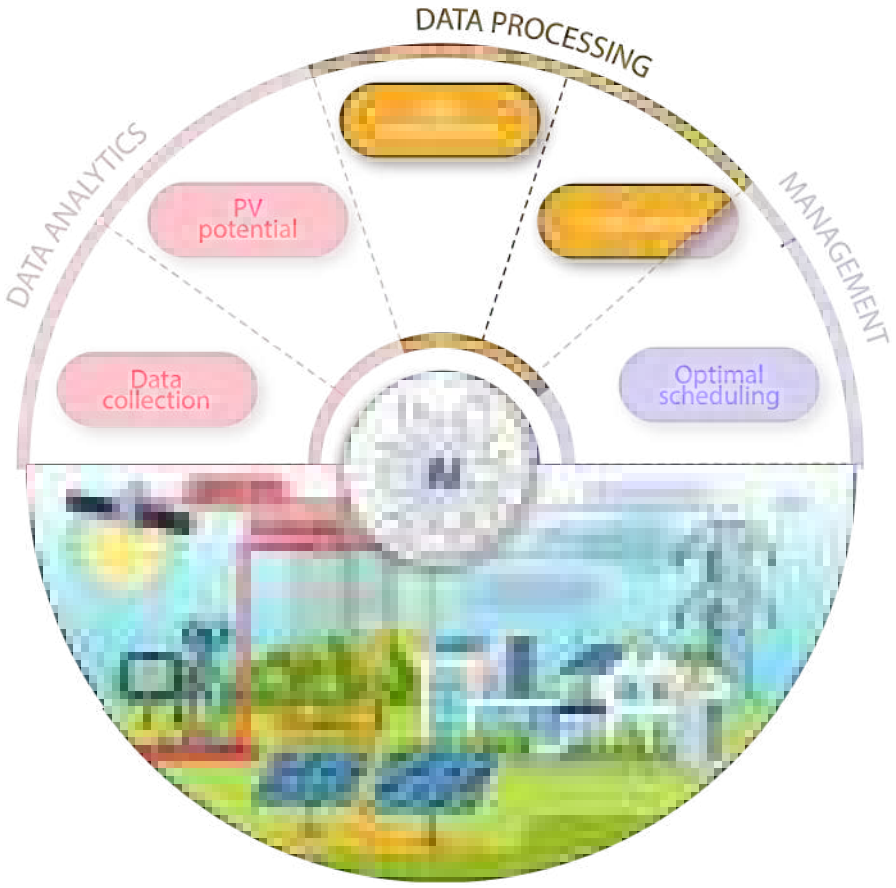

FIGURE 4.1: **Graphical Abstract of Chapter 4:** The databases are enhanced to provide more precise spatio-temporal data, allowing accurate solar irradiance forecasting models.

Renewable energy integration into power systems has attracted great interest in recent years because of the growing demand for electricity, the aim to diversify the energy basket in most countries, and the need to reduce CO_2 emissions by protecting the environment. Furthermore, islanded microgrids with clean-energy generation are suitable solutions to provide electricity in remote and hard-to-reach areas, promoting the welfare of poor communities [326].

The integration of renewable energy sources in the traditional power grid is currently one of the most important challenges, particularly with solar sources. The market of photovoltaic (PV) solar energy has increased in the last years, with an installed capacity of more than 586 GW around the world by 2019 (an increment of 20% with respect to 2018) [327]. Meanwhile, the total generation of electricity in the world is projected to increase to 36.5 trillion kWh by 2040 [328]. However, the integration of solar sources in

the power grid increases complexity in the management system because of the stochastic and intermittent behavior of these generators, causing problems such as voltage fluctuations and grid instability [329]. Therefore, predicting the behavior of solar radiation provides vital information for optimal sizing and control of solar systems in islanding or connected modes.

Design and implementation of efficient PV generation units in a specific location require a precise characterization of the solar energy available in the region of interest. Therefore, reliable historical data of solar radiation is needed to understand the long-term spatial and temporal variability of the solar resource. Clearly, the temporal behavior of solar radiation is the main variable used to estimate the generation capacity of a PV facility.

4.1.1 Solar radiation data sources

Historical solar radiation data can be obtained by in-situ measurements or satellite remote sensing through meteorological stations and geostationary meteorological satellites. Accuracy and quality of solar radiation data play a crucial role in the successful implementation of a solar energy system and depend on the data sources. To design new precise models with all Artificial Intelligence techniques, the first step and the most sensitive one to make the optimal choice is data collection and preprocessing. If bad data-based or not enough precise measures are chosen, the estimation of irradiation and associated parameters done by AI models are erroneous or not enough precise.

4.1.1.1 Solar radiation by ground measurements:

Meteorological stations provide in-situ measurements with a high accuracy. The most commonly used measuring instruments of solar radiation used in meteorological stations are pyranometers and pyrheliometers which measure the global horizontal irradiance (GHI) and the direct normal irradiance (DNI), respectively. The GHI is the total amount of radiation received by a surface horizontal to the ground, while the DNI is the amount of radiation received in a straight line from the direction of the sun. Although the ground measures provide accurate and high-time resolution data, the cost of installing and maintaining a network of meteorological stations results in geographically sparse stations. Also, the challenge of maintaining continuous operation with calibrated sensors may cause an interruption in data collection. Detailed information about issues and calibration of meteorological stations can be seen in [330–333]. Measurements provided

by meteorological stations are a reliable source of radiation and other weather data, however, calibration and maintenance problems can result in data gaps that must be overcome with other data sources [334].

4.1.1.2 Satellite-based solar radiation:

Geostationary meteorological satellites provide continuous image data of environmental information such as temperature, wind direction and speed, cloud cover, and radiation, covering a wide spectrum of temporal and spatial scales. Solar irradiance models convert satellite images captured by geostationary meteorological satellites into surface radiation using methods that combine radiative transfer theory and observations. Solar irradiance models can be classified into single-step and two-step physical models. In the first step of the two-step physical model, some atmospheric properties such as aerosol, cloud, and atmospheric moisture are obtained from the satellite sensor. Then, in the second step, the model solves the radiative transfer equation with the previous information to estimate the surface solar radiation. More details about the radiative transfer equation and the two-step model are available in [335] and references therein, and [336, Chapter 4]. The improvement in satellite technologies and the increase of computational capacity have enhanced the precision of two-step physical models, allowing an increase in spatial and temporal resolution. However, satellite estimations are limited by spatial resolution for accessible databases. Therefore, the spatial resolution of available geostationary meteorological satellites may not be sufficient to conduct a detailed study of solar radiation behavior at a precise geographic location [337]. More detailed information can be found in [338] and references therein.

4.1.2 Site Adaptation

In-situ measurements have precise locations and direct solar radiation measures, but it is difficult to maintain uninterrupted operation for long periods, whereas satellite remote sensing presents high time-resolution and is serially complete, but it is not as accurate as in-situ measurements. To address the problems in each source, satellite-based measurements can be calibrated with in-situ measurements for a target site, obtaining a database of long-term solar information with improved spatio-temporal information. This process is known in the literature as *site-adaptation*. Different site-adaptation techniques have been developed based on statistical analyses that try to adjust either the frequency distribution of the satellite-estimations to that of the in-situ data, or the model to convert

the satellite images into ground irradiance values [244]. However, as far as we know, methods that capture the point-to-point and probably nonlinear relationship between the satellite and in-situ data have not been explored yet. We propose a method to estimate this relationship in this work.

4.1.3 Scientific Contributions and highlights

The main contribution of this chapter is to propose a methodology based on machine and deep learning algorithms to develop accurate site-adaptation and solar radiation forecasting models, as the main scheme is illustrated in Figure 4.2. Our hypothesis is two-fold: *i)* using machine learning to be able to progressively construct a model that accurately captures the point-to-point relationship between meteorological station measurements and satellite data, potentially outperforming current models based on statistical analyses. This new model will induce an optimal estimator to obtain an improved database without the assumption of a complete and regular data acquisition, which represents an advantage in the presence of missing data; *ii)* the improved data inducing the development of highly accurate solar radiation forecasting models. To evaluate this hypothesis, we first present relevant related work on site-adaptation and forecasting models (Section 4.2). Then, we propose site-adaptation models with machine learning techniques (Section 4.3.1) and time-series forecasting models based on deep neural networks using the improved database (Section 4.3.2). Through a case study in Section 4.4, we evaluate the performance of the site-adaptation and forecasting models based on machine learning techniques and compare them to commonly used models in the literature, showing the benefits of using the proposed methodology. Finally, some conclusions and future research directions are presented in Section 4.5.

4.2 Related work

Several site-adaptation methods have been developed to improve the accuracy of satellite-derived data through in-situ data. Satellite-derived irradiance data include an estimation error due to approximations that transform satellite images into ground irradiance values. This imprecision generates a bias between the estimates and the in-situ radiation values [338]. Site-adaptation models can be divided into two main groups: physically-based methods and statistical methods. Physically-based methods convert satellite measurements into surface solar radiation [336]. For site-adaptation purposes, the inputs of

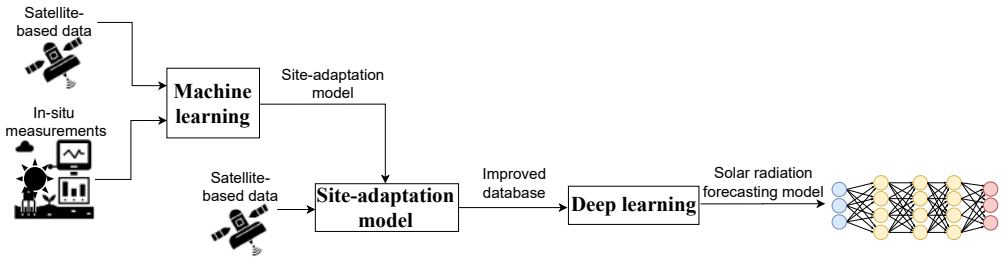

FIGURE 4.2: Diagram of the proposed approach to construct an accurate solar radiation forecasting model: After collecting and pre-processing solar radiation data from satellite-based data and in-situ measurements, a site-adaptation is developed through machine learning. Then, the site-adaptation model is used to obtain an improved database of solar radiation, and with the improved database, a solar radiation forecasting model is developed through deep learning.

the physically-based methods (e.g., cloud variables and aerosol turbidity) are processed to improve solar radiation measurements. Statistical models use in-situ data to adjust satellite-derived data by correcting the bias or adjusting the frequency distribution between these two databases. For instance, a linear method to eliminate bias estimates the mean bias deviation (MBD) between satellite and in-situ radiation data and removes it from the whole dataset [339]. Some methods use exogenous or ancillary variables, such as clear index and sun elevation angle, to adjust the satellite-based data through multivariate linear regression of the satellite-based data, exogenous variables, and the in-situ data [340]. Also, other methods approximate the cumulative distribution function of satellite-derived data to the one of the in-situ data, in a process known as the quantile mapping method (QM) [341]. A detailed description of site-adaptation methods can be found in [244] and the references therein.

Working with a refined database, time-series forecasting models have been extensively studied to predict solar irradiance for different time horizons. Some studies focused on typical methods for time-series analysis such as autoregressive integrated moving average models [342]. Other works have focused on regression techniques that are commonly used in machine learning applications such as linear regression, support vector machines, artificial neural networks (ANNs), and decision trees [343]. There are also methods that combine multiple learning algorithms to improve the forecasting such as boosting, bagging, random forest, and predictors ensemble [344]. However, ANNs have probably been one of the most widely used solar forecasting methods, especially since the last ten years [345, 346]. The wide use of ANNs can be explained by the enhancement in computational capability, large storage availability, and improvement achieved in accuracy by different ANN architectures [347]. Around 79% of the methods used in meteorological

forecasting are based on neural networks and specialized neural network structures have been developed for time series. In this work, we propose the use of deep neural networks to forecast solar radiation [22].

4.3 Methodology

This section describes the processes used in the development of this research as described in Figure 4.2. The method can be divided into two sequential subsystems or steps: the site-adaptation with machine learning and the solar radiation forecasting using deep learning.

4.3.1 Machine learning for solar database improving with site-adaptation techniques

To improve the database from the two origins, satellite-based solar radiation measurements must be matched with in-situ measurements. Statistical methods have been developed in the literature to improve satellite-based solar radiation using ground measurements during overlapping periods [348–350]. However, in the proposed approach, we aim to capture the point-to-point relationship between satellite-based data and in-situ measurements with the help of machine learning regression models. In this way, the obtained model will be able to easily deal with measurements that have not been regularly collected and the presence of missing data by using nonlinear relationships.

Figure 4.3 shows the proposed model for site-adaptation based on a series of data taking into account GHI, DHI, DNI, zenith angle, temperature, wind speed, and the exact timing for each series of estimations. Input variables or predictors are issues from the satellite-based data, and the output of this model is the estimation of in-situ measurements, achieving a site-adaptation of the satellite-based data with an hourly frequency. Even though the variable to be adjusted is solar radiation, input variables include diffuse horizontal irradiance (DHI), GNI, DNI, solar zenith angle, temperature, wind speed, and hour of the day. Having input variables other than solar irradiance, which are also part of the analyzed phenomenon, can potentially facilitate the regression process. Commercial and public databases can easily provide this meteorological information, and as we will show in the results section, machine learning algorithms can estimate the importance of each input variable for the regression task.

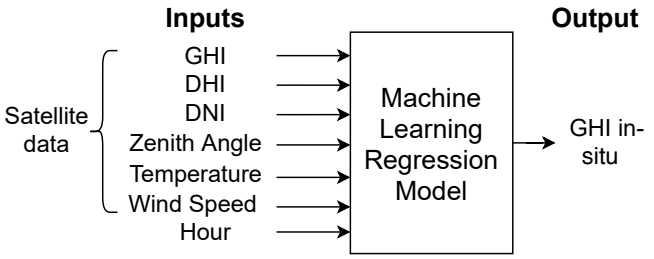

FIGURE 4.3: Block diagram for the site-adaptation model. Inputs are the satellite-based data: GHI, DHI, DNI, solar zenith angle, temperature, wind speed, plus the hour, while the output is the GHI in-situ.

Because in-situ measurements provide high accuracy and the satellite-based data provide high temporal resolution, applying a regression model over the whole satellite database results in a database with an improved spatial-temporal resolution.

There are several machine learning regression models that can be classified into two main groups: linear and nonlinear models. Linear regression models are the simplest ones and allow us to have a straightforward interpretation of the model properties. However, linear regression models may have significant limitations for pattern recognition, such as strictly linear relationships, sensitivity to outliers, and the assumption of independence in the data [351]. On the other hand, nonlinear regression models are capable of modeling more complex relationships in the variables. However, an overly complex model can cause overfitting, and in consequence, there is a trade-off between complexity and generalization for nonlinear regression models [352]. In this study, we explore the implementation of linear regression, neural networks, random forests, and AdaBoost, which have been shown to provide excellent performance in a wide variety of applications [353].

4.3.2 Deep learning for solar radiation forecasting

With the improved database obtained by the machine learning-based model, the next step is the forecast stage. The algorithms for time-series forecasting find patterns of behavior over time. We propose neural networks to forecast solar irradiance motivated by the fact that 79% of the methods used in meteorological predictions for the last ten years are based on neural networks [22]. In this field, we have chosen to use the long short-term memory (LSTM) networks and the gated recurrent units (GRU) networks, which are designed for processing sequential data and work with sequences of an arbitrary length, unlike traditional feedforward networks that work with fixed-sized inputs [354, 355]. This choice was oriented because LSTM and GRU networks are very useful for different tasks such as

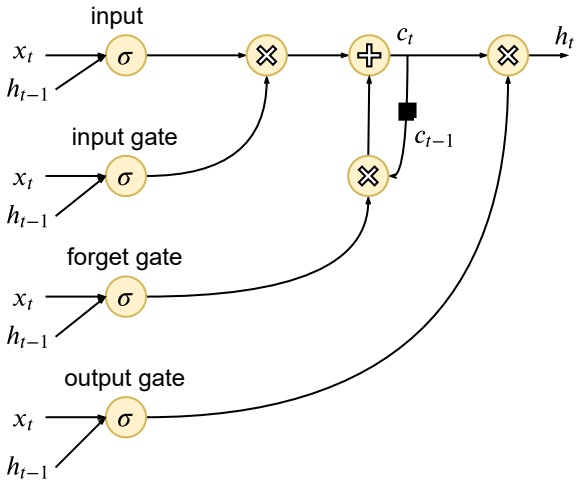

FIGURE 4.4: Diagram of an LSTM network unit. The unit is composed of four neurons, each of which receives as input the current state x_t and the previous state h_{t-1}. The input gate can enable or disable the state of the input neuron generating the state c_t, which has a linear self-loop represented by the black square. The forget gate controls the weight of the self-loop. The output gate can enable or disable the state of the unit h_t.

voice recognition, automatic translation, speech-to-text, and time series prediction [351], and have been used in the renewable energy area to forecast wind turbine power and solar radiation [356, 357]. LSTM and GRU architectures can be used for long-term and short-term forecasting. In the long term, they are used to study the viability of solar energy implementations, whereas in the short term, or in real-time, to manage the power supply [358]. Figure 4.4 shows an example of a diagram representing an LSTM network. Instead of a simple self-loop as in traditional recurrent networks, LSTM networks are composed of different cells that have a self-loop and three gating units to regulate the flow of information. The cell entries represent the current and previous states. The input gate enables or disables the state of the input neuron generating the state c_t, which has a linear self-loop. The forget gate controls the weight of the self-loop, selecting which previous states are forgotten and which remain, and then, allowing for both long and short-term memory. Finally, the output gate enables or disables the state of the unit h_t. GRU networks have a similar structure to LSTM. However, in the GRU structure, a single gating unit simultaneously controls the forget gate and the state unit h_t.

Time-series forecasting can be approached as a sequence-to-sequence model (named seq2seq) that predicts an output sequence given an input. The seq2seq prediction problems are challenging because the number of elements in the input sequence may vary

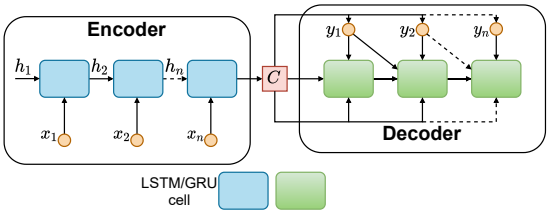

FIGURE 4.5: Encoder-Decoder or sequence-to-sequence model. The encoder creates an internal representation C. The decoder transforms C into the corresponding output vector.

from the output sequence. For example, to predict one day of solar radiation, at least one week of previous data could be required [359]. As the length of input and output sequences may vary, one approach to solve seq2seq problems is the Encoder-Decoder architecture [360, 361]. The structure of the Encoder-Decoder model is presented in Figure 4.5. In the encoder stage, the model summarizes the GHI input sequence and creates an internal representation C, which is a vector whose size is determined by the number of neurons in the last encoder layer. More than one layer can be used in this stage. Then, in the decoder stage, the internal representation C is transformed into the desired output sequence. In the same way, more than one layer can be used [362, 363]. In the encoder and decoder stages, we implemented LSTM and GRU networks.

Different time horizons can be studied to achieve a complete picture of solar radiation behavior, and the selected structure can be adapted to distinct sizes of inputs and outputs. For instance, solar annual horizons are considered to establish the global management of the electrical supply by estimating the large-scale energy potential, while monthly or weekly horizons are used for energy management such as demand response, energy efficiency, and market analyses. Short horizons such as hours, minutes, and seconds of prediction are useful for real-time power management schemes such as detailed dispatch of small units, grid stability strategies, and provision of ancillary services [347].

4.4 Site adaptation and Forecasting case study

To illustrate the functionality of the proposed model, we have selected a target site and tested the proposed methodology along with a competing one that has been used for site adaptation. Here, we first describe the target site with the satellite database and in-situ database. Then, we present the results of the site adaptation models and the forecast models.

4.4.1 Target region and databases

A region in Colombia, South America, was selected to evaluate the performance of the proposed model. Colombia has great potential for the development and implementation of renewable energy sources, however, about 68% of the energy is produced by hydroelectric plants whose generation has fluctuations due to rain regimes, and only 0.06% of the energy comes from solar sources [364]. In addition, there are remote regions where the electricity supply is deficient, increasing the socio-economic problems that hinder the progress of the region. Regions outside the power grid in Colombia represent approximately 52% of the whole territory, with more than 470.000 homes without electricity and around 180.000 users with energy from diesel plants [111, 365]. In particular, we had focused on a specific geographic location in the southwest, where implementation costs, difficult access, and the variability of solar radiation due to atmospheric conditions, have made its energization a challenge. The first step is to collect satellite and ground data on solar radiation, then with the collected data, implement site-adaptation techniques by machine learning models, and finally develop solar radiation forecasting models.

The region of study is a rural zone in Nariño state, located at coordinates $0°53'02''$N $77°30'14''$O. To estimate the GHI, we have in-situ data provided by the Colombian Institute of Hydrology, Meteorology and Environmental Studies (IDEAM) [40]. This database has an hourly periodicity and is available since 2006. To collect satellite data, we use the National Solar Radiation Database (NSRDB), which is a widely used open public dataset [41]. This database contains meteorological information from 1998 to 2017, with measurements every 30 minutes and 4 km^2 resolution. Nevertheless, as satellite measurements cover an average area of 4 km^2, the values differ from ground measurements at a specific location. To address this difference, we proceed to create a machine learning-based site-adaptation model by adjusting the satellite measurements (NSRDB) with the measurements in situ (IDEAM). With the improved database, we construct time forecasting models for daily and weekly time horizons.

4.4.2 Experimental Results: Site Adaptation

The IDEAM database contains information from 2006 to 2019, whereas the NSRDB database contains data from 1998 to 2017. Therefore, to develop a site-adaptation model, we choose the overlapped information (i.e., data from 2006 to 2017). Figure 4.6 displays the timeline of NSRDB and IDEAM databases. The IDEAM database contains missing data that represent a 22% of the total database. The NSRDB database contains

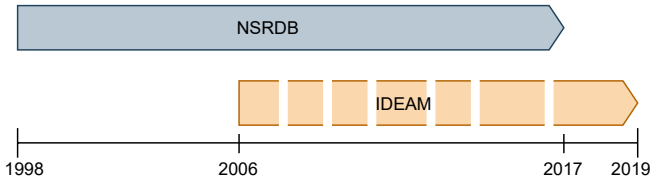

FIGURE 4.6: Timeline of NSRDB and IDEAM databases. Blank spaces in the IDEAM line indicate missing data.

TABLE 4.1: Correlation between IDEAM and NSRDB data.

	GHI IDEAM	**GHI NSRDB**	**DHI**	**DNI**	**Wind speed**	**Temp**	**Zentih**
GHI IDEAM	1	0.82	0.78	0.49	0.66	0.75	-0.73
GHI NSRDB	0.82	1	0.87	0.73	0.64	0.79	-0.79
DHI	0.78	0.87	1	0.34	0.69	0.82	-0.83
DNI	0.49	0.73	0.34	1	0.30	0.43	-0.43
Wind speed	0.66	0.64	0.62	0.30	1	0.8	-0.75
Temp	0.75	0.79	0.82	0.43	0.8	1	-0.83
Zentih	-0.73	-0.79	-0.83	-0.43	-0.75	-0.83	1

measurements of GHI, DNI, DHI, temperature, solar zenith angle, and wind speed, with a half-hour periodicity. To temporally match with the IDEAM database, the data is averaged to hourly measurements. Table 4.1 shows the correlation between the IDEAM radiation and NSRDB variables, where the correlation between GHI measurements is 0.82. Although this value shows a clear approximation between the satellite and the in-situ data, the objective of the site-adaptation model is to increase this correlation to a value as close as possible to one. For this stage, we use cross-validation to set the parameters in each model that best fit the data. The database is divided into 4 folds.

The implemented machine learning models are neural networks, linear regression, AdaBoost, and random forest on standardized measurements. To compare our results with a traditional method reported in the literature, we compute the quantile mapping method [244]. This method aims to adjust effectively the cumulative distribution function (CDF) of the satellite-derived data to the CDF of the in-situ data according to

$$\mathrm{GHI}_{\mathrm{imp}} = \mathrm{CDF}_{\mathrm{gnd}}^{-1}[\mathrm{CDF}_{\mathrm{sat}}(\mathrm{GHI}_{\mathrm{sat}})], \tag{4.1}$$

where $\mathrm{GHI}_{\mathrm{imp}}$ is the improved GHI data, $\mathrm{CDF}_{\mathrm{gnd}}^{-1}$ is the inverse CDF of the in-situ data, and $\mathrm{CDF}_{\mathrm{sat}}$ is the CDF of the satellite-based data. To estimate the CDF, we use

TABLE 4.2: Performance metrics (W/m^2 for RMSE and MAE) of site adaptation models according to cross-validation, in bold the best regression model.

Model	**Hyperparameters**	R^2	**RMSE**	**MAE**
Neural Networks	1 hidden layer 40 neurons	0.74	168	88
Neural Networks	3 hidden layers 20, 20, 5, neurons	0.75	167	85
Linear Regression		0.70	182	113
AdaBoost	Decision Tree (max depth=1) 20 estimators	0.57	219	172
Random Forest	**100 Estimators**	**0.96**	**66**	**33**
Quantile Mapping	Empirical distribution Function	0.58	210	110

the empirical distribution function, which is a non-parametric method. The complete process to estimate the CDF and its inverse is described in [366]. To evaluate the performance of the site-adaptation techniques, a cross-validation scheme with four folds is used, calculating the average of three performance indices (R^2, root mean squared error (RMSE), and mean absolute error (MAE)) on the validation folds. Table 4.2 presents a summary of the best parameters by model according to the cross-validation scheme. The chosen hyper-parameters are the ones that provide the best performance for each method.

The best performance model for our study is Random Forest with 100 estimators, obtaining the highest R^2 but the lowest RMSE and MAE. Figure 4.7 shows a scatter plot of GHI measurements from IDEAM (in situ) and from NSRDB (satellite) for the validation set, before and after applying the model based on random forest. Note that the scatter plot presents a more correlated behavior between GHI measurements by IDEAM and the improved satellite database. The ideal case would involve a slope of 45° in the straight line. As shown in Figure 4.7 (b), the slope increases after applying the model from 17° to 37°, achieving a better approximation to in-situ measurements. It can be noted that quantile mapping only has better performance indices than AdaBoost. Figure 4.8 shows the CDF of IDEAM, NSRDB, and the quantile-mapping adjusted data. The NSRDB database contains underestimated data with respect to the IDEAM database, which can also be seen in Figure 4.7. Even though the quantile mapping method brings the satellite-derived CDF closer to the in-situ CDF, the adjusted CDF is still underestimated concerning to in-situ data. An explanation for these results is that capturing the

FIGURE 4.7: Scatter plot between GHI measurements by IDEAM and by NSRDB in the validation set. (a) Before applying the site-adaptation model. (b) After applying the model. Note the increase in the slope from 17° to 37°, and correlation from 0.86 to 0.96.

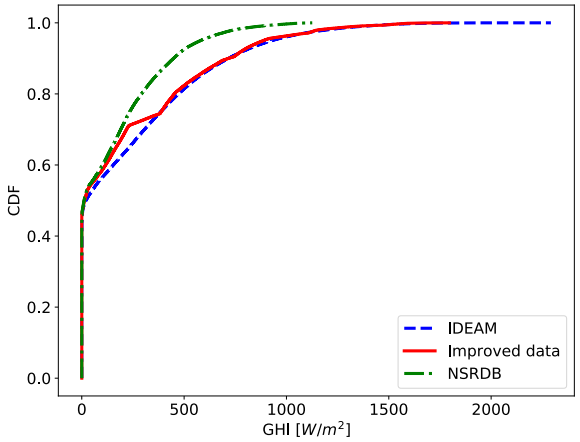

FIGURE 4.8: Site-adaptation with quantile mapping. Different line styles present the CDF for the IDEAM data (dashed line), the NSRDB data (dash-dotted line), and the improved database (solid line).

point-to-point nonlinear relation between measurements can potentially produce a better database improvement than techniques based on a holistic view of the data behavior.

Consequently, we have chosen to use Random Forest as the machine learning model to correct the whole NSRDB database and adjust it to the in-situ measurements. After applying the regression model, the correlation between GHI from in-situ and satellite data increased from 0.82 to 0.96. The results can be seen in Figure 4.9, where, for visualization purposes, we show only one week of data. The dashed line represents in-situ solar radiation, the dash-dot line the NSRDB radiation, and the solid line represents

the radiation obtained with the random forest model.

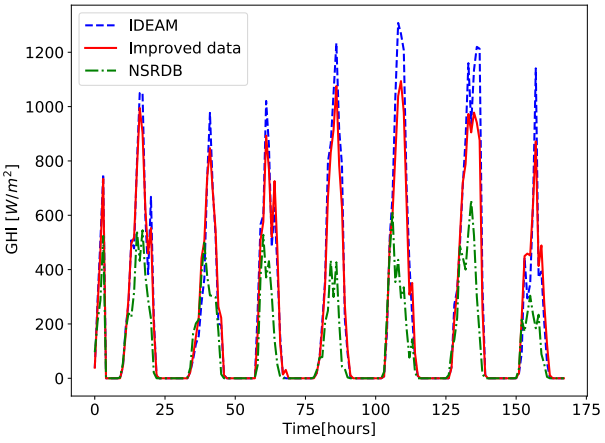

FIGURE 4.9: Site-adaptation with random forest. The horizontal axis is time in hours, and the vertical axis is GHI. The dashed line represents the IDEAM data, the dash-dotted line represents the NSRDB data, and the solid line represents the improved database.

To analyze the relevance of the inputs, the feature importance for the site adaptation using random forest is calculated and shown in Figure 4.10. As expected, the most important feature is the satellite GHI, which has the largest correlation coefficient, as it is presented in Table 4.1. The least important feature is wind speed. According to [367], there is a weak correlation between wind speed and radiation, where clear days can be windy or not. This indicates that the pattern learned by the machine learning model is consistent with what has been observed in physical phenomena regarding solar irradiance. Global radiation GHI can be expressed as the sum of DHI and DNI, which have a similar importance value. Moreover, we include the hour as an input variable, which has an importance value similar to DHI and DNI. As described in Table 1, the solar zenith angle and GHI have a negative correlation. An increase in the solar zenith angle implies a decrease in GHI [368]. According to the feature importance measure, the solar zenith angle is just over temperature and wind speed. Although temperature has been used to predict GHI achieving accurate models [369, 370], these models use daily and monthly averages. In our study, we include the temperature to conduct an hourly based estimation of GHI.

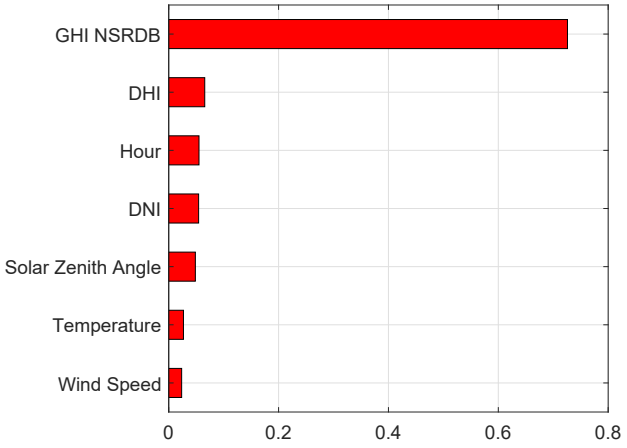

FIGURE 4.10: Random forest feature importance.

FIGURE 4.11: Split for training, validation, and test of the GHI forecasting models.

4.4.3 Experimental results: Time series forecasting

Using the site adaptation models based on random forests and quantile mapping, we adjusted the GHI satellite database from 1998 to 2017 with hourly periodicity, obtaining a total of 175,200 samples. From previous studies, we found that this number of samples is enough to train a GHI forecasting model based on neural networks [343, 356, 358, 359, 371, 372]. With the improved database, we trained daily and weekly multiple-output forecast models on an hourly basis, comparing the results of the forecasting with the two site adaptation models. The database is divided into three sets: 70% for training, 15% for validation, and 15% for test, corresponding to the data from years 1998 to 2011, 2012 to 2014, and 2015 to 2017, respectively as depicted in Figure 4.11. For the daily forecasting model, we trained encoder-decoder LSTM and GRU network models. For the LSTM model, we used 24, 72, and 168 neurons in the input layer, corresponding to 1, 3, and 7 previous days. Also, we included 12, 24, and 168 LSTM units in the encoder and decoder layers, and 24 neurons in the output layer. The output is a 24 size vector that represents one day. For the weekly forecasting model, we trained the encoder-decoder LSTM model with 168, 336, and 672 neurons in the input layer, corresponding to 1, 2, and 4 previous weeks. The LSTM units are the same as the daily model, and the 168 neurons in the output layer represent one week. Table 4.3 presents the parameters and

TABLE 4.3: Encoder-Decoder LSTM architecture and performance of daily and weekly forecasting models, in bold the best model for each horizon.

	Input size (hours)	LSTM units	MSE	Epochs	Output size (hours)
Daily		12	0.1141	24	
	168	**24**	**0.1113**	**31**	**24**
		168	0.1208	23	
		12	0.1145	34	
	72	24	0.1157	29	24
		168	0.1170	17	
		12	0.1144	26	
	24	24	0.1126	48	24
		168	0.1155	25	
Weekly		12	0.1425	32	
	672	24	0.1449	31	168
		168	0.1920	15	
		12	0.1405	34	
	336	**24**	**0.1399**	**23**	**168**
		168	0.1554	15	
		12	0.1466	25	
	168	24	0.1707	18	168
		168	0.2145	17	

performance of the models, where the performance measure is the mean squared error (MSE) in the validation set. An early stopping regularization was also applied to find the optimal epochs in each model. According to the results, the best daily model is achieved with 24 LSTM units, 168 input neurons (i.e., seven previous days), and 31 epochs. The best weekly model is achieved with 24 LSTM units, 336 input neurons (i.e., two previous weeks), and 23 epochs. We followed the same methodology to train the encoder-decoder GRU models, where the architecture and performance of the models are summarized in Table 4.4. The best daily model is achieved with 24 GRU units, 72 input neurons (i.e., three previous days), and 31 epochs. The best weekly model is achieved with 24 GRU units, 672 input neurons (i.e., four previous weeks), and 10 epochs. However, the results show that LSTM networks outperform GRU networks in both daily and weekly horizons. Therefore, we select the LSTM networks to work with from now on. We also trained daily and weekly forecasting models with the quantile-mapping obtained database to compare the results in the forecasting task using the two different approaches of site-adaptation. The forecasting models with the quantile-mapping database are implemented with the best parameters found previously.

Figures 4.12 and 4.13 show the results for GHI daily and weekly forecasting, respectively, according to the improved database obtained with the random forest model. The forecasted days are 01/08/2015, 01/12/2015, 01/12/2016, and 01/07/2017, while forecasted

TABLE 4.4: Encoder-Decoder GRU architecture and performance of daily and weekly forecasting models, in bold the best model for each horizon.

	Input size (hours)	**GRU units**	**MSE**	**Epochs**	**Output size (hours)**
Daily		12	0.1133	43	
	168	24	0.1130	46	24
		168	0.1153	15	
		12	0.1134	22	
	72	**24**	**0.1128**	**31**	**24**
		168	0.1195	15	
		12	0.1154	41	
	24	24	0.1135	27	24
		168	0.1194	22	
Weekly		12	0.1433	49	
	672	**24**	**0.1414**	**10**	**168**
		168	0.1533	14	
		12	0.1437	37	
	336	24	0.1542	29	168
		168	0.1547	2	
		12	0.1456	28	
	168	24	0.1528	24	168
		168	0.2267	15	

weeks are weeks 24 and 44 of 2015, week 24 of 2016, and week 44 of 2017. These days and weeks are randomly chosen. The solid line represents the actual value and the dashed line represents the forecasted value. In Table 4.5, we show the performance metrics for the daily and weekly forecasts according to the improved database using random forest and the improved database using quantile mapping. Here, the lowest value of R^2 for the database obtained with the random forest model is 0.91 and 0.88 for the daily and weekly forecasts, respectively. Values are 0.77 and 0.71 for the obtained database with the quantile mapping method. The results show the importance of a precise site adaptation model to improve the training data, and therefore, to develop accurate forecasting models.

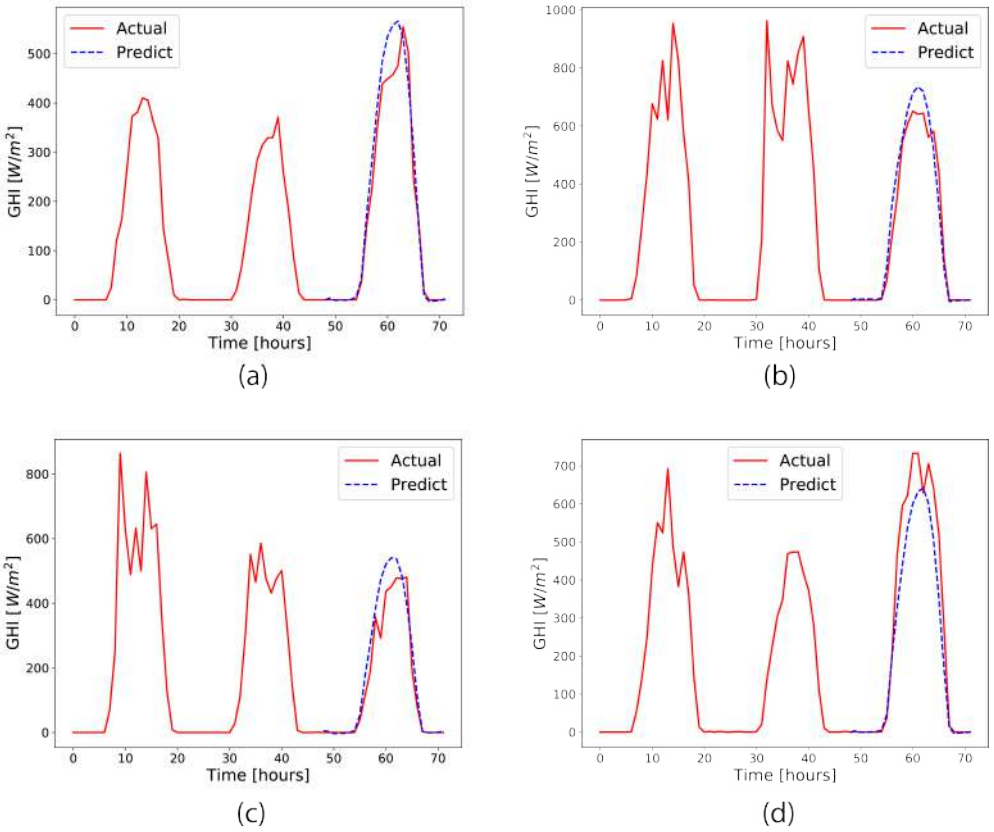

FIGURE 4.12: Actual and predicted GHI on a daily horizon. The solid line shows the actual value with the two previous days and the dashed line represents the obtained forecast. The figures present the forecasting for the days (a) 01/08/2015, (b) 01/12/2016, (c) 01/01/2017, and (d) 01/07/2017.

TABLE 4.5: Encoder-Decoder LSTM model performance. RF represents the improved database obtained with the random forest model, and QM represents the improved database obtained with the quantile mapping method.

		R^2		**RMSE**		**MAE**	
		RF	**QM**	**RF**	**QM**	**RF**	**QM**
Day	1	0.96	0.85	42	86	27	50
	2	0.96	0.88	54	98	37	54
	3	0.91	0.77	57	96	35	57
	4	0.93	0.81	79	137	49	86
Week	1	0.92	0.71	64	117	34	67
	2	0.91	0.75	100	153	54	79
	3	0.91	0.82	94	147	52	82
	4	0.88	0.76	82	148	46	81

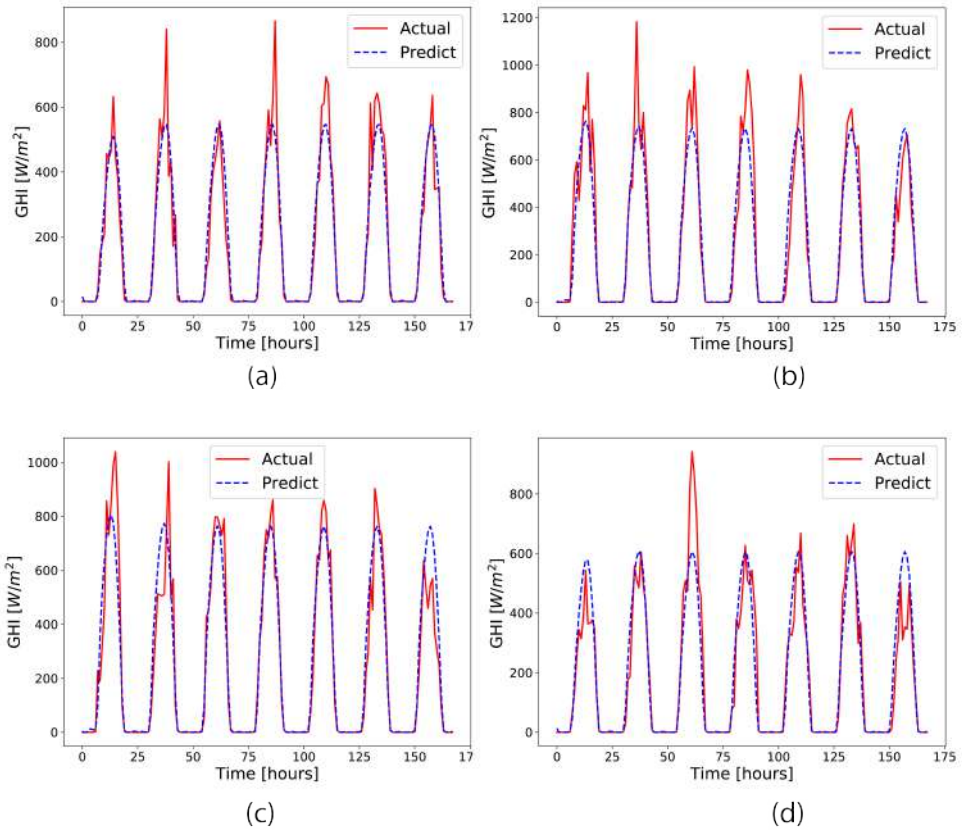

FIGURE 4.13: Actual and predicted GHI on a weekly horizon. The solid line is the actual value and the dashed line presents the obtained forecast. The figures present the forecasting for (a) week 24 of 2015, (b) week 44 of 2015 (c) week 24 of 2016, and (d) week 44 of 2017.

4.5 Conclusion

A methodology to develop site-adaptation techniques with machine learning algorithms has been implemented to capture the point-to-point relation between solar irradiance data from satellite and in-situ measurements. Using the machine learning-based improved database, we train solar irradiance forecasting models on the daily and weekly time frames. The results show a better performance for the database that was improved through machine learning techniques over the commonly used statistical methods for site-adaptation. The proposed methodology can be applied to any region where satellite and ground measurements are available by following the steps described in the site-adaptation section: training different machine learning algorithms to find the best model to approximate satellite-based data to in-situ solar irradiance. The performance of the models depends on meteorological data, which have different behavior depending

on the location. Therefore, several machine learning models should be implemented to find the optimal model according to a certain performance criterion.

The improved database and the accurate solar irradiance forecasting model are the fundamental basis for the optimal management of renewable energies. Predicting the potential photovoltaic production enables optimal management of a microgrid. This includes efficient management of energy storage systems, ensuring a constant and reliable energy supply, and reducing overall energy consumption costs.

Chapter 5

Optimal DC microgrid scheduling based on battery degradation cost and renewable energy forecasting

Abstract

This chapter introduces an advanced approach to the energy management of DC microgrids. The methodology integrates solar irradiance forecasting with optimal scheduling techniques to minimize energy costs while also addressing battery degradation. To ensure accurate solar photovoltaic production forecasts for the next 24 hours, the study employs long short-term memory networks. The chapter proposes a novel battery cost formulation, which assesses costs associated with various depths of discharge levels. Unlike other methodologies, our proposal allows the use of 100 percent of the battery state of charge, obtaining a behavior that is more faithful to reality, where the battery usage price encourages its use when a high state of charge is reached and avoids deep discharge levels. Preliminary results of this chapter were presented at the "Journées Nationales du Photovoltaïque" congress (JNPV 2022).

Table of Contents

5.1 Introduction

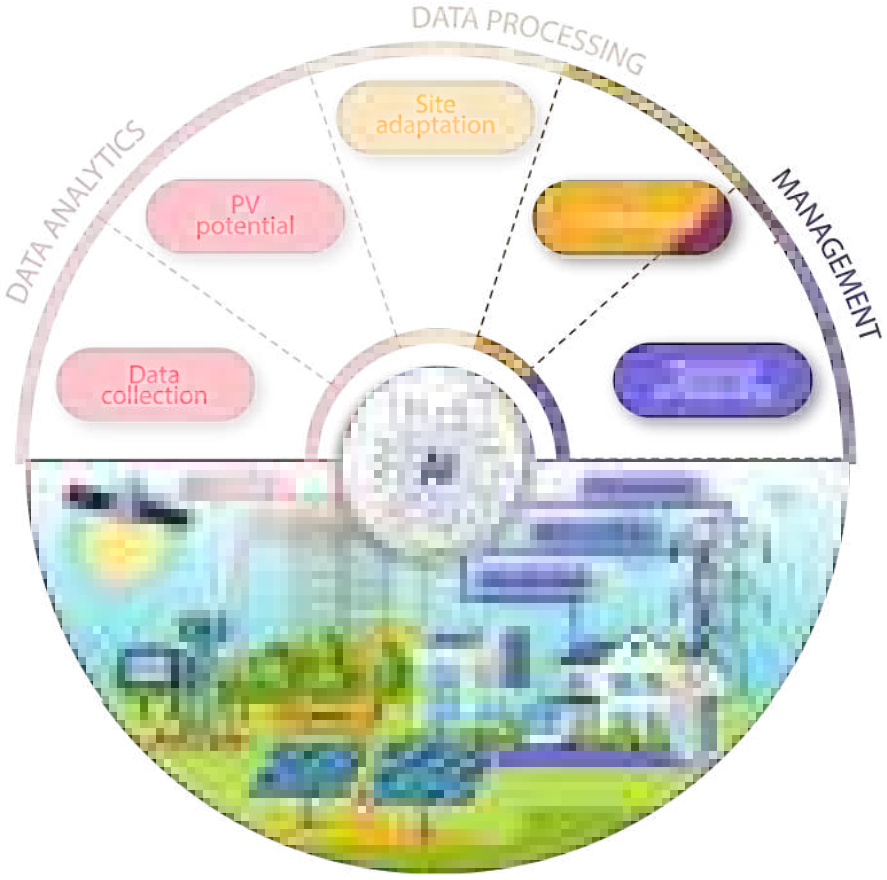

FIGURE 5.1: **Graphical Abstract of Chapter 5:** The forecasting models, along with optimal scheduling, are integrated to achieve efficient microgrid management.

The integration of renewable energy sources in microgrids has attracted considerable attention in recent years due to their environmental benefits, cost reductions, and potential to mitigate greenhouse gas emissions [216]. However, the incorporation of renewable energy sources, especially photovoltaic (PV) panels, presents challenges related to power generation variability and intermittency [45]. To address these challenges, accurate forecasting of solar irradiance is crucial [8]. Additionally, optimizing the scheduling of energy storage systems is essential to maximize the use of renewable energy and minimize energy costs [9, 373–375].

Despite the growing interest in integrating renewable energy sources and optimizing energy storage systems within microgrids, there is still a research gap regarding the joint challenges of battery degradation and renewable energy uncertainty within optimal scheduling [208]. While previous studies have separately explored optimal scheduling

techniques and battery degradation, comprehensive methodologies addressing both aspects at once are limited [172, 207, 376–378]. Moreover, existing research often relies on simplified degradation models or does not account for the uncertainties associated with renewable energy generation, particularly from PV panels [379, 380]. This gap calls for a novel approach that captures the dynamic nature of renewable energy generation, providing accurate solar irradiance forecasts, and evaluating battery degradation costs in a more realistic and comprehensive approach.

Solar radiation plays a key role in the performance of PV systems due to its direct relationship with electricity generation. Solar radiation serves as the primary energy source for PV systems [190]. When sunlight, in the form of photons, strikes the semiconductor material of PV panels, it excites electrons, creating an electric current. The intensity and duration of solar radiation directly influence the amount of electricity generated. Higher solar radiation levels result in increased energy production, making it a fundamental factor for PV system performance [381]. However, solar radiation is variable and intermittent. To address the uncertainty associated with renewable energy forecasts, the forecasting model relies on meteorological information. This choice aligns with established evidence highlighting that meteorological data plays a crucial role as a primary input for microgrid scheduling problems [177]. By utilizing meteorological information, the forecasting model can provide valuable insights into future renewable energy generation, enabling more accurate and reliable scheduling decisions within microgrid systems [379].

This chapter presents a novel methodology to optimize the scheduling of a battery energy storage system (BESS) in a DC microgrid, incorporating solar irradiance forecasting through long short-term memory (LSTM) neural networks. This study focuses on DC microgrids because they offer advantages such as simplified infrastructure, improved renewable energy integration, enhanced control, and power management, making them an attractive option for efficient and sustainable power distribution in various applications [382, 383]. The proposed methodology introduces an innovative formulation for evaluating battery degradation costs by considering information obtained from technical specifications. This formulation assesses the cost of battery utilization based on energy extracted at different depths of discharge (DoD).

The primary objective of this approach is to find an optimal balance between battery usage and degradation. To assess this hypothesis, we introduce the time-series solar irradiance forecasting model, the battery cost formulation, and the optimal scheduling optimization problem in Section 5.2. In Section 5.3, we conduct a case study using

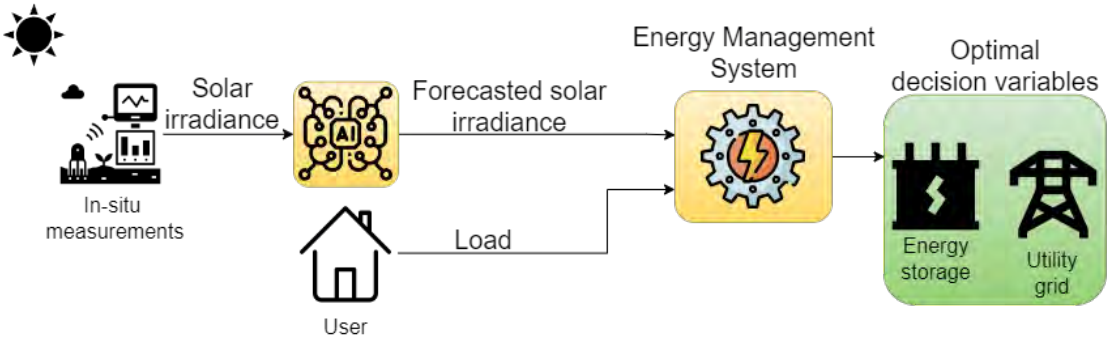

FIGURE 5.2: Diagram of the proposed methodology. The first step is to predict solar irradiance. Then, based on the forecasted irradiance and the load profile, the energy management system determines optimal battery power charging/discharging and grid consumption.

real-world data on PV energy production and lighting consumption from the LAAS-CNRS laboratory in Toulouse, France. We evaluate the performance of the proposed methodology and compare it with commonly used models in the literature, demonstrating the advantages of our approach. Finally, in Section 5.4, we present concluding remarks and outline potential directions for future research.

5.2 Methodology

We propose an advanced energy management system that utilizes a rolling horizon strategy to address the optimal scheduling problem in a DC microgrid, as shown in Figure 5.2. This strategy enables adaptive decision-making by implementing only the initial steps of the optimal schedule and recalculating a new schedule based on updated data [114, 384–386]. The EMS incorporates solar irradiance forecasting techniques and optimal scheduling to minimize the energy drawn from the grid while mitigating battery degradation.

The integration of renewable energies into microgrids represents a major challenge. As presented in Chapter 2.2, solar PV systems are one of the main sources of renewable energy. Solar radiation plays a key role in the performance of PV systems. Accurate modeling of solar radiation data is essential for both the design and optimization of solar PV systems. Any inaccuracy in this modeling process can lead to inefficient resource allocation and suboptimal asset management within microgrids [124].

We performed a comparative analysis of two methods of forecasting solar irradiance: probabilistic models and artificial intelligence (AI) techniques. Among the probabilistic

models, the Beta Probability Density Function (PDF) solar model stands out as the most commonly employed [378]. The most widely used AI technique for predicting solar irradiance is the long-term memory neural network (LSTM) [387]. Moreover, LSTM networks capture complex temporal dependencies and effectively model the time series patterns inherent in solar irradiance nature [8, 47, 356, 376, 388].

Our study aims to contrast the prediction performance of the Beta PDF solar model with that of AI techniques in the context of solar irradiance prediction. The solar forecasting model attempts to predict solar irradiance for a 24-hour horizon. The solar irradiance is then transformed into the expected PV power output. The solar irradiance data used in this study was obtained from the ADREAM building in the LAAS laboratory. The data was processed using an hourly average.

In the rolling horizon strategy, only the hour-ahead decision variables for grid power and BESS power are used. This hour-ahead scheduling allows for more frequent adjustments based on updated information, reducing the uncertainty caused by longer forecasting horizons [172, 389]. The optimization problem is formulated to minimize energy costs while considering the adverse effects of battery degradation [171, 390]. To evaluate the cost associated with different DoD levels, we use information obtained from technical specifications and propose a novel battery cost formulation. By incorporating this formulation, we aim to find an optimal balance between battery usage and degradation.

The proposed EMS, incorporating the rolling horizon strategy, offers significant potential for achieving efficient energy management in DC microgrid systems. By adapting the optimization process based on updated information and shorter forecasting horizons, our approach attempts to reduce energy costs and extend the lifespan of the battery.

5.2.1 Probabilistic modeling of solar generation

Probabilistic modeling of solar irradiance data has been employed for the economical operation and optimal management of microgrids. The most common probabilistic models include Monte Carlo sampling, Beta probability density function (PDF) estimation, Markov-chain-based model, and Weibull Distribution. From these models, Beta PDF is the most widely used function for modeling solar irradiance. Beta PDF is a versatile distribution that can be adjusted to model a wide range of shapes in the data.

The Beta PDF solar generation model attempts to find an hourly irradiance pattern at a specific location, and often follows a bimodal pattern, which can be represented

by combining two unimodal distribution functions, as presented in [378] and references therein. To characterize each of these unimodal distributions, the Beta PDF is formulated as follows:

$$B(\text{GHI}) = \begin{cases} \frac{\Gamma(\alpha)\Gamma(\beta)}{\Gamma(\alpha+\beta)}(\text{GHI})^{(\alpha-1)}(1-\text{GHI})^{(\beta-1)} \\ \quad \text{for } 0 \leq \text{GHI} \leq 1, \alpha \geq 0, \beta \geq 0 \\ 0 \quad \text{otherwise} \end{cases}$$

where GHI represents the global horizontal irradiance (kW/m^2). The parameters of the Beta distribution function (α, β) can be determined by utilizing the mean (μ) and standard deviation (σ) of the random variable:

$$\beta = (1-\mu)\left(\frac{\mu(1+\mu)}{\sigma^2} - 1\right) \tag{5.1}$$

$$\alpha = \frac{\mu\beta}{1-\mu} \tag{5.2}$$

We found the Beta PDF for each month of the year, finding the hourly irradiance patterns according to each month. We chose to adjust the Beta PDF for each month in order to capture and characterize the seasonal patterns of irradiance, and to obtain a better representation of the variability in solar irradiance throughout the year.

5.2.2 Solar irradiance forecasting with AI

Unlike solar models, which identify typical patterns on a monthly or seasonal basis, forecasting models are more realistic. Instead of sticking to a defined pattern, they take into account past behavior to predict future results. To forecast solar irradiance, we employed an LSTM network with an encoder-decoder structure. The LSTM network was chosen because it can capture long-term dependencies and handle temporal data effectively. Also because LSTM networks have been used for solar irradiance prediction in several works, and have shown better results than other architectures, as discussed in Chapter 4 and references [8, 45, 355, 356]

An LSTM network is a type of recurrent neural network (RNN) architecture that is specifically designed to capture and model long-term dependencies in sequential data.

Unlike traditional RNNs, LSTMs incorporate memory cells, which enable them to retain and utilize information over longer time intervals. This is achieved through a combination of gating mechanisms that control the flow of information, allowing LSTMs to selectively remember or forget information based on its relevance. The ability of an LSTM network to handle and learn from sequential data makes it ideal for tasks such as time series forecasting, natural language processing, and speech recognition. Its effectiveness lies in its capacity to overcome the vanishing gradient problem and capture both short-term and long-term dependencies, making it a powerful tool for modeling and predicting complex sequential patterns in diverse domains [351]. By utilizing the LSTM-based forecasting algorithm, we can provide accurate predictions of solar irradiance, which plays a crucial role in optimizing the energy management system of the microgrid and facilitating informed decision-making regarding the scheduling and utilization of renewable energy resources.

The solar irradiance database contains data from 2017 to 2021. In the forecasting model with LSTM networks, we used three years for training (2017-2019), one year for validation (2020), and one year for testing (2021). The model was trained to predict the next 24 hours based on the previous 24 hours of solar irradiance. Table 5.1 displays the performance metrics, including root mean squared error (RMSE), mean absolute error (MAE), and the coefficient of determination (R^2), for the validation set with different numbers of LSTM cells. The model with the best performance was achieved with 24 LSTM cells in both the encoder and the decoder. Table 5.2 presents the performance metrics for the testing set. Figure 5.3 displays the loss curve depicting the performance of the training and validation sets. This loss corresponds to the mean square error (MES), a measure of the degree to which the model predictions match the actual values. A lower loss value usually means better performance, as it indicates that the model predictions are closer to reality. This curve also allows us to qualitatively verify that the model is neither over-fit nor under-fit by verifying that the training loss (blue line) and validation loss (red line) are not far apart. For example, if the training loss continues to decrease but the validation loss remains the same or increases, it is an indication of overfitting. The model was trained using a batch size of 32, and an early stopping mechanism was employed with a patience parameter set to 10.

To qualitatively assess the performance of the LSTM model in capturing solar irradiance patterns, we specifically applied the LSTM-based model to the 5th day of each month, as illustrated in Figure 5.4. Table 5.3 quantitatively compares the results of the LSTM model with those of the Beta PDF model.

TABLE 5.1: Performance of the encoder-decoder LSTM architecture in the validation set.

	LSTM cells				
	12	**24**	48	64	72
RMSE	0.1078	**0.1071**	0.106	0.1094	0.1072
MAE	0.0578	**0.0556**	0.0556	0.0577	0.0561
R^2	0.7986	**0.8012**	0.8052	0.7925	0.8007

TABLE 5.2: Performance of the encoder-decoder LSTM architecture in the training set.

	24 LSTM cells
RMSE	0.1067
MAE	0.0559
R^2	0.8027

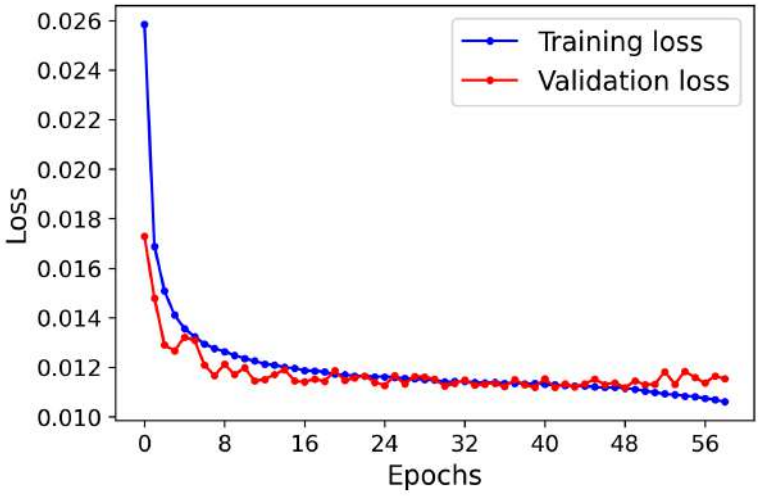

FIGURE 5.3: Loss curve of the performance of the training and validation sets for the best model (24 LSTM cells).

5.2.3 Battery cost formulation

As discussed in Chapter 2.3.3 batteries are the most common energy storage systems for microgrids due to their versatility, fast response times, and ability to efficiently store and release electricity, making them ideal for managing the intermittency of renewable energy sources and ensuring grid stability. In this subsection, we present a novel model for evaluating the cost of battery usage, which offers several advantages compared to existing methods. One key distinction is that we consider the entire range of state of charge (SoC) values, rather than restricting it to a specific range. Therefore, our model

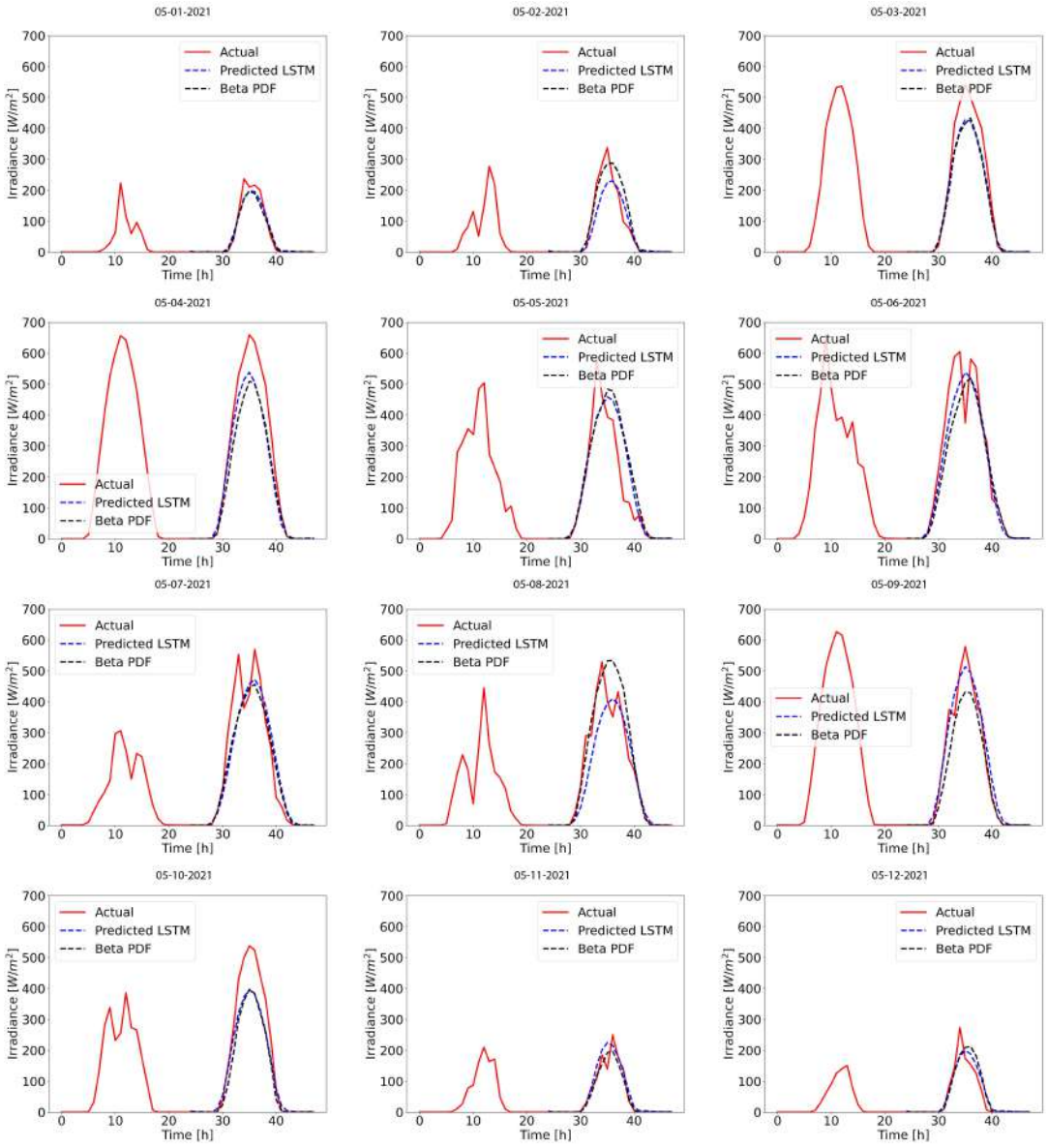

FIGURE 5.4: Predictions of solar irradiance specifically for the 5th day of each month. The solid line represents the actual value, and the dotted line represents the prediction.

offers a more thorough analysis of battery performance and cost dynamics by taking into account the entire spectrum of SoC levels.

Unlike other approaches that rely solely on the number of cycles, our model takes into account the energy that can be delivered by the battery at different levels of depth of discharge (DoD = 1 - SoC). This approach enables us to estimate the energy recovery characteristics of the battery across its entire operating range.

We propose to express the relationship between available energy and DoD as:

$$E(\text{DoD}) = \beta_0 + \beta_1 \text{DoD} + \beta_2 \text{DoD}^2, \tag{5.3}$$

where the coefficients $\beta_0, \beta_1, \beta_2$ are determined from the battery datasheet. This equation allows us to estimate the amount of energy that can be extracted from the battery at various DoD levels, including both shallow and deep discharges.

By considering the energy recovery characteristics of the battery, according to [9], we can estimate the cost of energy at a specific DoD ($C_E(\text{DoD}_t)$) as:

$$C_E(\text{DoD}_t) = \frac{\text{DoD}_t E_b C_{\text{cap}}}{E(\text{DoD})}, \tag{5.4}$$

where DoD_t represents the DoD value at a given time t, E_b represents the nominal energy capacity of the battery (kWh), and C_{cap} indicates the capital cost of the battery (€). Equation 5.5 gives the cost of use (€) with respect to the change in SoC at each time step:

$$C_{b,t}(p_{b,t}) = C_E(1 - \text{SoC}_t) - C_E(1 - \text{SoC}_{t-1}). \tag{5.5}$$

Finally, the change in time of the SoC is determined by:

$$\text{SoC}_{t+1} = \text{SoC}_t - \frac{\eta \Delta t}{E_b} p_{b,t} \tag{5.6}$$

where η is the battery efficiency (%), and Δt the time interval (h).

5.2.4 Optimal scheduling optimization

The objective of the optimization problem is to minimize the energy cost within a DC microgrid, comprising solar panels, a BESS, and a grid connection. The optimization strategy for charging and discharging the BESS considers battery life-time and the cost associated with grid usage.

The optimization problem is formulated as follows:

$$\begin{aligned} \min_{p\in\mathbb{R}^{2n}} & \sum_{t=t_i}^{t_f} C_{g,t}(p_{g,t}) + C_{b,t}(p_{b,t}) \\ \text{s.t.} \quad & p_{g,t} \leq p_{l,t} - p_{pv,t} - p_{b,t} \\ & p_{b,\min}(\text{SoC}) \leq p_{b,t} \leq p_{b,\max} \\ & 0\% \leq \text{SoC} \leq 100\% \\ & p_{g,t} \geq 0, \end{aligned} \tag{5.7}$$

where $C_{g,t}$ represents the time-varying cost of grid usage (€), $C_{b,t}$ represents the cost of the BESS usage determined by Equation 5.5. The decision variables $p_{g,t}$ and $p_{b,t}$ represent the power(kW) taken from the grid and the BESS power respectively. The BESS power can be positive, when it is discharging, or negative, when it is charging. pl, t denotes the power consumed by the load (kW), and $p_{pv,t}$ the power obtained by the PV system (kW). Finally, $p_{b,\max}$ represents the maximum discharging power (kW), and the charging power $p_{b,\min}(\text{SoC})$ is kept constant at the maximum value for SoC values ranging from 0 to 80%. For SoC values greater than 80%, we refer to the manufacturer datasheet to determine the maximum charging power curve.

The time-varying cost of grid usage is calculated as:

$$C_{g,t} = \lambda_t p_{g,t}, \tag{5.8}$$

where λ_t is the electricity price.

The methodology allows the BESS to eventually reach 100% SoC, where the battery cost is low, promoting the use of the BESS when fully charged. For SoC levels below 20%, the battery cost is high, preventing the BESS from being fully discharged, thus limiting the battery degradation. According to methodologies such as the one presented in [9], the battery cost model relies on the number of cycles per DoD:

$$N_{cycle} = \beta_0 \text{DoD}^{-\beta_1} \exp\{\beta_2(1 - \text{DoD})\}, \tag{5.9}$$

where β_0, β_1, and β_2 are curve-fitting coefficients. However, in this formulation for low DoD, the number of cycles tends to infinity, forcing the state of charge to be limited, typically to 80-90%. Therefore, in contrast to existing literature, which commonly limits the SoC range to 20-80% [9, 374], our battery operation is closer to reality and allows for maximum battery capacity utilization.

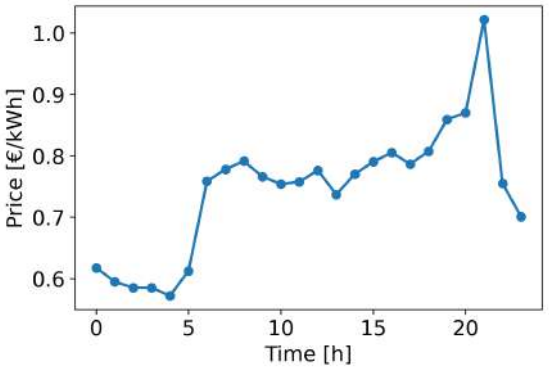

FIGURE 5.5: Kilowatt-hour (kWh) price profile for France.

Finally, in the BESS scheduling following the rolling horizon strategy, with each passing hour, the actual PV data is refreshed, enabling a forecast for the forthcoming 24 hours. The optimization problem is then solved for the entire optimization horizon, but the decision variables are selected only for the upcoming hour, accounting for the latest information. This iterative process ensures the continuous adaptation of the scheduling strategy to changing conditions.

5.3 Case study

The microgrid used in this case study is a DC microgrid, where the load is the lighting of the second floor of the ADREAM building at LAAS-CNRS, and the microgrid is connected to the grid. It should be clarified that the sizing of the proposed microgrid was not determined with optimal sizing methods. The primary aim of this case study is to show the advantages of the proposed method, particularly in regard to reducing battery costs and optimizing grid utilization.

To address the optimization problem, we used the hourly energy prices from the French electricity market [391]. The price profile in euro per kilowatt-hour (€/kWh) used in this section was obtained from Nord Pool Group. This profile corresponds to an average price in France. Figure 5.5 shows the price profile, where a maximum peak at 8 p.m. is observed.

The load profile corresponds to the lighting load of the third floor of the ADREAM building at LAAS. The BESS under consideration is a 12V, 100Ah lead battery, manufactured by Ultracel, with an approximate price of €205. According to the manufacturer, this battery offers 3600 cycles at 20%, 1200 cycles at 50% DoD, and 400 cycles at 90% DoD.

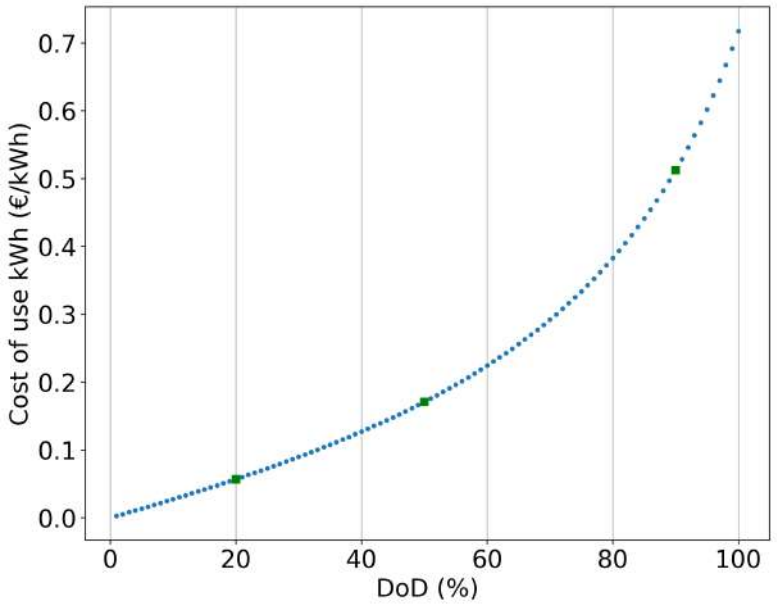

FIGURE 5.6: Cost of use in €/kWh. Green squares represent data from the datasheet.

By applying the formulations presented in Equations 5.3 and 5.4, we obtained the cost of use in euros per kilowatt-hour for one battery (€/kWh), as shown in Figure 5.6.

According to [392], the charging efficiency of lead batteries demonstrates variation based on several factors such as the SoC, temperatures, and charging rates. In the battery used in this study, the charging power exhibits fluctuations in relation to SoC, as illustrated in Figure 5.7, where green squares are data from the manufacturer. Within the SoC range of 0% to approximately 70%, the charging power, represented by the red line, exhibits an almost linear relationship. For higher levels of SoC the charging power shows a linear decline. We decline this fitted charging power curve in our methodology to achieve a more realistic behavior of the battery performance.

5.3.1 Solar forecasting vs Solar generation modeling

In this subsection, we show the benefits of the solar irradiance forecasting model, described in Section 5.2.2, compared to the typical Beta PDF solar generation model introduced in Section 5.2.1.

We compare the solutions obtained from the optimization problem stated in Equation 5.7 using both the LSTM-based approach and the Beta PDF formulation. This comparison serves to highlight the advantages of the forecasting methodology. Then, we proceed to

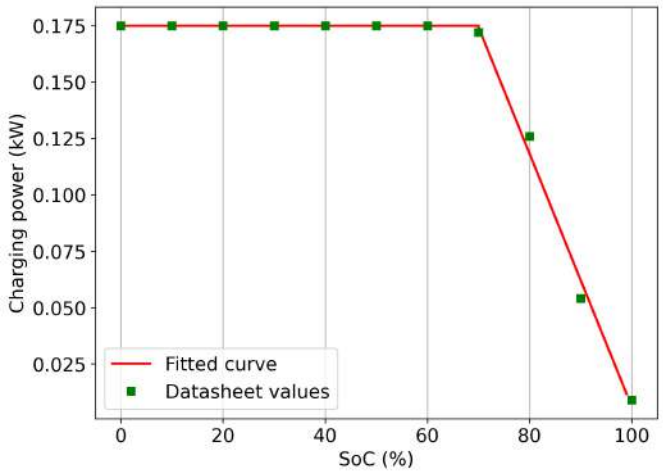

FIGURE 5.7: Variation of the charging power according to the battery state of charge. Green squares represent data from the manufacturer, and the red line is a linear fit.

a comparison between our approach and the method presented by Lee [9], integrating the forecasting methodology into the Lee method.

For each of the proposed methodologies, the LSTM and Beta PDF approach for BESS scheduling, the algorithm was executed under different initial SoC levels: 20%, 50%, and 80%. These specific levels were selected to assess how the optimization scheduling algorithm responds to varying initial conditions. Additionally, the algorithm was executed over the course of one week for each month of the year. The total cost for the twelve weeks, obtained with each method, is presented in Figure 5.8. The results indicate that, with an initial SoC of 20% and 50%, the LSTM-based method resulted in lower costs compared to the Beta PDF method. At initial SoC levels of 80%, the LSTM-based method resulted in the same total cost as the Beta PDF method.

Although the differences in the total energy price presented between the two methods, it is important to compare the performance of the methods to approximate the real power delivered by the PV panels. While the LSTM-based method is continuously updating with actual information and performing new predictions, the Beta PDF method assumes a constant PV profile for each month.

Therefore, to assess the efficacy of each model in capturing solar irradiance patterns, Table 5.3 presents the performance metrics for time series regression. For the Beta PDF formulation, the mean solar irradiance for each month was used and compared against the actual values recorded on the mentioned days. As shown in Table 5.3, the LSTM model outperforms the Beta PDF formulation in terms of RMSE, MAE, and R^2 for most of the forecasted days, demonstrating higher accuracy in predicting solar irradiance. The

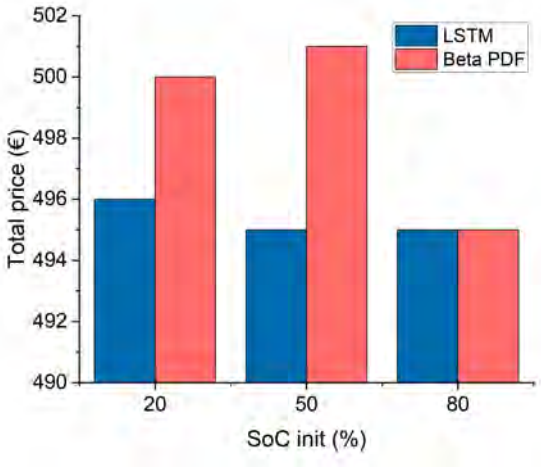

FIGURE 5.8: Total price (in €) for the optimal scheduling problem at different initial SoC levels (%). The total price is represented in blue when forecasting is performed using LSTM networks and in red when using the Beta PDF distribution.

TABLE 5.3: Forecast model performance metrics of LSTM vs Beta PDF.

	LSTM			Beta PDF		
Day	RMSE	MAE	R^2	RMSE	MAE	R^2
01-05-2021	16.9	9.1	0.96	17.7	8.45	0.95
02-05-2021	39.0	19.5	0.86	33.77	17.5	0.89
03-05-2021	54.5	31.7	0.88	145.5	84.7	0.50
04-05-2021	63.6	39.6	0.93	75.0	49.2	0.91
05-05-2021	73.8	41.5	0.82	132.2	81.4	0.35
06-05-2021	61.4	39.5	0.92	76.5	47.4	0.88
07-05-2021	71.3	43.5	0.88	63.6	36.5	0.90
08-05-2021	63.0	31.2	0.87	145.2	86.2	0.58
09-05-2021	29.9	18.6	0.98	54.4	30.2	0.92
10-05-2021	63.8	37.6	0.90	70.35	43.5	0.88
11-05-2021	22.1	10.9	0.91	35.5	19.5	0.5
12-05-2021	25.1	13.6	0.89	56.2	28.1	0.1

main limitation of using the Beta PDF formulation for predicting solar irradiance is that the fixed bimodal distribution may not accurately capture the dynamic and complex nature of solar irradiance patterns.

The Beta PDF method may generate a PV profile that deviates from reality, which could lead to situations where an attempt is made to charge the batteries when in fact there is

no PV production. In other words, the system could request power from the solar panels even though there is no PV production. These discrepancies can cause several problems in the optimal battery scheduling process.

5.3.2 Optimal scheduling results

We now compare our battery cost formulation against the battery cost model proposed by Lee [9]. In both cases, we use solar irradiance forecasting, and the load profile and energy price remain consistent with the previous scenario. We also compare the results with a base case without BESS to verify the benefits of energy storage systems in the proposed methodology.

Figures 5.9, 5.10, and 5.11 compare the performance of the two proposed methods for BESS scheduling. These figures display the results for different initial SoC levels: 20%, 50%, and 80% for each week. The proposed method consistently achieves lower intake power costs and total costs compared to the Lee method across all SoC levels, except for week five with an initial SoC of 80%. The graph illustrating the total cost includes the base case, represented by the green line. The base case represents the system without BESS, consisting only of PV panels and the grid. It is evident that the base case presents higher costs than any of the proposed methodologies. This is mainly attributed to the lighting profile, characterized by a peak demand in the morning and evening and a low demand in the central hours of the day. This pattern contrasts with the PV profile. This discrepancy underscores the advantage of energy storage, which allows the system to store surplus energy during peak PV production for use during periods when the panels are not generating electricity.

In Table 5.4, a comparison is made between intake power cost, battery cost, and total cost. The findings consistently demonstrate cost advantages of our proposed method over the Lee method. Specifically, concerning input energy cost and total cost, the proposed method proves to be more economical. Although this might lead to slightly higher battery usage costs, it ultimately results in savings in overall energy expenses over the medium and long term, optimizing BESS utilization. Across all initial SoC, our method consistently achieves a 3.5% reduction in total costs compared to the Lee method.

In Figures 5.12, 5.13, and 5.14, we present graphical representations of the SoC over a 12-week testing period. These figures serve as a visual comparison between our proposed methodology, denoted by the red line, and the approach outlined by Lee [9], represented

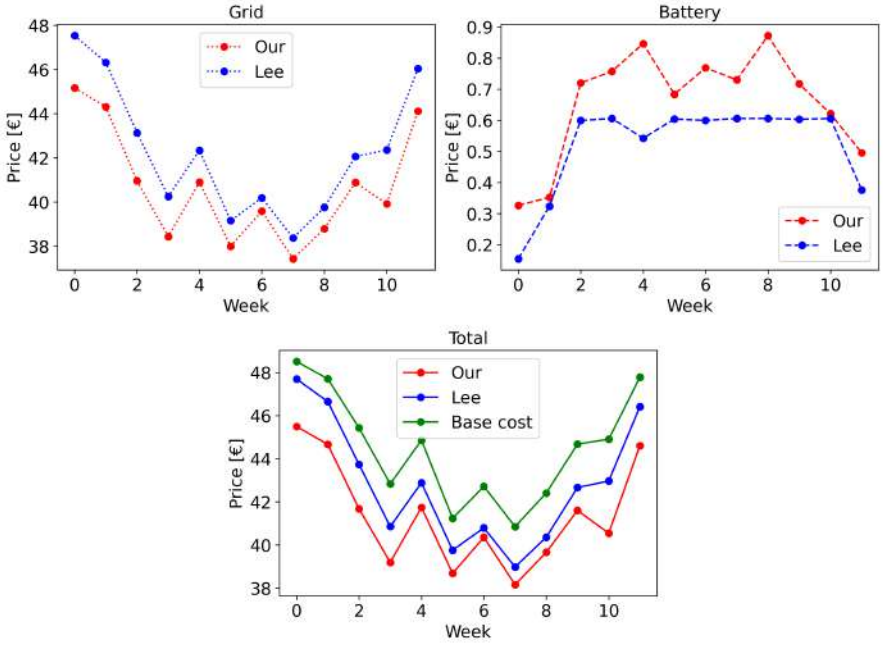

FIGURE 5.9: Total price (in €) for the optimal scheduling problem at an initial SoC of 20%. The red lines represent our method, while the blue lines represent Lee's method. (a) is the grid cost, (b) the battery cost, and (c) the total costs.

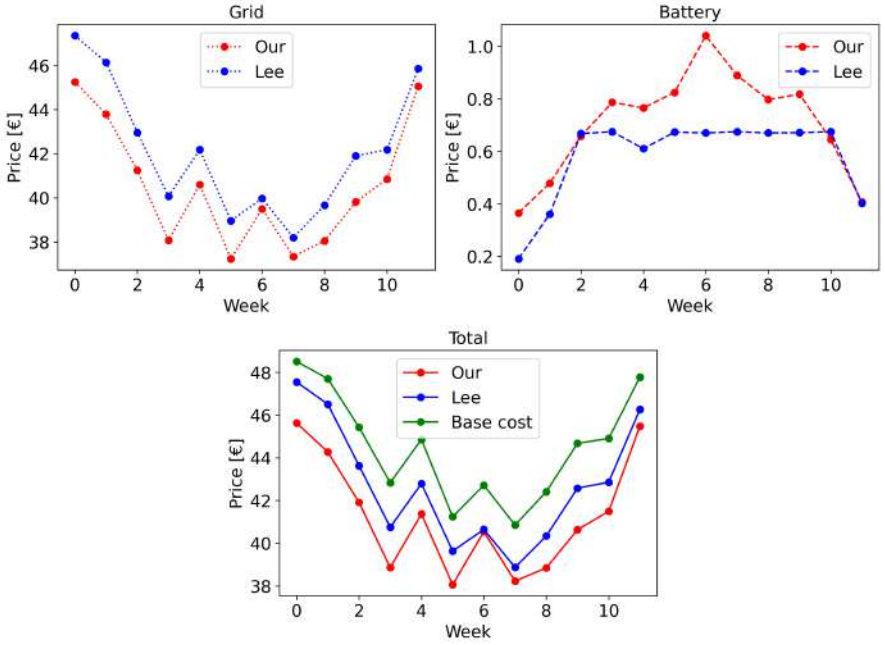

FIGURE 5.10: Total price (in €) for the optimal scheduling problem at an initial SoC of 50%. The red lines represent our method, while the blue lines represent Lee's method. (a) is the grid cost, (b) the battery cost, and (c) the total costs.

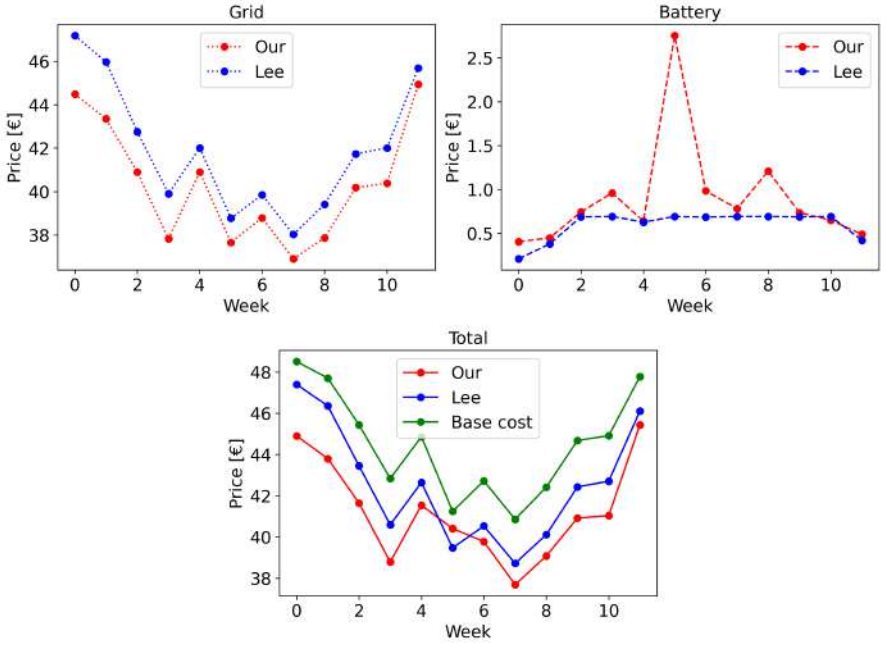

FIGURE 5.11: Total price (in €) for the optimal scheduling problem at an initial SoC of 80%. The red lines represent our method, while the blue lines represent Lee's method. (a) is the grid cost, (b) the battery cost, and (c) the total costs.

TABLE 5.4: Total costs of the proposed BESS scheduling method against method presented in [9].

	Initial SoC (%)	Intake power cost [€]	Battery usage cost [€]	Total cost [€]
Proposed method	20	488	7.89	496
	50	487	8.48	495
	80	484	10.8	495
Lee method	20	508	6.23	514
	50	505	6.94	512
	80	503	7.16	510

by the blue dashed line. These comparisons are conducted across various initial SoC values.

Notably, our methodology introduces a distinctive feature by avoiding imposing hard constraints on SoC values, in contrast to the 20% and 80% limits. This flexibility in our approach allows, depending on the PV production, the SoC to reach 100%, thereby maximizing battery utilization and effectively reducing grid consumption. We also do not impose a strong constraint for low SoC levels. However, as can be seen in Figures 5.12, 5.13 and 5.14, very rarely does the SoC drop below 20%. This is because, for low SoC levels, the battery utilization cost is high. Therefore, this methodology, based on battery cost relative to SoC, strikes a balance between minimizing grid consumption and extending battery life.

These graphical representations provide valuable insights into the dynamic behavior of the SoC under different initial conditions. They demonstrate the adaptability and potential advantages of our approach in optimizing energy storage system management within microgrids. Furthermore, they underscore the relationship between SoC, grid consumption, and battery life, reinforcing the significance of our methodology in achieving sustainable and efficient microgrid operation.

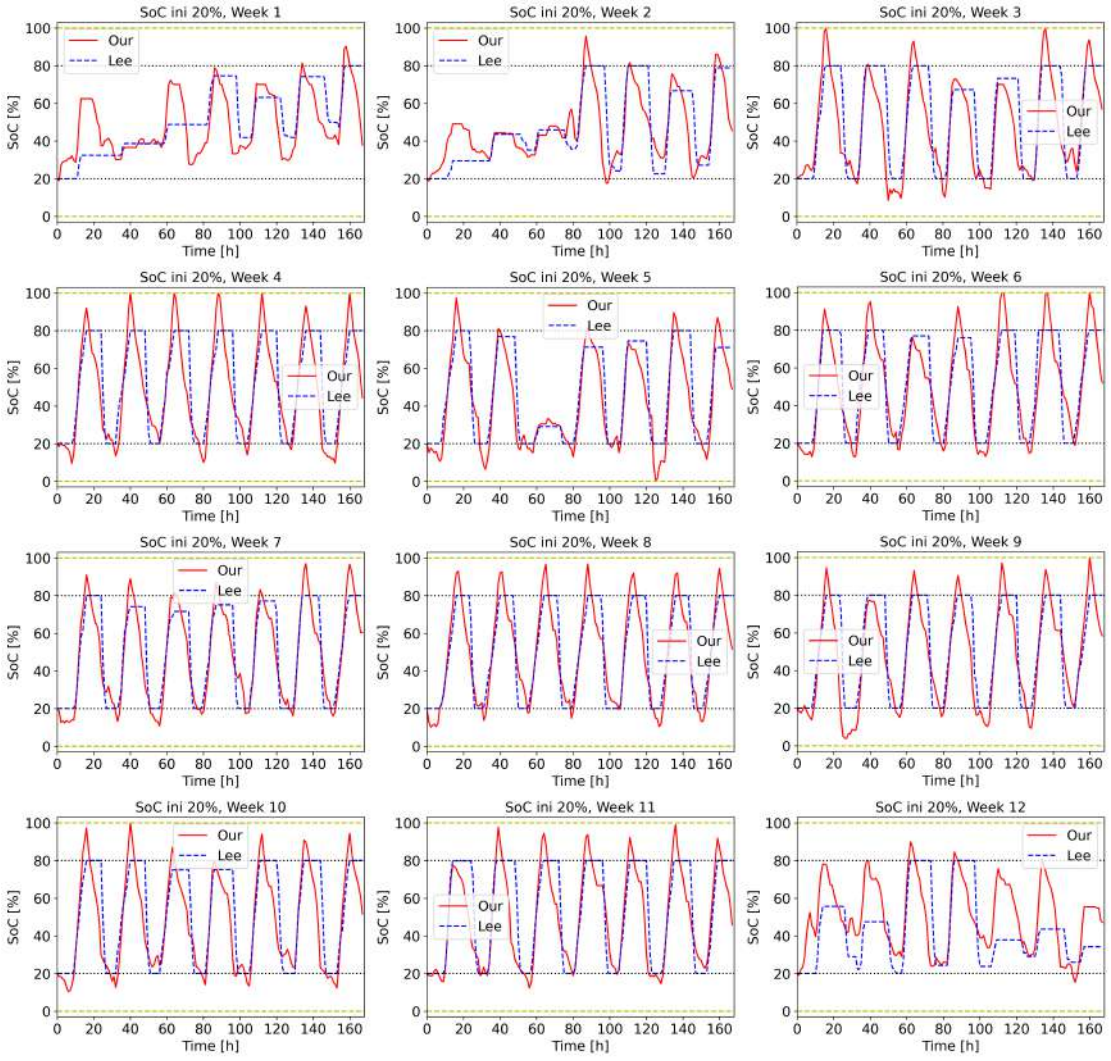

FIGURE 5.12: SoC over time for the 12 weeks of testing, our method (red line) and Lee method (blue dashed line), at initial SoC of 20%.

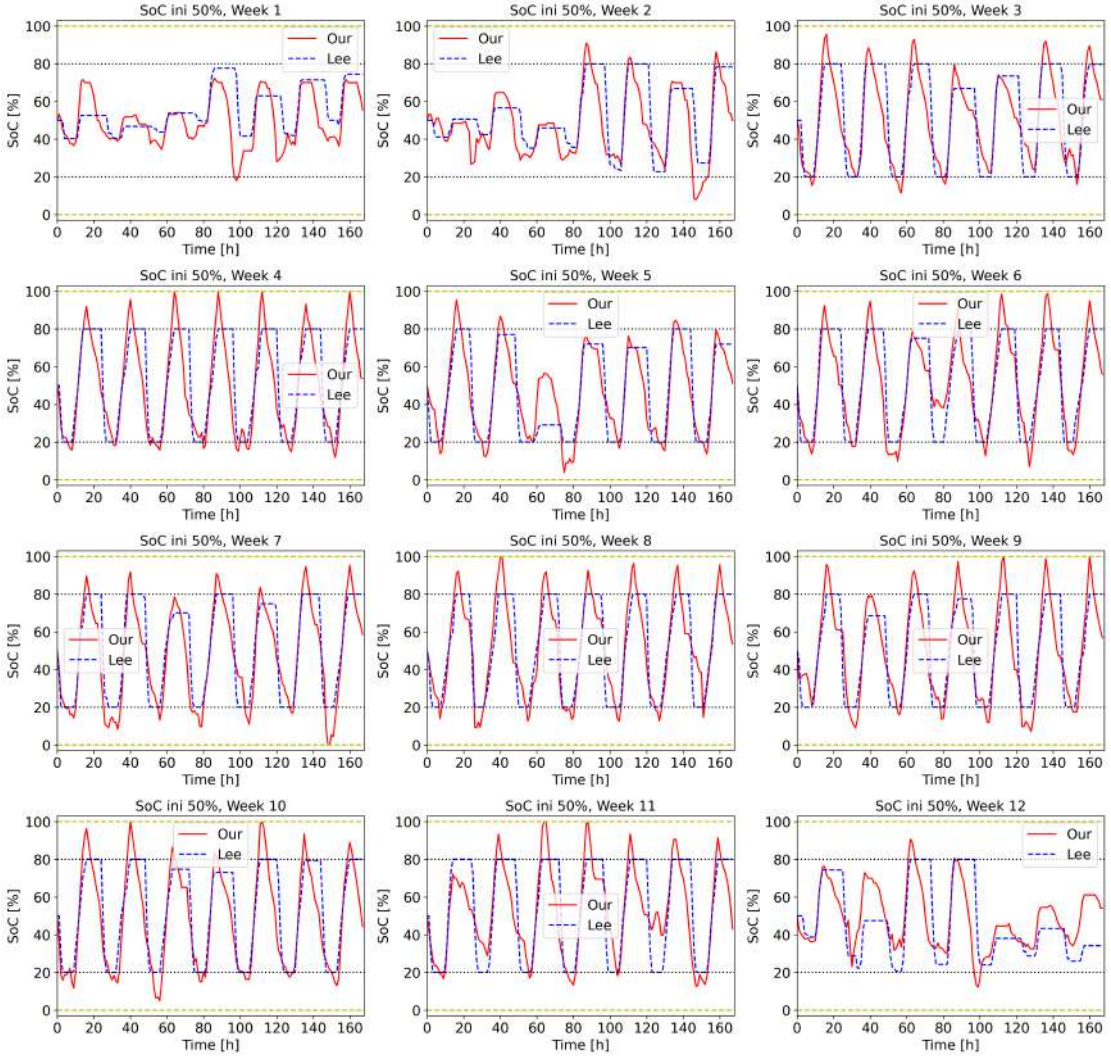

FIGURE 5.13: SoC over time for the 12 weeks of testing, our method (red line) and Lee method (blue dashed line), at initial SoC of 50%.

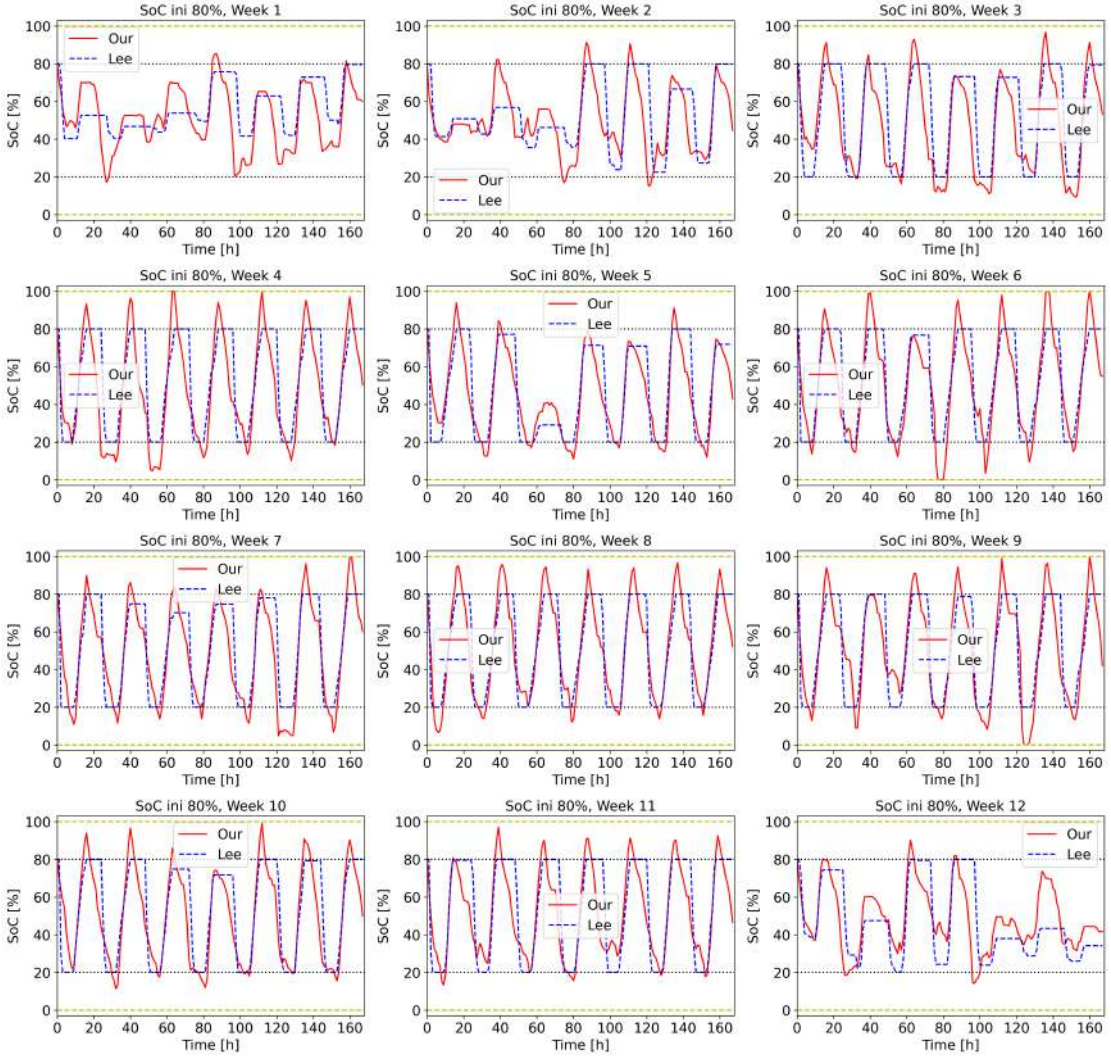

FIGURE 5.14: SoC over time for the 12 weeks of testing, our method (red line) and Lee method (blue dashed line), at initial SoC of 80%.

Finally, for a comprehensive visual analysis of the results, Figure 11, in the appendix section, graphically presents the outcomes of the BESS scheduling employing our proposed method, spanning one full day of system operation. In this figure, a dynamic representation unfolds, showcasing the evolving decision variables, namely grid power and battery power, over time, adhering to the rolling horizon strategy. In the battery power plot, positive values denote the discharge of the battery, while negative values signify the battery charging process. The dynamism in the figure becomes apparent as it progresses hour by hour. With each passing hour, the actual PV data is updated, enabling a forecast for the forthcoming 24 hours. Subsequently, the optimization problem is solved for the entire optimization horizon. However, the unique characteristic of this

method is that the decision variables are continually updated for the upcoming hour, factoring in the most recent information. This iterative and adaptive process ensures the continuous fine-tuning and adjustment of the scheduling strategy, effectively responding to the ever-changing operational conditions. For a comparative perspective, Figure 12, in the appendix section, presents analogous visualizations obtained through the utilization of the Lee method.

5.4 Conclusion

We introduced an innovative method for managing energy in DC microgrids, integrating solar irradiance forecasting and optimal scheduling while considering battery degradation expenses. We assessed battery degradation costs based on technical data, allowing us to determine how much energy the batteries generated concerning the depth of discharge (DoD). Our findings reveal that this approach provides more cost-effective and efficient scheduling of the Battery Energy Storage System (BESS). Specifically, our results displayed a 3.5% cost reduction compared to methods that rely on cycle count for estimating battery costs. These outcomes underscore the effectiveness of our approach in optimizing BESS operation and minimizing associated expenses, positioning it as a promising solution for energy management systems. Furthermore, our results indicate enhanced performance when incorporating solar irradiance forecasting alongside the rolling horizon strategy.

Chapter 6

Conclusion and Future Work

This thesis has made significant contributions to the field of renewable energy. We have addressed critical aspects of photovoltaic power potential, climate change impact assessment, artificial intelligence techniques for solar irradiance forecasting, and optimal renewable energy management. The findings and methodologies presented here contribute significantly to the field of renewable energy, offering valuable insights and practical solutions for sustainable energy generation and management.

Chapter 2 laid the groundwork for the global renewable energy landscape, the current context, and the challenges, and introduced microgrids as an alternative to integrate renewable energies in an efficient way. Photovoltaic energy emerged as a focal point due to its widespread interest and potential in the scientific community, governments, and the private sector. We presented how the challenges of photovoltaic energy have been addressed by artificial intelligence. Finally, we pointed out the current gaps that allowed us to formulate the central research question of this thesis.

Chapter 3 introduced the critical role of meteorological data in assessing photovoltaic power potential. The Colombian Solar Atlas was presented, an interactive tool that allows users to estimate photovoltaic potential in Colombia. The Atlas provides data ranging from 1998 to 2019, including future projections up to 2099. Furthermore, the chapter introduced the potential impact of climate change on photovoltaic power potential in South America. Through an analysis of solar irradiance, air temperature, and wind speed changes under different climate scenarios, we highlighted the significance of solar irradiance as the primary driver of photovoltaic potential. This chapter provides essential information for selecting optimal regions for solar energy projects, and presents

essential databases for designing artificial intelligence algorithms for optimal microgrid management.

Chapter 4 introduced a methodology for site-adaptation techniques using machine learning algorithms to achieve an improved spatio-temporal database allowing for accurate solar irradiance forecasting. By comparing machine learning-based approaches to traditional statistical methods, we demonstrated the superior performance of our approach. The improved database allows for a more accurate solar forecasting model. The forecasting model is fundamental for effective renewable energy management.

Chapter 5 presented a novel methodology for the energy management of DC microgrids. This methodology incorporated solar irradiance forecasting, optimal scheduling, and battery degradation cost considerations. Our results showed that this approach leads to more efficient and cost-effective scheduling of Battery Energy Storage Systems (BESS). It offers promising prospects for enhancing energy management systems, improving BESS performance, and reducing associated costs.

This thesis not only deepens our understanding of renewable energy, but also paves the way towards more sustainable and efficient energy generation and management practices. The methodologies and perspectives presented here hold promise for a greener and more sustainable energy future. We also hope to help communities in the non-interconnected zones through the Colombian Solar Atlas.

The lines of future work arising from this thesis include several aspects. Regarding the prediction of meteorological variables, especially solar irradiance, several works have already been presented that address this issue. However, the inclusion of other meteorological stations that provide not only temporal information, but also spatial information, can contribute to obtain spatio-temporal prediction models, and the performance of these models should be compared with the classical temporal models.

Concerning the optimal scheduling of microgrids, in this thesis, we focus on DC microgrids for a specific location with particular characteristics. It may be interesting to contrast with other locations having a different PV profile and a different grid price. It is also necessary to work on the sizing of the microgrid. This step is crucial to compare operating costs. Additionally, evaluating the health status of the batteries is important. While this thesis focused on analyzing the depth of discharge and the state of charge, a long-term analysis of battery health status can provide better indicators of battery degradation with the proposed method.

References

[1] REN21, "RENEWABLES 2023 GLOBAL STATUS REPORT ENERGY SUPPLY," tech. rep., REN21, 2023.

[2] Energy Institute, "In partnership with Statistical Review of World Energy 2023 | 72 nd edition," tech. rep., Energy Institute, 2023.

[3] D. A. Torres, J. Alexandra, B. Medina, O. Leandra, R. Luengas, S. Serrano Díaz, O. Hernán, R. Alfonso, W. Leofan, and C. Chivata, "INFORME SECTORIAL DE LA PRESTACIÓN DEL SERVICIO DE ENERGÍA ELÉCTRICA 2020," tech. rep., Superintendencia de Servicios Públicos Domiciliarios, 2020.

[4] XM, "Reporte integral de sostenibilidad, operación y mercado 2021," tech. rep., XM, Bogota, 2021.

[5] S. Ali, Z. Zheng, M. Aillerie, J.-P. Sawicki, M.-C. Péra, and D. Hissel, "A Review of DC Microgrid Energy Management Systems Dedicated to Residential Applications," *Energies*, vol. 14, no. 14, 2021.

[6] A. Bidram and A. Davoudi, "Hierarchical Structure of Microgrids Control System," *IEEE Transactions on Smart Grid*, vol. 3, no. 4, pp. 1963–1976, 2012.

[7] S. Choudhury, "Review of energy storage system technologies integration to microgrid: Types, control strategies, issues, and future prospects," *Journal of Energy Storage*, vol. 48, p. 103966, 2022.

[8] J. F. Gaviria, G. Narváez, C. Guillen, L. F. Giraldo, and M. Bressan, "Machine learning in photovoltaic systems: A review," *Renewable Energy*, vol. 196, pp. 298–318, 8 2022.

[9] J.-O. Lee and Y.-S. Kim, "Novel battery degradation cost formulation for optimal scheduling of battery energy storage systems," *International Journal of Electrical Power & Energy Systems*, vol. 137, p. 107795, 5 2022.

[10] D. Gielen, R. Gorini, N. Wagner, R. Leme, L. Gutierrez, G. Prakash, E. Asmelash, L. Janeiro, G. Gallina, G. Vale, and others, "Global energy transformation: a roadmap to 2050," tech. rep., Hydrogen Knowledge Centre, 2019.

[11] J. Conti, P. Holtberg, J. Diefenderfer, A. LaRose, J. T. Turnure, and L. Westfall, "International Energy Outlook 2016 With Projections to 2040," tech. rep., USDOE Energy Information Administration (EI) (United States), 5 2016.

[12] O. A. Al-Shahri, F. B. Ismail, M. Hannan, M. H. Lipu, A. Q. Al-Shetwi, R. Begum, N. F. Al-Muhsen, and E. Soujeri, "Solar photovoltaic energy optimization methods, challenges and issues: A comprehensive review," *Journal of Cleaner Production*, vol. 284, p. 125465, 2 2021.

[13] B. N. Stram, "Key challenges to expanding renewable energy," *Energy Policy*, vol. 96, pp. 728–734, 2016.

[14] A. M. R. Lede, M. G. Molina, M. Martinez, and P. E. Mercado, "Microgrid architectures for distributed generation: A brief review," in *2017 IEEE PES Innovative Smart Grid Technologies Conference - Latin America (ISGT Latin America)*, pp. 1–6, IEEE, 9 2017.

[15] R. Lasseter and P. Paigi, "Microgrid: a conceptual solution," in *2004 IEEE 35th Annual Power Electronics Specialists Conference (IEEE Cat. No.04CH37551)*, vol. 6, pp. 4285–4290, IEEE, 2004.

[16] E. Gaona, C. Trujillo, and J. Guacaneme, "Rural microgrids and its potential application in Colombia," *Renewable and Sustainable Energy Reviews*, vol. 51, pp. 125–137, 11 2015.

[17] J. Lopes, C. Moreira, and A. Madureira, "Defining Control Strategies for MicroGrids Islanded Operation," *IEEE Transactions on Power Systems*, vol. 21, pp. 916–924, 5 2006.

[18] S. K. Jha, P. Stoa, and K. Uhlen, "Socio-economic impact of a rural microgrid," in *2016 4th International Conference on the Development in the in Renewable Energy Technology (ICDRET)*, pp. 1–4, IEEE, 1 2016.

[19] S. Choudhury, "A comprehensive review on issues, investigations, control and protection trends, technical challenges and future directions for Microgrid technology," *International Transactions on Electrical Energy Systems*, vol. 30, p. e12446, 9 2020.

[20] D. E. Olivares, A. Mehrizi-Sani, A. H. Etemadi, C. A. Cañizares, R. Iravani, M. Kazerani, A. H. Hajimiragha, O. Gomis-Bellmunt, M. Saeedifard, R. Palma-Behnke, and others, "Trends in microgrid control," *IEEE Transactions on smart grid*, vol. 5, no. 4, pp. 1905–1919, 2014.

[21] T. Berghout, M. Benbouzid, T. Bentrcia, X. Ma, S. Djurović, and L.-H. Mouss, "Machine Learning-Based Condition Monitoring for PV Systems: State of the Art and Future Prospects," *Energies*, vol. 14, p. 6316, 10 2021.

[22] C. Voyant, G. Notton, S. Kalogirou, M. L. Nivet, C. Paoli, F. Motte, and A. Fouilloy, "Machine learning methods for solar radiation forecasting: A review," *Renewable Energy*, vol. 105, pp. 569–582, 2017.

[23] G. M. Tina, C. Ventura, S. Ferlito, and S. De Vito, "A state-of-art-review on machine-learning based methods for PV," *Applied Sciences*, vol. 11, no. 16, p. 7550, 2021.

[24] H. Yousuf, A. Y. Zainal, M. Alshurideh, and S. A. Salloum, "Artificial intelligence models in power system analysis," in *Artificial Intelligence for Sustainable Development: Theory, Practice and Future Applications*, pp. 231–242, Springer, 2021.

[25] A. B. Kanase-Patil, A. P. Kaldate, S. D. Lokhande, H. Panchal, M. Suresh, and V. Priya, "A review of artificial intelligence-based optimization techniques for the sizing of integrated renewable energy systems in smart cities," *Environmental Technology Reviews*, vol. 9, pp. 111–136, 1 2020.

[26] N.-P. Yu, C.-C. Liu, and J. Price, "Evaluation of market rules using a multi-agent system method," *IEEE Transactions on Power Systems*, vol. 25, no. 1, pp. 470–479, 2009.

[27] A. Chaouachi, R. M. Kamel, R. Andoulsi, and K. Nagasaka, "Multiobjective Intelligent Energy Management for a Microgrid," *IEEE Transactions on Industrial Electronics*, vol. 60, pp. 1688–1699, 4 2013.

[28] R. Lu, S. H. Hong, and X. Zhang, "A Dynamic pricing demand response algorithm for smart grid: Reinforcement learning approach," *Applied Energy*, vol. 220, pp. 220–230, 6 2018.

[29] E. Kuznetsova, Y.-F. Li, C. Ruiz, E. Zio, G. Ault, and K. Bell, "Reinforcement learning for microgrid energy management," *Energy*, vol. 59, pp. 133–146, 9 2013.

[30] W. Liu, P. Zhuang, H. Liang, J. Peng, and Z. Huang, "Distributed Economic Dispatch in Microgrids Based on Cooperative Reinforcement Learning," *IEEE Transactions on Neural Networks and Learning Systems*, vol. 29, pp. 2192–2203, 6 2018.

[31] P. Kofinas, A. Dounis, and G. Vouros, "Fuzzy Q-Learning for multi-agent decentralized energy management in microgrids," *Applied Energy*, vol. 219, pp. 53–67, 6 2018.

[32] D. Y. Yamashita, I. Vechiu, and J.-P. Gaubert, "A review of hierarchical control for building microgrids," *Renewable and Sustainable Energy Reviews*, vol. 118, p. 109523, 2020.

[33] M. B. Hayat, D. Ali, K. C. Monyake, L. Alagha, and N. Ahmed, "Solar energy-A look into power generation, challenges, and a solar-powered future," *International Journal of Energy Research*, vol. 43, pp. 1049–1067, 3 2019.

[34] J.-F. Gaviria, M.-I. Torres, G.-E. Narvaez, H. R. Chamorro, J. F. Jimenez, L. F. Giraldo, and M. Bressan, "Kiosol: An Intelligent Distributed Energy Resources Living Laboratory," in *2021 IEEE 22nd Workshop on Control and Modelling of Power Electronics (COMPEL)*, pp. 1–6, IEEE, 11 2021.

[35] E. Miranda, J. F. G. Fierro, G. Narváez, L. F. Giraldo, and M. Bressan, "Prediction of site-specific solar diffuse horizontal irradiance from two input variables in Colombia," *Heliyon*, vol. 7, p. e08602, 12 2021.

[36] T. M. Razykov, C. S. Ferekides, D. Morel, E. Stefanakos, H. S. Ullal, and H. M. Upadhyaya, "Solar photovoltaic electricity: Current status and future prospects," *Solar energy*, vol. 85, no. 8, pp. 1580–1608, 2011.

[37] M. Bressan, Y. El Basri, A. Galeano, and C. Alonso, "A shadow fault detection method based on the standard error analysis of I-V curves," *Renewable Energy*, vol. 99, pp. 1181–1190, 12 2016.

[38] M. E. Khodayar, "Rural electrification and expansion planning of off-grid microgrids," *The Electricity Journal*, vol. 30, pp. 68–74, 5 2017.

[39] E. O. Ogunniyi and H. Pienaar, "Overview of battery energy storage system advancement for renewable (photovoltaic) energy applications," in *2017 International Conference on the Domestic Use of Energy (DUE)*, pp. 233–239, 2017.

[40] M. de Ambiente y Desarrollo Sostenible, "IDEAM - Instituto de Hidrología, Meteorología y Estudios Ambientales." urlhttp://www.ideam.gov.co/, 2019.

[41] M. Sengupta, Y. Xie, A. Lopez, A. Habte, G. Maclaurin, and J. Shelby, "The National Solar Radiation Data Base (NSRDB)," *Renewable and Sustainable Energy Reviews*, vol. 89, no. September 2017, pp. 51–60, 2018.

[42] F. Giorgi and W. J. Gutowski, "Regional Dynamical Downscaling and the CORDEX Initiative," *Annual Review of Environment and Resources*, vol. 40, pp. 467–490, 11 2015.

[43] D. P. Van Vuuren, E. Stehfest, M. G. J. den Elzen, T. Kram, J. van Vliet, S. Deetman, M. Isaac, K. K. Goldewijk, A. Hof, A. M. Beltran, and others, "RCP2. 6: exploring the possibility to keep global mean temperature increase below 2 C," *Climatic change*, vol. 109, no. 1, pp. 95–116, 2011.

[44] K. Riahi, S. Rao, V. Krey, C. Cho, V. Chirkov, G. Fischer, G. Kindermann, N. Nakicenovic, and P. Rafaj, "RCP 8.5—A scenario of comparatively high greenhouse gas emissions," *Climatic change*, vol. 109, no. 1, pp. 33–57, 2011.

[45] G. Narvaez, L. F. Giraldo, M. Bressan, and A. Pantoja, "Machine learning for site-adaptation and solar radiation forecasting," *Renewable Energy*, vol. 167, pp. 333–342, 4 2021.

[46] G. Narvaez, L. F. Giraldo, M. Bressan, and A. Pantoja, "The impact of climate change on photovoltaic power potential in Southwestern Colombia," *Heliyon*, vol. 8, p. e11122, 10 2022.

[47] G. Narvaez, M. Bressan, A. Pantoja, and L. F. Giraldo, "Climate change impact on photovoltaic power potential in South America," *Environmental Research Communications*, vol. 5, p. 081004, 8 2023.

[48] G. Narvaez, L. F. Giraldo, M. Bressan, C. A. Guillen, M. A. Pabón, N. Díaz, M. F. Porras, B. H. Medina, F. Jiménez, G. Jiménez-Estévez, A. Pantoja, and C. Alonso, "An interactive tool for visualization and prediction of solar radiation and photovoltaic generation in Colombia," *Big Earth Data*, pp. 1–26, 3 2023.

[49] P. A. Owusu and S. Asumadu-Sarkodie, "A review of renewable energy sources, sustainability issues and climate change mitigation," *Cogent Engineering*, vol. 3, p. 1167990, 12 2016.

[50] C. Lupangu and R. C. Bansal, "A review of technical issues on the development of solar photovoltaic systems," *Renewable and Sustainable Energy Reviews*, vol. 73, pp. 950–965, 6 2017.

[51] I. Hadjipaschalis, A. Poullikkas, and V. Efthimiou, "Overview of current and future energy storage technologies for electric power applications," *Renewable and Sustainable Energy Reviews*, vol. 13, pp. 1513–1522, 8 2009.

[52] A. Molina, M. Falvey, and R. Rondanelli, "A solar radiation database for Chile," *Scientific Reports*, vol. 7, p. 14823, 11 2017.

[53] J. T. Dellosa and E. C. Palconit, "Artificial Intelligence (AI) in Renewable Energy Systems: A Condensed Review of its Applications and Techniques," in *2021 IEEE International Conference on Environment and Electrical Engineering and 2021 IEEE Industrial and Commercial Power Systems Europe (EEEIC / I&CPS Europe)*, pp. 1–6, 2021.

[54] L. Zhang, J. Ling, and M. Lin, "Artificial intelligence in renewable energy: A comprehensive bibliometric analysis," *Energy Reports*, vol. 8, pp. 14072–14088, 2022.

[55] S. K. Jha, J. Bilalovic, A. Jha, N. Patel, and H. Zhang, "Renewable energy: Present research and future scope of Artificial Intelligence," *Renewable and Sustainable Energy Reviews*, vol. 77, pp. 297–317, 2017.

[56] B. Haibe-Kains, G. A. Adam, A. Hosny, F. Khodakarami, T. Shraddha, R. Kusko, S.-A. Sansone, W. Tong, R. D. Wolfinger, C. E. Mason, W. Jones, J. Dopazo, C. Furlanello, L. Waldron, B. Wang, C. McIntosh, A. Goldenberg, A. Kundaje, C. S. Greene, T. Broderick, M. M. Hoffman, J. T. Leek, K. Korthauer, W. Huber, A. Brazma, J. Pineau, R. Tibshirani, T. Hastie, J. P. A. Ioannidis, J. Quackenbush, H. J. W. L. Aerts, and M. A. Q. C. M. S. B. o. Directors, "Transparency and reproducibility in artificial intelligence," *Nature*, vol. 586, no. 7829, pp. E14–E16, 2020.

[57] A. Ashfaq, M. Kamran, F. Rehman, N. Sarfaraz, H. U. Ilyas, and H. H. Riaz, "Role of Artificial Intelligence in Renewable Energy and its Scope in Future," in *2022 5th International Conference on Energy Conservation and Efficiency (ICECE)*, pp. 1–6, 2022.

[58] Y. Zhou, "Artificial intelligence in renewable systems for transformation towards intelligent buildings," *Energy and AI*, vol. 10, p. 100182, 2022.

[59] A. N. Abdalla, M. S. Nazir, H. Tao, S. Cao, R. Ji, M. Jiang, and L. Yao, "Integration of energy storage system and renewable energy sources based on artificial intelligence: An overview," *Journal of Energy Storage*, vol. 40, p. 102811, 2021.

[60] M. M. Vanegas Cantarero, "Of renewable energy, energy democracy, and sustainable development: A roadmap to accelerate the energy transition in developing countries," *Energy Research & Social Science*, vol. 70, p. 101716, 12 2020.

[61] F. Henao, J. P. Viteri, Y. Rodríguez, J. Gómez, and I. Dyner, "Annual and interannual complementarities of renewable energy sources in Colombia," *Renewable and Sustainable Energy Reviews*, vol. 134, p. 110318, 12 2020.

[62] E. Heylen, G. Deconinck, and D. Van Hertem, "Review and classification of reliability indicators for power systems with a high share of renewable energy sources," *Renewable and Sustainable Energy Reviews*, vol. 97, pp. 554–568, 2018.

[63] M. Iqbal, M. Azam, M. Naeem, A. S. Khwaja, and A. Anpalagan, "Optimization classification, algorithms and tools for renewable energy: A review," *Renewable and Sustainable Energy Reviews*, vol. 39, pp. 640–654, 2014.

[64] T.-Z. Ang, M. Salem, M. Kamarol, H. S. Das, M. A. Nazari, and N. Prabaharan, "A comprehensive study of renewable energy sources: Classifications, challenges and suggestions," *Energy Strategy Reviews*, vol. 43, p. 100939, 2022.

[65] N. Kannan and D. Vakeesan, "Solar energy for future world: - A review," *Renewable and Sustainable Energy Reviews*, vol. 62, pp. 1092–1105, 2016.

[66] G. K. Singh, "Solar power generation by PV (photovoltaic) technology: A review," *Energy*, vol. 53, pp. 1–13, 2013.

[67] S. A. Kalogirou, S. Karellas, V. Badescu, and K. Braimakis, "Exergy analysis on solar thermal systems: A better understanding of their sustainability," *Renewable Energy*, vol. 85, pp. 1328–1333, 2016.

[68] M. B. Hayat, D. Ali, K. C. Monyake, L. Alagha, and N. Ahmed, "Solar energy—A look into power generation, challenges, and a solar-powered future," *International Journal of Energy Research*, vol. 43, pp. 1049–1067, 3 2019.

[69] E. Kabir, P. Kumar, S. Kumar, A. A. Adelodun, and K.-H. Kim, "Solar energy: Potential and future prospects," *Renewable and Sustainable Energy Reviews*, vol. 82, pp. 894–900, 2018.

[70] G. M. Joselin Herbert, S. Iniyan, E. Sreevalsan, and S. Rajapandian, "A review of wind energy technologies," *Renewable and Sustainable Energy Reviews*, vol. 11, no. 6, pp. 1117–1145, 2007.

[71] M. I. Blanco, "The economics of wind energy," *Renewable and Sustainable Energy Reviews*, vol. 13, no. 6, pp. 1372–1382, 2009.

[72] A. D. Şahin, "Progress and recent trends in wind energy," *Progress in Energy and Combustion Science*, vol. 30, no. 5, pp. 501–543, 2004.

[73] P. Veers, K. Dykes, E. Lantz, S. Barth, C. L. Bottasso, O. Carlson, A. Clifton, J. Green, P. Green, H. Holttinen, D. Laird, V. Lehtomäki, J. K. Lundquist, J. Manwell, M. Marquis, C. Meneveau, P. Moriarty, X. Munduate, M. Muskulus, J. Naughton, L. Pao, J. Paquette, J. Peinke, A. Robertson, J. Sanz Rodrigo, A. M. Sempreviva, J. C. Smith, A. Tuohy, and R. Wiser, "Grand challenges in the science of wind energy," *Science*, vol. 366, p. eaau2027, 10 2019.

[74] J. O. Dabiri, J. R. Greer, J. R. Koseff, P. Moin, and J. Peng, "A new approach to wind energy: Opportunities and challenges," *AIP Conference Proceedings*, vol. 1652, pp. 51–57, 3 2015.

[75] P. Pinson, "Wind Energy: Forecasting Challenges for Its Operational Management," *Statistical Science*, vol. 28, pp. 564–585, 11 2013.

[76] N. Kishor, R. P. Saini, and S. P. Singh, "A review on hydropower plant models and control," *Renewable and Sustainable Energy Reviews*, vol. 11, no. 5, pp. 776–796, 2007.

[77] A. Bartle, "Hydropower potential and development activities," *Energy Policy*, vol. 30, no. 14, pp. 1231–1239, 2002.

[78] D. K. Okot, "Review of small hydropower technology," *Renewable and Sustainable Energy Reviews*, vol. 26, pp. 515–520, 2013.

[79] C. S. Kaunda, C. Z. Kimambo, and T. K. Nielsen, "Hydropower in the Context of Sustainable Energy Supply: A Review of Technologies and Challenges," *ISRN Renewable Energy*, vol. 2012, p. 730631, 2012.

[80] R. Saidur, E. A. Abdelaziz, A. Demirbas, M. S. Hossain, and S. Mekhilef, "A review on biomass as a fuel for boilers," *Renewable and Sustainable Energy Reviews*, vol. 15, no. 5, pp. 2262–2289, 2011.

[81] A. Tursi, "A review on biomass: importance, chemistry, classification, and conversion," *Biofuel Research Journal*, vol. 6, no. 2, pp. 962–979, 2019.

[82] T. Bridgwater, "Biomass for energy," *Journal of the Science of Food and Agriculture*, vol. 86, pp. 1755–1768, 9 2006.

[83] J. W. Lund and T. L. Boyd, "Direct utilization of geothermal energy 2015 worldwide review," *Geothermics*, vol. 60, pp. 66–93, 2016.

[84] D. L. Gallup, "Production engineering in geothermal technology: A review," *Geothermics*, vol. 38, no. 3, pp. 326–334, 2009.

[85] E. Barbier, "Geothermal energy technology and current status: an overview," *Renewable and Sustainable Energy Reviews*, vol. 6, no. 1, pp. 3–65, 2002.

[86] INTERNATIONAL ENERGY AGENCY, "World Energy Outlook 2022," tech. rep., INTERNATIONAL ENERGY AGENCY, 2022.

[87] International Energy Agency, "Guidebook for Improved Electricity Access Statistics," tech. rep., International Energy Agency, 2023.

[88] W. Su, J. Wang, and J. Roh, "Stochastic Energy Scheduling in Microgrids With Intermittent Renewable Energy Resources," *IEEE Transactions on Smart Grid*, vol. 5, no. 4, pp. 1876–1883, 2014.

[89] A. D. Mills and R. H. Wiser, "Implications of geographic diversity for short-term variability and predictability of solar power," in *2011 IEEE Power and Energy Society General Meeting*, pp. 1–9, 2011.

[90] M. Šúri, T. A. Huld, E. D. Dunlop, and H. A. Ossenbrink, "Potential of solar electricity generation in the European Union member states and candidate countries," *Solar Energy*, vol. 81, pp. 1295–1305, 10 2007.

[91] K. Surana and S. M. Jordaan, "The climate mitigation opportunity behind global power transmission and distribution," *Nature Climate Change*, vol. 9, no. 9, pp. 660–665, 2019.

[92] I. Worighi, A. Maach, A. Hafid, O. Hegazy, and J. Van Mierlo, "Integrating renewable energy in smart grid system: Architecture, virtualization and analysis," *Sustainable Energy, Grids and Networks*, vol. 18, p. 100226, 6 2019.

[93] Z. Dobrotkova, K. Surana, and P. Audinet, "The price of solar energy: Comparing competitive auctions for utility-scale solar PV in developing countries," *Energy Policy*, vol. 118, pp. 133–148, 7 2018.

[94] L. Dusonchet and E. Telaretti, "Economic analysis of different supporting policies for the production of electrical energy by solar photovoltaics in western European Union countries," *Energy Policy*, vol. 38, pp. 3297–3308, 7 2010.

[95] A. Sangwongwanich, Y. Yang, D. Sera, and F. Blaabjerg, "Lifetime Evaluation of Grid-Connected PV Inverters Considering Panel Degradation Rates and Installation Sites," *IEEE Transactions on Power Electronics*, vol. 33, no. 2, pp. 1225–1236, 2018.

[96] L. Eyraud, B. Clements, and A. Wane, "Green investment: Trends and determinants," *Energy Policy*, vol. 60, pp. 852–865, 9 2013.

[97] J. P. Painuly, "Barriers to renewable energy penetration; a framework for analysis," *Renewable Energy*, vol. 24, pp. 73–89, 9 2001.

[98] World Bank Group, "BEYOND CONNECTIONS Energy Access Redefined," tech. rep., World Bank Group, 2015.

[99] S. Impram, S. Varbak Nese, and B. Oral, "Challenges of renewable energy penetration on power system flexibility: A survey," *Energy Strategy Reviews*, vol. 31, p. 100539, 2020.

[100] B. Muruganantham, R. Gnanadass, and N. P. Padhy, "Challenges with renewable energy sources and storage in practical distribution systems," *Renewable and Sustainable Energy Reviews*, vol. 73, pp. 125–134, 2017.

[101] G. M. Shafiullah, A. M. T. Oo, D. Jarvis, A. B. M. S. Ali, and P. Wolfs, "Potential challenges: Integrating renewable energy with the smart grid," in *2010 20th Australasian Universities Power Engineering Conference*, pp. 1–6, 2010.

[102] S. Ould Amrouche, D. Rekioua, T. Rekioua, and S. Bacha, "Overview of energy storage in renewable energy systems," *International Journal of Hydrogen Energy*, vol. 41, no. 45, pp. 20914–20927, 2016.

[103] W. Pantoja, J. A. Perez-Taborda, and A. Avila, "Tug-of-War in the Selection of Materials for Battery Technologies," *Batteries*, vol. 8, no. 9, p. 105, 2022.

[104] M. H. Rehmani, M. Reisslein, A. Rachedi, M. Erol-Kantarci, and M. Radenkovic, "Integrating Renewable Energy Resources Into the Smart Grid: Recent Developments in Information and Communication Technologies," *IEEE Transactions on Industrial Informatics*, vol. 14, no. 7, pp. 2814–2825, 2018.

[105] M. Yekini Suberu, M. Wazir Mustafa, and N. Bashir, "Energy storage systems for renewable energy power sector integration and mitigation of intermittency," *Renewable and Sustainable Energy Reviews*, vol. 35, pp. 499–514, 7 2014.

[106] A. Savaresi, "The Paris Agreement: a new beginning?," *Journal of Energy & Natural Resources Law*, vol. 34, pp. 16–26, 1 2016.

[107] O. Pupo-Roncallo, J. Campillo, D. Ingham, K. Hughes, and M. Pourkashanian, "Large scale integration of renewable energy sources (RES) in the future Colombian energy system," *Energy*, vol. 186, p. 115805, 11 2019.

[108] G. Carvajal-Romo, M. Valderrama-Mendoza, D. Rodríguez-Urrego, and L. Rodríguez-Urrego, "Assessment of solar and wind energy potential in La Guajira, Colombia: Current status, and future prospects," *Sustainable Energy Technologies and Assessments*, vol. 36, p. 100531, 12 2019.

[109] M. Jimenez, C. J. Franco, and I. Dyner, "Diffusion of renewable energy technologies: The need for policy in Colombia," *Energy*, vol. 111, pp. 818–829, 9 2016.

[110] T. Gómez-Navarro and D. Ribó-Pérez, "Assessing the obstacles to the participation of renewable energy sources in the electricity market of Colombia," *Renewable and Sustainable Energy Reviews*, vol. 90, pp. 131–141, 7 2018.

[111] D. Rodríguez-Urrego and L. Rodríguez-Urrego, "Photovoltaic energy in Colombia: Current status, inventory, policies and future prospects," *Renewable and Sustainable Energy Reviews*, vol. 92, no. May 2017, pp. 160–170, 2018.

[112] J. Arias-Gaviria, S. X. Carvajal-Quintero, and S. Arango-Aramburo, "Understanding dynamics and policy for renewable energy diffusion in Colombia," *Renewable Energy*, vol. 139, pp. 1111–1119, 8 2019.

[113] L. Hernández-Callejo, S. Gallardo-Saavedra, and V. Alonso-Gómez, "A review of photovoltaic systems: Design, operation and maintenance," *Solar Energy*, vol. 188, pp. 426–440, 8 2019.

[114] R. Palma-Behnke, C. Benavides, F. Lanas, B. Severino, L. Reyes, J. Llanos, and D. Saez, "A Microgrid Energy Management System Based on the Rolling Horizon Strategy," *IEEE Transactions on Smart Grid*, vol. 4, pp. 996–1006, 6 2013.

[115] M. S. Javed, J. Jurasz, M. McPherson, Y. Dai, and T. Ma, "Quantitative evaluation of renewable-energy-based remote microgrids: curtailment, load shifting, and reliability," *Renewable and Sustainable Energy Reviews*, vol. 164, p. 112516, 2022.

[116] J. A. P. Lopes, A. G. Madureira, and C. Moreira, "A View of Microgrids," in *Advances in Energy Systems*, ch. 9, pp. 149–166, Wiley Online Library, 3 2019.

[117] Q. Ai, X. Wang, and X. He, "The impact of large-scale distributed generation on power grid and microgrids," *Renewable Energy*, vol. 62, pp. 417–423, 2014.

[118] G. Shahgholian, "A brief review on microgrids: Operation, applications, modeling, and control," *International Transactions on Electrical Energy Systems*, vol. 31, p. e12885, 6 2021.

[119] A. Khalid, A. Stevenson, and A. I. Sarwat, "Overview of Technical Specifications for Grid-Connected Microgrid Battery Energy Storage Systems," *IEEE Access*, vol. 9, pp. 163554–163593, 2021.

[120] M. E. T. Souza and L. C. G. Freitas, "Grid-Connected and Seamless Transition Modes for Microgrids: An Overview of Control Methods, Operation Elements, and General Requirements," *IEEE Access*, vol. 10, pp. 97802–97834, 2022.

[121] J. Li, Y. Xue, L. Tian, and X. Yuan, "Research on optimal configuration strategy of energy storage capacity in grid-connected microgrid," *Protection and Control of Modern Power Systems*, vol. 2, no. 1, p. 35, 2017.

[122] T. L. Vandoorn, J. D. M. De Kooning, B. Meersman, and L. Vandevelde, "Review of primary control strategies for islanded microgrids with power-electronic interfaces," *Renewable and Sustainable Energy Reviews*, vol. 19, pp. 613–628, 2013.

[123] A. A. Anderson and S. Suryanarayanan, "Review of energy management and planning of islanded microgrids," *CSEE Journal of Power and Energy Systems*, vol. 6, no. 2, pp. 329–343, 2020.

[124] J. M. Raya-Armenta, N. Bazmohammadi, J. G. Avina-Cervantes, D. Sáez, J. C. Vasquez, and J. M. Guerrero, "Energy management system optimization in islanded microgrids: An overview and future trends," *Renewable and Sustainable Energy Reviews*, vol. 149, p. 111327, 2021.

[125] J. J. Justo, F. Mwasilu, J. Lee, and J.-W. Jung, "AC-microgrids versus DC-microgrids with distributed energy resources: A review," *Renewable and Sustainable Energy Reviews*, vol. 24, pp. 387–405, 2013.

[126] Y. Khayat, Q. Shafiee, R. Heydari, M. Naderi, T. Dragičević, J. W. Simpson-Porco, F. Dörfler, M. Fathi, F. Blaabjerg, J. M. Guerrero, and H. Bevrani, "On the Secondary Control Architectures of AC Microgrids: An Overview," *IEEE Transactions on Power Electronics*, vol. 35, no. 6, pp. 6482–6500, 2020.

[127] K. S. Rajesh, S. S. Dash, R. Rajagopal, and R. Sridhar, "A review on control of ac microgrid," *Renewable and Sustainable Energy Reviews*, vol. 71, pp. 814–819, 2017.

[128] B. Patnaik, M. Mishra, R. C. Bansal, and R. K. Jena, "AC microgrid protection – A review: Current and future prospective," *Applied Energy*, vol. 271, p. 115210, 2020.

[129] A. T. Elsayed, A. A. Mohamed, and O. A. Mohammed, "DC microgrids and distribution systems: An overview," *Electric Power Systems Research*, vol. 119, pp. 407–417, 2015.

[130] T. Dragičević, X. Lu, J. C. Vasquez, and J. M. Guerrero, "DC Microgrids—Part I: A Review of Control Strategies and Stabilization Techniques," *IEEE Transactions on Power Electronics*, vol. 31, no. 7, pp. 4876–4891, 2016.

[131] F. S. Al-Ismail, "DC Microgrid Planning, Operation, and Control: A Comprehensive Review," *IEEE Access*, vol. 9, pp. 36154–36172, 2021.

[132] U. Manandhar, A. Ukil, and T. K. K. Jonathan, "Efficiency comparison of DC and AC microgrid," in *2015 IEEE Innovative Smart Grid Technologies - Asia (ISGT ASIA)*, pp. 1–6, 2015.

[133] D. Fregosi, S. Ravula, D. Brhlik, J. Saussele, S. Frank, E. Bonnema, J. Scheib, and E. Wilson, "A comparative study of DC and AC microgrids in commercial buildings across different climates and operating profiles," in *2015 IEEE First International Conference on DC Microgrids (ICDCM)*, pp. 159–164, 2015.

[134] M. H. Andishgar, E. Gholipour, and R.-a. Hooshmand, "An overview of control approaches of inverter-based microgrids in islanding mode of operation," *Renewable and Sustainable Energy Reviews*, vol. 80, pp. 1043–1060, 2017.

[135] Z. Cheng, J. Duan, and M. Y. Chow, "To Centralize or to Distribute: That Is the Question: A Comparison of Advanced Microgrid Management Systems," *IEEE Industrial Electronics Magazine*, vol. 12, no. 1, pp. 6–24, 2018.

[136] F. Yang, X. Feng, and Z. Li, "Advanced Microgrid Energy Management System for Future Sustainable and Resilient Power Grid," *IEEE Transactions on Industry Applications*, vol. 55, no. 6, pp. 7251–7260, 2019.

[137] L. Ahmethodzic and M. Music, "Comprehensive review of trends in microgrid control," *Renewable Energy Focus*, vol. 38, pp. 84–96, 2021.

[138] A. G. Tsikalakis and N. D. Hatziargyriou, "Centralized control for optimizing microgrids operation," in *2011 IEEE Power and Energy Society General Meeting*, pp. 1–8, 2011.

[139] A. Kaur, J. Kaushal, and P. Basak, "A review on microgrid central controller," *Renewable and Sustainable Energy Reviews*, vol. 55, pp. 338–345, 2016.

[140] D. Espín-Sarzosa, R. Palma-Behnke, and O. Núñez-Mata, "Energy Management Systems for Microgrids: Main Existing Trends in Centralized Control Architectures," *Energies*, vol. 13, no. 3, 2020.

[141] Y. Gu, X. Xiang, W. Li, and X. He, "Mode-Adaptive Decentralized Control for Renewable DC Microgrid With Enhanced Reliability and Flexibility," *IEEE Transactions on Power Electronics*, vol. 29, no. 9, pp. 5072–5080, 2014.

[142] Q. Li, F. Chen, M. Chen, J. M. Guerrero, and D. Abbott, "Agent-Based Decentralized Control Method for Islanded Microgrids," *IEEE Transactions on Smart Grid*, vol. 7, no. 2, pp. 637–649, 2016.

[143] J. M. Guerrero, M. Chandorkar, T. L. Lee, and P. C. Loh, "Advanced Control Architectures for Intelligent Microgrids—Part I: Decentralized and Hierarchical Control," *IEEE Transactions on Industrial Electronics*, vol. 60, no. 4, pp. 1254–1262, 2013.

[144] M. Shirkhani, J. Tavoosi, S. Danyali, A. K. Sarvenoee, A. Abdali, A. Mohammadzadeh, and C. Zhang, "A review on microgrid decentralized energy/voltage control structures and methods," *Energy Reports*, vol. 10, pp. 368–380, 2023.

[145] E. Espina, J. Llanos, C. Burgos-Mellado, R. Cárdenas-Dobson, M. Martínez-Gómez, and D. Sáez, "Distributed Control Strategies for Microgrids: An Overview," *IEEE Access*, vol. 8, pp. 193412–193448, 2020.

[146] Q. Zhou, M. Shahidehpour, A. Paaso, S. Bahramirad, A. Alabdulwahab, and A. Abusorrah, "Distributed Control and Communication Strategies in Networked Microgrids," *IEEE Communications Surveys & Tutorials*, vol. 22, no. 4, pp. 2586–2633, 2020.

[147] A. Mehrizi-Sani, "Chapter 2 - Distributed Control Techniques in Microgrids," in *Microgrid* (M. S. Mahmoud, ed.), pp. 43–62, Butterworth-Heinemann, 2017.

[148] K. Zuo and L. Wu, "A review of decentralized and distributed control approaches for islanded microgrids: Novel designs, current trends, and emerging challenges," *The Electricity Journal*, vol. 35, no. 5, p. 107138, 2022.

[149] J. Quesada, R. Sebastián, M. Castro, and J. A. Sainz, "Control of inverters in a low voltage microgrid with distributed battery energy storage. Part I: Primary control," *Electric Power Systems Research*, vol. 114, pp. 126–135, 9 2014.

[150] Q. Shafiee, J. M. Guerrero, and J. C. Vasquez, "Distributed Secondary Control for Islanded Microgrids—A Novel Approach," *IEEE Transactions on Power Electronics*, vol. 29, no. 2, pp. 1018–1031, 2014.

[151] S. Moayedi and A. Davoudi, "Distributed Tertiary Control of DC Microgrid Clusters," *IEEE Transactions on Power Electronics*, vol. 31, no. 2, pp. 1717–1733, 2016.

[152] A. Abhishek, A. Ranjan, S. Devassy, B. Kumar Verma, S. K. Ram, and A. K. Dhakar, "Review of hierarchical control strategies for DC microgrid," *IET Renewable Power Generation*, vol. 14, pp. 1631–1640, 7 2020.

[153] S. Hajiaghasi, A. Salemnia, and M. Hamzeh, "Hybrid energy storage system for microgrids applications: A review," *Journal of Energy Storage*, vol. 21, pp. 543–570, 2019.

[154] R. Georgious, R. Refaat, J. Garcia, and A. A. Daoud, "Review on Energy Storage Systems in Microgrids," *Electronics*, vol. 10, no. 17, 2021.

[155] X. Tan, Q. Li, and H. Wang, "Advances and trends of energy storage technology in Microgrid," *International Journal of Electrical Power & Energy Systems*, vol. 44, pp. 179–191, 1 2013.

[156] H. Zsiborács, N. H. Baranyai, A. Vincze, L. Zentkó, Z. Birkner, K. Máté, and G. Pintér, "Intermittent Renewable Energy Sources: The Role of Energy Storage in the European Power System of 2040," *Electronics*, vol. 8, no. 7, 2019.

[157] M. Mahmoud, M. Ramadan, A.-G. Olabi, K. Pullen, and S. Naher, "A review of mechanical energy storage systems combined with wind and solar applications," *Energy Conversion and Management*, vol. 210, p. 112670, 2020.

[158] T. S. Mathis, N. Kurra, X. Wang, D. Pinto, P. Simon, and Y. Gogotsi, "Energy Storage Data Reporting in Perspective—Guidelines for Interpreting the Performance of Electrochemical Energy Storage Systems," *Advanced Energy Materials*, vol. 9, p. 1902007, 10 2019.

[159] Z. Yang, J. Zhang, M. C. W. Kintner-Meyer, X. Lu, D. Choi, J. P. Lemmon, and J. Liu, "Electrochemical Energy Storage for Green Grid," *Chemical Reviews*, vol. 111, pp. 3577–3613, 5 2011.

[160] K. Zou, W. Deng, P. Cai, X. Deng, B. Wang, C. Liu, J. Li, H. Hou, G. Zou, and X. Ji, "Prelithiation/Presodiation Techniques for Advanced Electrochemical Energy Storage Systems: Concepts, Applications, and Perspectives," *Advanced Functional Materials*, vol. 31, p. 2005581, 1 2021.

[161] H. Chen, T. N. Cong, W. Yang, C. Tan, Y. Li, and Y. Ding, "Progress in electrical energy storage system: A critical review," *Progress in Natural Science*, vol. 19, no. 3, pp. 291–312, 2009.

[162] B. Zakeri and S. Syri, "Electrical energy storage systems: A comparative life cycle cost analysis," *Renewable and Sustainable Energy Reviews*, vol. 42, pp. 569–596, 2015.

[163] N. S. Wade, P. C. Taylor, P. D. Lang, and P. R. Jones, "Evaluating the benefits of an electrical energy storage system in a future smart grid," *Energy Policy*, vol. 38, no. 11, pp. 7180–7188, 2010.

[164] W. Smith, "The role of fuel cells in energy storage," *Journal of Power Sources*, vol. 86, pp. 74–83, 3 2000.

[165] M. S. Shin, H. S. Kim, D. S. Jang, S. N. Lee, Y. S. Lee, and H. G. Yoon, "Numerical and experimental study on the design of a stratified thermal storage system," *Applied Thermal Engineering*, vol. 24, pp. 17–27, 1 2004.

[166] M. Liu, W. Saman, and F. Bruno, "Review on storage materials and thermal performance enhancement techniques for high temperature phase change thermal storage systems," *Renewable and Sustainable Energy Reviews*, vol. 16, pp. 2118–2132, 5 2012.

[167] S. Jegadheeswaran and S. D. Pohekar, "Performance enhancement in latent heat thermal storage system: A review," *Renewable and Sustainable Energy Reviews*, vol. 13, pp. 2225–2244, 12 2009.

[168] M. Moncecchi, C. Brivio, S. Mandelli, and M. Merlo, "Battery Energy Storage Systems in Microgrids: Modeling and Design Criteria," *Energies*, vol. 13, no. 8, 2020.

[169] Y. Zhang, C.-g. Zhou, J. Yang, S.-c. Xue, H.-l. Gao, X.-h. Yan, Q.-y. Huo, S.-w. Wang, Y. Cao, J. Yan, K.-z. Gao, and L.-x. Wang, "Advances and challenges in improvement of the electrochemical performance for lead-acid batteries: A comprehensive review," *Journal of Power Sources*, vol. 520, p. 230800, 2022.

[170] P. K. Nayak, E. M. Erickson, F. Schipper, T. R. Penki, N. Munichandraiah, P. Adelhelm, H. Sclar, F. Amalraj, B. Markovsky, and D. Aurbach, "Review on Challenges and Recent Advances in the Electrochemical Performance of High Capacity Li- and Mn-Rich Cathode Materials for Li-Ion Batteries," *Advanced Energy Materials*, vol. 8, p. 1702397, 3 2018.

[171] P. L. C. García-Miguel, J. Alonso-Martínez, S. Arnaltes Gómez, M. García Plaza, and A. P. Asensio, "A Review on the Degradation Implementation for the Operation of Battery Energy Storage Systems," *Batteries*, vol. 8, p. 110, 9 2022.

[172] D. Michaelson, H. Mahmood, and J. Jiang, "A Predictive Energy Management System Using Pre-Emptive Load Shedding for Islanded Photovoltaic Microgrids," *IEEE Transactions on Industrial Electronics*, vol. 64, pp. 5440–5448, 7 2017.

[173] W. Ropero-Castaño, N. Muñoz-Galeano, E. F. Caicedo-Bravo, P. Maya-Duque, and J. M. López-Lezama, "Sizing Assessment of Islanded Microgrids Considering Total Investment Cost and Tax Benefits in Colombia," *Energies*, vol. 15, no. 14, 2022.

[174] I. Granit, "Microgrids through the Energy-Water-Food Security Nexus in La Guajira, Colombia: Increasing water and food security or jeopardizing groundwater levels?," *Energy Research & Social Science*, vol. 93, p. 102814, 11 2022.

[175] C. Hoyos-Velandia, L. Ramirez-Hurtado, J. Quintero-Restrepo, R. Moreno-Chuquen, and F. Gonzalez-Longatt, "Cost Functions for Generation Dispatching in Microgrids for Non-Interconnected Zones in Colombia," *Energies*, vol. 15, no. 7, 2022.

[176] Y. Yoldaş, A. Önen, S. M. Muyeen, A. V. Vasilakos, and I. Alan, "Enhancing smart grid with microgrids: Challenges and opportunities," *Renewable and Sustainable Energy Reviews*, vol. 72, pp. 205–214, 5 2017.

[177] A. Agüera-Pérez, J. C. Palomares-Salas, J. J. González de la Rosa, and O. Florencias-Oliveros, "Weather forecasts for microgrid energy management: Review, discussion and recommendations," *Applied Energy*, vol. 228, pp. 265–278, 10 2018.

[178] M. Faisal, M. A. Hannan, P. J. Ker, A. Hussain, M. B. Mansor, and F. Blaabjerg, "Review of Energy Storage System Technologies in Microgrid Applications: Issues and Challenges," *IEEE Access*, vol. 6, pp. 35143–35164, 2018.

[179] S. T. Blesslin, G. J. J. Wessley, V. Kanagaraj, S. Kamatchi, A. Radhika, and D. A. Janeera, "Microgrid Optimization and Integration of Renewable Energy Resources: Innovation, Challenges and Prospects," in *Integration of Renewable Energy Sources with Smart Grid*, ch. 11, pp. 239–262, Wiley Online Library, 10 2021.

[180] S. X. Chen, H. B. Gooi, and M. Q. Wang, "Sizing of Energy Storage for Microgrids," *IEEE Transactions on Smart Grid*, vol. 3, no. 1, pp. 142–151, 2012.

[181] E. Gul, G. Baldinelli, P. Bartocci, F. Bianchi, P. Domenighini, F. Cotana, and J. Wang, "A techno-economic analysis of a solar PV and DC battery storage system for a community energy sharing," *Energy*, vol. 244, p. 123191, 4 2022.

[182] A. Omazic, G. Oreski, M. Halwachs, G. C. Eder, C. Hirschl, L. Neumaier, G. Pinter, and M. Erceg, "Relation between degradation of polymeric components in crystalline silicon PV module and climatic conditions: A literature review," *Solar Energy Materials and Solar Cells*, vol. 192, pp. 123–133, 4 2019.

[183] A. M. Humada, S. Y. Darweesh, K. G. Mohammed, M. Kamil, S. F. Mohammed, N. K. Kasim, T. A. Tahseen, O. I. Awad, and S. Mekhilef, "Modeling of PV system and parameter extraction based on experimental data: Review and investigation," *Solar Energy*, vol. 199, pp. 742–760, 3 2020.

[184] C. Zhang, J. Zhang, Y. Hao, Z. Lin, and C. Zhu, "A simple and efficient solar cell parameter extraction method from a single current-voltage curve," *Journal of Applied Physics*, vol. 110, 9 2011.

[185] R. W. Andrews, A. Pollard, and J. M. Pearce, "Improved parametric empirical determination of module short circuit current for modelling and optimization of solar photovoltaic systems," *Solar Energy*, vol. 86, pp. 2240–2254, 9 2012.

[186] M. Bressan, *Développement d'un outil de supervision et de contrôle pour une installation solaire photovoltaïque.* PhD thesis, Université de Perpignan, 2014.

[187] A. Gutiérrez Galeano, *Study of Photovoltaic System Integration in Microgrids through Real-Time Modeling and Emulation of its Components Using HiLeS.* PhD thesis, Université Toulouse 3 Paul Sabatier, 2017.

[188] L. Antonio García-Gutiérrez, *Development of an Active-Fault Tolerant Control Applied to PV systems.* PhD thesis, Université Toulouse 3 Paul Sabatier, 2020.

[189] M. Gaetani-Liseo and M. Gaetani, *Prise en compte des systèmes de stockage de l'énergie et de leurs dégradations dans la gestion et le dimensionnement des micro-réseaux : influence de la précision des modèles.* PhD thesis, Université Toulouse 3 Paul Sabatier, 2022.

[190] M. M. Fouad, L. A. Shihata, and E. S. I. Morgan, "An integrated review of factors influencing the perfomance of photovoltaic panels," *Renewable and Sustainable Energy Reviews*, vol. 80, pp. 1499–1511, 12 2017.

[191] C. Brunet, O. Savadogo, P. Baptiste, M. A. Bouchard, C. Cholez, C. Gendron, and N. Merveille, "The three paradoxes of the energy transition - Assessing sustainability of large-scale solar photovoltaic through multi-level and multi-scalar perspective in Rwanda," *Journal of Cleaner Production*, vol. 288, p. 125519, 3 2021.

[192] Z. A. Elum and A. S. Momodu, "Climate change mitigation and renewable energy for sustainable development in Nigeria: A discourse approach," *Renewable and Sustainable Energy Reviews*, vol. 76, pp. 72–80, 2017.

[193] K. R. Abbasi, M. Shahbaz, J. Zhang, M. Irfan, and R. Alvarado, "Analyze the environmental sustainability factors of China: The role of fossil fuel energy and renewable energy," *Renewable Energy*, vol. 187, pp. 390–402, 2022.

[194] T. V. Ramachandra and B. V. Shruthi, "Spatial mapping of renewable energy potential," *Renewable and Sustainable Energy Reviews*, vol. 11, no. 7, pp. 1460–1480, 2007.

[195] J. Ondraczek, "Are we there yet? Improving solar PV economics and power planning in developing countries: The case of Kenya," *Renewable and Sustainable Energy Reviews*, vol. 30, pp. 604–615, 2 2014.

[196] M. Šúri, T. A. Huld, and E. D. Dunlop, "PV-GIS: a web-based solar radiation database for the calculation of PV potential in Europe," *International Journal of Sustainable Energy*, vol. 24, pp. 55–67, 6 2005.

[197] T. AlSkaif, S. Dev, L. Visser, M. Hossari, and W. van Sark, "A systematic analysis of meteorological variables for PV output power estimation," *Renewable Energy*, vol. 153, pp. 12–22, 6 2020.

[198] P. Denholm and R. M. Margolis, "Evaluating the limits of solar photovoltaics (PV) in traditional electric power systems," *Energy Policy*, vol. 35, pp. 2852–2861, 5 2007.

[199] S. M. Besarati, R. V. Padilla, D. Y. Goswami, and E. Stefanakos, "The potential of harnessing solar radiation in Iran: Generating solar maps and viability study of PV power plants," *Renewable Energy*, vol. 53, pp. 193–199, 5 2013.

[200] M. Wild, D. Folini, F. Henschel, N. Fischer, and B. Müller, "Projections of long-term changes in solar radiation based on CMIP5 climate models and their influence on energy yields of photovoltaic systems," *Solar Energy*, vol. 116, pp. 12–24, 2015.

[201] S. Jerez, I. Tobin, R. Vautard, J. P. Montávez, J. M. López-Romero, F. Thais, B. Bartok, O. B. Christensen, A. Colette, M. Déqué, G. Nikulin, S. Kotlarski, E. van Meijgaard, C. Teichmann, and M. Wild, "The impact of climate change on photovoltaic power generation in Europe," *Nature Communications*, vol. 6, p. 10014, 12 2015.

[202] P. C. Stern, B. K. Sovacool, and T. Dietz, "Towards a science of climate and energy choices," *Nature Climate Change*, vol. 6, no. 6, pp. 547–555, 2016.

[203] S. Feron, R. R. Cordero, A. Damiani, and R. B. Jackson, "Climate change extremes and photovoltaic power output," *Nature Sustainability*, vol. 4, pp. 270–276, 11 2020.

[204] F. Giorgi, C. Jones, and G. Asrar, "Addressing climate information needs at the regional level: the CORDEX framework," *... Organization (WMO) Bulletin*, vol. 58, no. July, pp. 175–183, 2009.

[205] P. Luhunga, J. Botai, and F. Kahimba, "Evaluation of the performance of CORDEX regional climate models in simulating present climate conditions of Tanzania," *Journal of Southern Hemisphere Earth Systems Science*, vol. 66, no. 1, p. 32, 2016.

[206] H. C. Hesse, M. Schimpe, D. Kucevic, and A. Jossen, "Lithium-Ion Battery Storage for the Grid—A Review of Stationary Battery Storage System Design Tailored for Applications in Modern Power Grids," *Energies*, vol. 10, no. 12, 2017.

[207] J. Cao, D. Harrold, Z. Fan, T. Morstyn, D. Healey, and K. Li, "Deep Reinforcement Learning-Based Energy Storage Arbitrage With Accurate Lithium-Ion Battery Degradation Model," *IEEE Transactions on Smart Grid*, vol. 11, pp. 4513–4521, 9 2020.

[208] Y. Yang, S. Bremner, C. Menictas, and M. Kay, "Modelling and optimal energy management for battery energy storage systems in renewable energy systems: A review," *Renewable and Sustainable Energy Reviews*, vol. 167, p. 112671, 2022.

[209] C.-L. Kuo, J.-L. Chen, S.-J. Chen, C.-C. Kao, H.-T. Yau, and C.-H. Lin, "Photovoltaic Energy Conversion System Fault Detection Using Fractional-Order Color Relation Classifier in Microdistribution Systems," *IEEE Transactions on Smart Grid*, vol. 8, pp. 1163–1172, 5 2017.

[210] M. S. Naderi, G. B. Gharehpetian, M. Abedi, and T. R. Blackburn, "Modeling and detection of transformer internal incipient fault during impulse test," *IEEE Transactions on Dielectrics and Electrical Insulation*, vol. 15, no. 1, pp. 284–291, 2008.

[211] M. Hajji, M.-F. Harkat, A. Kouadri, K. Abodayeh, M. Mansouri, H. Nounou, and M. Nounou, "Multivariate feature extraction based supervised machine learning for fault detection and diagnosis in photovoltaic systems," *European Journal of Control*, vol. 59, pp. 313–321, 5 2021.

[212] S.-M. Xue and C. Liu, "Line-to-line fault analysis and location in a VSC-based low-voltage DC distribution network," *Energies*, vol. 11, no. 3, p. 536, 2018.

[213] R. Kase and S. Nishikawa, "Fault detection of bypass circuit of PV module—Detection technology of open circuit fault location," in *2016 19th International Conference on Electrical Machines and Systems (ICEMS)*, pp. 1–4, 2016.

[214] A. Y. Appiah, X. Zhang, B. B. K. Ayawli, and F. Kyeremeh, "Long Short-Term Memory Networks Based Automatic Feature Extraction for Photovoltaic Array Fault Diagnosis," *IEEE Access*, vol. 7, pp. 30089–30101, 2019.

[215] W. Gao and R. J. Wai, "A Novel Fault Identification Method for Photovoltaic Array via Convolutional Neural Network and Residual Gated Recurrent Unit," *IEEE Access*, vol. 8, pp. 159493–159510, 2020.

[216] M. F. Zia, E. Elbouchikhi, and M. Benbouzid, "Microgrids energy management systems: A critical review on methods, solutions, and prospects," *Applied energy*, vol. 222, pp. 1033–1055, 2018.

[217] V. François-Lavet, D. Taralla, D. Ernst, and R. Fonteneau, "Deep reinforcement learning solutions for energy microgrids management," in *European Workshop on Reinforcement Learning (EWRL 2016)*, 2016.

[218] A. Kathirgamanathan, K. Twardowski, E. Mangina, and D. P. Finn, "A Centralised Soft Actor Critic Deep Reinforcement Learning Approach to District Demand Side Management through CityLearn," in *Proceedings of the 1st International Workshop on Reinforcement Learning for Energy Management in Buildings & Cities*, (New York, NY, USA), pp. 11–14, ACM, 11 2020.

[219] K. Shivam, J.-C. Tzou, and S.-C. Wu, "A multi-objective predictive energy management strategy for residential grid-connected PV-battery hybrid systems based on machine learning technique," *Energy Conversion and Management*, vol. 237, p. 114103, 2021.

[220] S. Leonori, A. Martino, F. M. F. Mascioli, and A. Rizzi, "Microgrid energy management systems design by computational intelligence techniques," *Applied Energy*, vol. 277, p. 115524, 2020.

[221] S. A. Kumar, M. S. P. Subathra, N. M. Kumar, M. Malvoni, N. J. Sairamya, S. T. George, E. S. Suviseshamuthu, and S. S. Chopra, "A Novel Islanding Detection Technique for a Resilient Photovoltaic-Based Distributed Power Generation System Using a Tunable-Q Wavelet Transform and an Artificial Neural Network," *Energies*, vol. 13, p. 4238, 8 2020.

[222] T. Khatib and W. Elmenreich, "An Improved Method for Sizing Standalone Photovoltaic Systems Using Generalized Regression Neural Network," *International Journal of Photoenergy*, vol. 2014, pp. 1–8, 2014.

[223] J. M. Malof, B. Li, B. Huang, K. Bradbury, and A. Stretslov, "Mapping solar array location, size, and capacity using deep learning and overhead imagery," *Preprint at https://arxiv. org/abs/1902.10895*, 2019.

[224] M. Glavic, "(Deep) Reinforcement learning for electric power system control and related problems: A short review and perspectives," *Annual Reviews in Control*, vol. 48, pp. 22–35, 2019.

[225] M. Arjun and J. B. Zubin, "Artificial Neural Network Based Hybrid MPPT for Photovoltaic Modules," in *2018 International CET Conference on Control, Communication, and Computing (IC4)*, pp. 140–145, IEEE, 7 2018.

[226] G. Valverde and T. Van Cutsem, "Model predictive control of voltages in active distribution networks," *IEEE Transactions on Smart Grid*, vol. 4, no. 4, pp. 2152–2161, 2013.

[227] T. Sansawatt, J. O'Donnell, L. F. Ochoa, and G. P. Harrison, "Decentralised voltage control for active distribution networks," in *2009 44th International Universities Power Engineering Conference (UPEC)*, pp. 1–5, 2009.

[228] S. Takayama and A. Ishigame, "Autonomous decentralized control of distribution network voltage using reinforcement learning," *IFAC-PapersOnLine*, vol. 51, no. 28, pp. 209–214, 2018.

[229] H. K. Ahn and N. Park, "Deep RNN-Based Photovoltaic Power Short-Term Forecast Using Power IoT Sensors," *Energies*, vol. 14, p. 436, 1 2021.

[230] V. Suresh, P. Janik, J. Rezmer, and Z. Leonowicz, "Forecasting solar PV output using convolutional neural networks with a sliding window algorithm," *Energies*, vol. 13, no. 3, p. 723, 2020.

[231] C. Voyant, G. Notton, S. Kalogirou, M. L. Nivet, C. Paoli, F. Motte, and A. Fouilloy, "Machine learning methods for solar radiation forecasting: A review," *Renewable Energy*, vol. 105, pp. 569–582, 2017.

[232] A. Mellit and S. Kalogirou, "Assessment of machine learning and ensemble methods for fault diagnosis of photovoltaic systems," *Renewable Energy*, vol. 184, pp. 1074–1090, 2022.

[233] A. Eskandari, J. Milimonfared, and M. Aghaei, "Fault Detection and Classification for Photovoltaic Systems Based on Hierarchical Classification and Machine Learning Technique," *IEEE Transactions on Industrial Electronics*, vol. 68, no. 12, pp. 12750–12759, 2021.

[234] A. Mellit, S. A. Kalogirou, L. Hontoria, and S. Shaari, "Artificial intelligence techniques for sizing photovoltaic systems: A review," *Renewable and Sustainable Energy Reviews*, vol. 13, no. 2, pp. 406–419, 2009.

[235] A. Mellit and S. A. Kalogirou, "Artificial intelligence techniques for photovoltaic applications: A review," *Progress in Energy and Combustion Science*, vol. 34, no. 5, pp. 574–632, 2008.

[236] T. Berghout, M. Benbouzid, X. Ma, S. Djurović, and L. H. Mouss, "Machine Learning for Photovoltaic Systems Condition Monitoring: A Review," in *IECON 2021 – 47th Annual Conference of the IEEE Industrial Electronics Society*, pp. 1–5, 2021.

[237] M. Mansouri, M. Trabelsi, H. Nounou, and M. Nounou, "Deep Learning-Based Fault Diagnosis of Photovoltaic Systems: A Comprehensive Review and Enhancement Prospects," *IEEE Access*, vol. 9, pp. 126286–126306, 2021.

[238] R. Trivedi and S. Khadem, "Implementation of artificial intelligence techniques in microgrid control environment: Current progress and future scopes," *Energy and AI*, vol. 8, p. 100147, 2022.

[239] L. Ahmethodžić, M. Musić, and S. Huseinbegović, "Microgrid Energy Management: Classification, Review and Challenges," *CSEE Journal of Power and Energy Systems*, vol. 9, no. 4, pp. 1425–1438, 2023.

[240] L. Tightiz and J. Yoo, "A Review on a Data-Driven Microgrid Management System Integrating an Active Distribution Network: Challenges, Issues, and New Trends," *Energies*, vol. 15, no. 22, 2022.

[241] S. Killinger, D. Lingfors, Y.-M. Saint-Drenan, P. Moraitis, W. van Sark, J. Taylor, N. A. Engerer, and J. M. Bright, "On the search for representative characteristics of PV systems: Data collection and analysis of PV system azimuth, tilt, capacity, yield and shading," *Solar Energy*, vol. 173, pp. 1087–1106, 2018.

[242] C. Washburn and M. Pablo-Romero, "Measures to promote renewable energies for electricity generation in Latin American countries," *Energy Policy*, vol. 128, pp. 212–222, 5 2019.

[243] S. A. Arefifar, F. Paz, and M. Ordonez, "Improving Solar Power PV Plants Using Multivariate Design Optimization," *IEEE Journal of Emerging and Selected Topics in Power Electronics*, vol. 5, no. 2, pp. 638–650, 2017.

[244] J. Polo, S. Wilbert, J. A. Ruiz-Arias, R. Meyer, C. Gueymard, M. Súri, L. Martín, T. Mieslinger, P. Blanc, I. Grant, J. Boland, P. Ineichen, J. Remund, R. Escobar, A. Troccoli, M. Sengupta, K. P. Nielsen, D. Renne, N. Geuder, and T. Cebecauer, "Preliminary survey on site-adaptation techniques for satellite-derived and reanalysis solar radiation datasets," *Solar Energy*, vol. 132, pp. 25–37, 2016.

[245] European Comission, "PVGIS users manual," 2020.

[246] A. Halevy, P. Norvig, and F. Pereira, "The Unreasonable Effectiveness of Data," *IEEE Intelligent Systems*, vol. 24, no. 2, pp. 8–12, 2009.

[247] D. Rangel-Martinez, K. D. P. Nigam, and L. A. Ricardez-Sandoval, "Machine learning on sustainable energy: A review and outlook on renewable energy systems,

catalysis, smart grid and energy storage," *Chemical Engineering Research and Design*, vol. 174, pp. 414–441, 2021.

[248] Colombian Ministry of Environment, "Instituto de Hidrología, Meteorología y Estudios Ambientales - IDEAM," 2005.

[249] R. Gelaro, W. McCarty, M. J. Suárez, R. Todling, A. Molod, L. Takacs, C. A. Randles, A. Darmenov, M. G. Bosilovich, R. Reichle, K. Wargan, L. Coy, R. Cullather, C. Draper, S. Akella, V. Buchard, A. Conaty, A. M. da Silva, W. Gu, G.-K. Kim, R. Koster, R. Lucchesi, D. Merkova, J. E. Nielsen, G. Partyka, S. Pawson, W. Putman, M. Rienecker, S. D. Schubert, M. Sienkiewicz, and B. Zhao, "The Modern-Era Retrospective Analysis for Research and Applications, Version 2 (MERRA-2)," *Journal of Climate*, vol. 30, pp. 5419–5454, 7 2017.

[250] "CORDEX-CORE." https://cordex.org/experiment-guidelines/cordex-core/cordex-core-simulations/, 2022.

[251] F. Giorgi, E. Coppola, D. Jacob, C. Teichmann, S. Abba Omar, M. Ashfaq, N. Ban, K. Bülow, M. Bukovsky, L. Buntemeyer, T. Cavazos, J. Ciarlo', R. P. da Rocha, S. Das, F. di Sante, J. P. Evans, X. Gao, G. Giuliani, R. H. Glazer, P. Hoffmann, E.-S. Im, G. Langendijk, L. Lierhammer, M. Llopart, S. Mueller, R. Luna-Nino, R. Nogherotto, E. Pichelli, F. Raffaele, M. Reboita, D. Rechid, A. Remedio, T. Remke, W. Sawadogo, K. Sieck, J. A. Torres-Alavez, and T. Weber, "The CORDEX-CORE EXP-I Initiative: Description and Highlight Results from the Initial Analysis," *Bulletin of the American Meteorological Society*, vol. 103, pp. E293–E310, 2 2022.

[252] C. Teichmann, D. Jacob, A. R. Remedio, T. Remke, L. Buntemeyer, P. Hoffmann, A. Kriegsmann, L. Lierhammer, K. Bülow, T. Weber, and others, "Assessing mean climate change signals in the global CORDEX-CORE ensemble," *Climate Dynamics*, vol. 57, no. 5, pp. 1269–1292, 2021.

[253] W. Sawadogo, M. S. o. Reboita, A. Faye, R. P. da Rocha, R. C. Odoulami, C. F. Olusegun, M. O. Adeniyi, B. J. Abiodun, M. B. Sylla, I. Diallo, and others, "Current and future potential of solar and wind energy over Africa using the RegCM4 CORDEX-CORE ensemble," *Climate Dynamics*, vol. 57, no. 5, pp. 1647–1672, 2021.

[254] J.-J. Morcrette, L. Smith, and Y. Fouquart, "Pressure and temperature dependence of the absorption in longwave radiation parameterizations," *Beitraege zur Physik der Atmosphaere (ISSN 0005-8173*, vol. 59, pp. 455–469, 1986.

[255] M. A. Giorgetta and M. Wild, "The water vapour continuum and its representation in ECHAM4," tech. rep., Max-Planck-Institut für Meteorologie, 1995.

[256] J. T. Kiehl, J. J. Hack, G. B. Bonan, B. A. Boville, and B. P. Briegleb, "Description of the NCAR Community Climate Model (CCM3). Technical note," tech. rep., National Center for Atmospheric Research, Boulder, CO (United States). Climate and Global Dynamics Div., 1996.

[257] A. Slingo, "A GCM parameterization for the shortwave radiative properties of water clouds," *Journal of Atmospheric Sciences*, vol. 46, no. 10, pp. 1419–1427, 1989.

[258] D. Rechid, T. J. Raddatz, and D. Jacob, "Parameterization of snow-free land surface albedo as a function of vegetation phenology based on MODIS data and applied in climate modelling," *Theoretical and applied Climatology*, vol. 95, no. 3, pp. 245–255, 2009.

[259] R. E. Dickinson, A. Henderson-Sellers, and P. J. Kennedy, "Biosphere-atmosphere transfer scheme (BATS) version le as coupled to the NCAR community climate model. Technical note.[NCAR (National Center for Atmospheric Research)]," tech. rep., National Center for Atmospheric Research, Boulder, CO (United States). Scientific Computing Div., 1993.

[260] J. W. Deardorff, "Efficient prediction of ground surface temperature and moisture, with inclusion of a layer of vegetation," *Journal of Geophysical Research*, vol. 83, no. C4, p. 1889, 1978.

[261] J.-F. Louis, "A parametric model of vertical eddy fluxes in the atmosphere," *Boundary-Layer Meteorology*, vol. 17, pp. 187–202, 9 1979.

[262] N. Elguindi, X. Bi, F. Giorgi, B. Nagarajan, J. Pal, F. Solmon, S. Rauscher, A. Zakey, T. O'Brien, R. Nogherotto, and G. Giuliani, "Regional climate model RegCM: reference manual version 4.7," *Abdus Salam ICTP, Trieste*, 2017.

[263] L. DÜMENIL and E. TODINI, "A rainfall–runoff scheme for use in the Hamburg climate model," in *Advances in Theoretical Hydrology*, pp. 129–157, Elsevier, 1992.

[264] F. Giorgi and G. T. Bates, "The climatological skill of a regional model over complex terrain," *Monthly Weather Review*, vol. 117, no. 11, pp. 2325–2347, 1989.

[265] F. Giorgi and M. R. Marinucci, "Validation of a regional atmospheric model over Europe: Sensitivity of wintertime and summertime simulations to selected physics

parametrizations and lower boundary conditions," *Quarterly Journal of the Royal Meteorological Society*, vol. 117, pp. 1171–1206, 10 1991.

[266] G. A. Grell, "Prognostic evaluation of assumptions used by cumulus parameterizations," *Monthly weather review*, vol. 121, no. 3, pp. 764–787, 1993.

[267] K. A. Emanuel and M. Živković-Rothman, "Development and evaluation of a convection scheme for use in climate models," *Journal of the Atmospheric Sciences*, vol. 56, no. 11, pp. 1766–1782, 1999.

[268] M. Tiedtke, "A comprehensive mass flux scheme for cumulus parameterization in large-scale models," *Monthly weather review*, vol. 117, no. 8, pp. 1779–1800, 1989.

[269] T. E. Nordeng, "Extended versions of the convective parametrization scheme at ECMWF and their impact on the mean and transient activity of the model in the tropics.," *Research Department Technical Memorandum*, vol. 206, pp. 1–41, 1994.

[270] A. Seth and F. Giorgi, "The effects of domain choice on summer precipitation simulation and sensitivity in a regional climate model," *Journal of Climate*, vol. 11, no. 10, pp. 2698–2712, 1998.

[271] T. Semmler, D. Jacob, K. H. Schlünzen, and R. Podzun, "Influence of sea ice treatment in a regional climate model on boundary layer values in the Fram Strait region," *Monthly Weather Review*, vol. 132, no. 4, pp. 985–999, 2004.

[272] X. Zeng and A. Beljaars, "A prognostic scheme of sea surface skin temperature for modeling and data assimilation," *Geophysical Research Letters*, vol. 32, no. 14, 2005.

[273] H. Sundqvist, "A parameterization scheme for non-convective condensation including prediction of cloud water content," *Quarterly Journal of the Royal Meteorological Society*, vol. 104, no. 441, pp. 677–690, 1978.

[274] E. Roeckner, K. Arpe, L. Bengtsson, M. Christoph, M. Claussen, L. Dümenil, M. Esch, M. A. Giorgetta, U. Schlese, and U. Schulzweida, "The atmospheric general circulation model ECHAM-4: Model description and simulation of present-day climate," tech. rep., Max-Planck-Institut für Meteorologie, 1996.

[275] B. Laurent, B. Marticorena, G. Bergametti, J. F. Léon, and N. M. Mahowald, "Modeling mineral dust emissions from the Sahara desert using new surface properties and soil database," *Journal of Geophysical Research*, vol. 113, p. D14218, 7 2008.

[276] S. C. Alfaro and L. Gomes, "Modeling mineral aerosol production by wind erosion: Emission intensities and aerosol size distributions in source areas," *Journal of Geophysical Research: Atmospheres*, vol. 106, pp. 18075–18084, 8 2001.

[277] M. Tiedtke, "Representation of clouds in large-scale models," *Monthly Weather Review*, vol. 121, no. 11, pp. 3040–3061, 1993.

[278] A. M. Tompkins, K. Gierens, and G. Rädel, "Ice supersaturation in the ECMWF integrated forecast system," *Quarterly Journal of the Royal Meteorological Society: A journal of the atmospheric sciences, applied meteorology and physical oceanography*, vol. 133, no. 622, pp. 53–63, 2007.

[279] R. Nogherotto, A. M. Tompkins, G. Giuliani, E. Coppola, and F. Giorgi, "Numerical framework and performance of the new multiple-phase cloud microphysics scheme in RegCM4. 5: precipitation, cloud microphysics, and cloud radiative effects," *Geoscientific Model Development*, vol. 9, no. 7, pp. 2533–2547, 2016.

[280] A. A. M. Holtslag, E. I. F. De Bruijn, and H. L. Pan, "A high resolution air mass transformation model for short-range weather forecasting," *Monthly Weather Review*, vol. 118, no. 8, pp. 1561–1575, 1990.

[281] T. A. O'Brien, P. Y. Chuang, L. C. Sloan, I. C. Faloona, and D. L. Rossiter, "Coupling a new turbulence parametrization to RegCM adds realistic stratocumulus clouds," *Geoscientific Model Development*, vol. 5, no. 4, pp. 989–1008, 2012.

[282] E. E. Small, L. C. Sloan, S. Hostetler, and F. Giorgi, "Simulating the water balance of the Aral Sea with a coupled regional climate-lake model," *Journal of Geophysical Research: Atmospheres*, vol. 104, no. D6, pp. 6583–6602, 1999.

[283] X. Zeng, M. Zhao, and R. E. Dickinson, "Intercomparison of bulk aerodynamic algorithms for the computation of sea surface fluxes using TOGA COARE and TAO data," *Journal of Climate*, vol. 11, no. 10, pp. 2628–2644, 1998.

[284] National Renewable Energy Laboratory, "NSRDB Data Viewer," 2022.

[285] European Commission Joint Research Centre, "Photovoltaic Geographical Information System," 2019.

[286] European Comission, "Data Sources and Calculation Methods," 2020.

[287] The World Bank, "Global Solar Atlas," 2017.

[288] M. Suri, J. Betak, K. Rosina, D. Chrkavy, N. Suriova, T. Cebecauer, M. Caltik, and B. Erdelyi, "Global photovoltaic power potential by country," 2020.

[289] SOLARGIS, "What can you do with Solargis?," 2021.

[290] The World Bank, "Global Solar Atlas - Getting Started," 2017.

[291] Chilean Ministry of Energy, "Explorador Solar," 2022.

[292] M. Institute of Hydrology and E. Studies, "Atlas Interactivo," 2022.

[293] R. Urraca, A. M. Gracia-Amillo, E. Koubli, T. Huld, J. Trentmann, A. Riihelä, A. V. Lindfors, D. Palmer, R. Gottschalg, and F. Antonanzas-Torres, "Extensive validation of CM SAF surface radiation products over Europe," *Remote sensing of environment*, vol. 199, pp. 171–186, 2017.

[294] M. M. Breunig, H.-P. Kriegel, R. T. Ng, and J. Sander, "LOF," in *Proceedings of the 2000 ACM SIGMOD international conference on Management of data*, (New York, NY, USA), pp. 93–104, ACM, 5 2000.

[295] C. Piani, G. P. Weedon, M. Best, S. M. Gomes, P. Viterbo, S. Hagemann, and J. O. Haerter, "Statistical bias correction of global simulated daily precipitation and temperature for the application of hydrological models," *Journal of hydrology*, vol. 395, no. 3-4, pp. 199–215, 2010.

[296] M. Enayati, O. Bozorg-Haddad, J. Bazrafshan, S. Hejabi, and X. Chu, "Bias correction capabilities of quantile mapping methods for rainfall and temperature variables," *Journal of Water and Climate Change*, vol. 12, pp. 401–419, 3 2021.

[297] D. Li, J. Feng, Z. Xu, B. Yin, H. Shi, and J. Qi, "Statistical Bias Correction for Simulated Wind Speeds Over CORDEX-East Asia," *Earth and Space Science*, vol. 6, pp. 200–211, 2 2019.

[298] N. Aste, C. Del Pero, F. Leonforte, and M. Manfren, "A simplified model for the estimation of energy production of PV systems," *Energy*, vol. 59, pp. 503–512, 9 2013.

[299] E. Caamaño and E. Lorenzo, "Modelling and financial analysis tools for PV grid-connected systems," *Progress in Photovoltaics: Research and Applications*, vol. 4, pp. 295–305, 7 1996.

[300] L. M. Ayompe, A. Duffy, S. J. McCormack, and M. Conlon, "Validated real-time energy models for small-scale grid-connected PV-systems," *Energy*, vol. 35, pp. 4086–4091, 10 2010.

[301] G. T. Klise and J. S. Stein, "SANDIA REPORT Models Used to Assess the Performance of Photovoltaic Systems," tech. rep., Sandia National Laboratories, 12 2009.

[302] D. Myers, "INVENTORY OF SOLAR RADIATION/SOLAR ENERGY SYSTEMS ESTIMATORS, MODELS, SITE-SPECIFIC DATA, AND PUBLICATIONS," tech. rep., National Renewable Energy Laboratory, 7 2009.

[303] J. Boland, B. Ridley, and B. Brown, "Models of diffuse solar radiation," *Renewable Energy*, vol. 33, pp. 575–584, 4 2008.

[304] W. De Soto, S. A. Klein, and W. A. Beckman, "Improvement and validation of a model for photovoltaic array performance," *Solar energy*, vol. 80, no. 1, pp. 78–88, 2006.

[305] A. Dobos, "PVWatts Version 5 Manual," tech. rep., National Renewable Energy Laboratory (NREL), Golden, CO (United States), 9 2014.

[306] L. Narvarte and E. Lorenzo, "Tracking and ground cover ratio," *Progress in photovoltaics: research and applications*, vol. 16, no. 8, pp. 703–714, 2008.

[307] W. C. Skamarock, J. B. Klemp, J. Dudhia, D. O. Gill, Z. Liu, J. Berner, W. Wang, J. G. Powers, M. G. Duda, D. M. Barker, and others, "A description of the advanced research WRF model version 4," *National Center for Atmospheric Research: Boulder, CO, USA*, vol. 145, p. 145, 2019.

[308] X. Zhao, G. Huang, C. Lu, X. Zhou, and Y. Li, "Impacts of climate change on photovoltaic energy potential: A case study of China," *Applied Energy*, vol. 280, p. 115888, 2020.

[309] J. C. Pérez, A. González, J. P. D\'\iaz, F. J. Expósito, and J. Felipe, "Climate change impact on future photovoltaic resource potential in an orographically complex archipelago, the Canary Islands," *Renewable Energy*, vol. 133, pp. 749–759, 2019.

[310] D. C. Jordan and S. R. Kurtz, "Photovoltaic Degradation Rates-an Analytical Review," *Progress in Photovoltaics: Research and Applications*, vol. 21, pp. 12–29, 1 2013.

[311] W. Sawadogo, B. J. Abiodun, and E. C. Okogbue, "Impacts of global warming on photovoltaic power generation over West Africa," *Renewable Energy*, vol. 151, pp. 263–277, 2020.

[312] A. Bichet, B. Hingray, G. Evin, A. Diedhiou, C. M. F. Kebe, and S. Anquetin, "Potential impact of climate change on solar resource in Africa for photovoltaic energy: analyses from CORDEX-AFRICA climate experiments," *Environmental Research Letters*, vol. 14, p. 124039, 12 2019.

[313] I. Losada Carreño, M. T. Craig, M. Rossol, M. Ashfaq, F. Batibeniz, S. E. Haupt, C. Draxl, B.-M. Hodge, and C. Brancucci, "Potential impacts of climate change on wind and solar electricity generation in Texas," *Climatic Change*, vol. 163, pp. 745–766, 11 2020.

[314] P. Meisen and S. Krumpel, "Renewable Energy Potential of Latin America," *San Diego: Global Energy Network Institute*, 2009.

[315] L. d. S. N. S. Barbosa, D. Bogdanov, P. Vainikka, and C. Breyer, "Hydro, wind and solar power as a base for a 100% renewable energy supply for South and Central America," *PLOS ONE*, vol. 12, p. e0173820, 3 2017.

[316] S. R. Santos da Silva, M. I. Hejazi, G. Iyer, T. B. Wild, M. Binsted, F. Miralles-Wilhelm, P. Patel, A. C. Snyder, and C. R. Vernon, "Power sector investment implications of climate impacts on renewable resources in Latin America and the Caribbean," *Nature Communications*, vol. 12, p. 1276, 2 2021.

[317] G. P. Peters, R. M. Andrew, T. Boden, J. G. Canadell, P. Ciais, C. Le Quéré, G. Marland, M. R. Raupach, and C. Wilson, "The challenge to keep global warming below 2 ˆC," *Nature Climate Change*, vol. 3, 8 2013.

[318] V. Masson-Delmotte, P. Zhai, A. Pirani, S. L. Connors, C. Péan, S. Berger, N. Caud, Y. Chen, L. Goldfarb, M. I. Gomis, and others, "Climate change 2021: the physical science basis," tech. rep., Intergovernmental Panel on Climate Change (IPCC), 2021.

[319] M. Rummukainen, "State-of-the-art with regional climate models," *Wiley Interdisciplinary Reviews: Climate Change*, vol. 1, no. 1, pp. 82–96, 2010.

[320] C. Park, S.-W. Shin, G. Kim, D.-H. Cha, S.-K. Min, D. Lee, Y.-H. Byun, and J.-U. Kim, "What determines future changes in photovoltaic potential over East Asia?," *Renewable Energy*, vol. 185, pp. 338–347, 2022.

[321] P. Hui, Y. Li, Y. Chen, L. Zhang, F. Wei, S. Wang, and J. Tang, "The impact of radiation parameterization schemes on the regional climate simulations over the CORDEX-EA domain," *Atmospheric Research*, vol. 224, pp. 81–98, 8 2019.

[322] M. Falco, A. F. Carril, C. G. Menéndez, P. G. Zaninelli, and L. Z. X. Li, "Assessment of CORDEX simulations over South America: added value on seasonal climatology and resolution considerations," *Climate Dynamics*, vol. 52, pp. 4771–4786, 4 2019.

[323] Z. Kundzewicz, V. Krysanova, R. Benestad, ø. Hov, M. Piniewski, and I. Otto, "Uncertainty in climate change impacts on water resources," *Environmental Science & Policy*, vol. 79, pp. 1–8, 1 2018.

[324] M. T. Nóbrega, W. Collischonn, C. E. M. Tucci, and A. R. d. Paz, "Uncertainty in climate change impacts on water resources in the Rio Grande Basin, Brazil," *Hydrology and Earth System Sciences*, vol. 15, no. 2, pp. 585–595, 2011.

[325] A. Fantini, F. Raffaele, C. Torma, S. Bacer, E. Coppola, F. Giorgi, B. Ahrens, C. Dubois, E. Sanchez, and M. Verdecchia, "Assessment of multiple daily precipitation statistics in ERA-Interim driven Med-CORDEX and EURO-CORDEX experiments against high resolution observations," *Climate Dynamics*, vol. 51, pp. 877–900, 8 2018.

[326] G. Jiménez-Estévez, R. Palma-Behnke, D. Ortiz-Villalba, O. Núñez Mata, and C. Silva Montes, "It Takes a Village: Social SCADA and Approaches to Community Engagement in Isolated Microgrids," *IEEE Power and Energy Magazine*, vol. 12, pp. 60–69, 7 2014.

[327] IRENA, *Renewable capacity statistics 2020*. International Renewable Energy Agency (IRENA), 2020.

[328] L. E. Singer and D. Peterson, *International energy outlook 2010*, vol. 0484. U.S. Energy Information Administration Forrestal, 2011.

[329] A. Rico Espinosa, M. Bressan, and L. F. Giraldo, "Failure signature classification in solar photovoltaic plants using RGB images and convolutional neural networks," *Renewable Energy*, vol. 162, pp. 249–256, 12 2020.

[330] G. Salazar, P. Utrillas, A. Esteve, J. Martínez-Lozano, and M. Aristizabal, "Estimation of daily average values of the Ångström turbidity coefficient β using a Corrected Yang Hybrid Model," *Renewable Energy*, vol. 51, pp. 182–188, 3 2013.

[331] A. Merlone, G. Lopardo, F. Sanna, S. Bell, R. Benyon, R. A. Bergerud, F. Bertiglia, J. Bojkovski, N. Böse, M. Brunet, A. Cappella, G. Coppa, D. del Campo, M. Dobre, J. Drnovsek, V. Ebert, R. Emardson, V. Fernicola, K. Flakiewicz, T. Gardiner, C. Garcia-Izquierdo, E. Georgin, A. Gilabert, A. Grykałowska, E. Grudniewicz, M. Heinonen, M. Holmsten, D. Hudoklin, J. Johansson, H. Kajastie, H. Kaykısızlı, P. Klason, L. Kňazovická, A. Lakka, A. Kowal, H. Müller, C. Musacchio, J. Nwaboh, P. Pavlasek, A. Piccato, L. Pitre, M. de Podesta, M. K. Rasmussen, H. Sairanen, D. Smorgon, F. Sparasci, R. Strnad, A. Szmyrka-Grzebyk, and R. Underwood, "The MeteoMet project - metrology for meteorology: challenges and results," *Meteorological Applications*, vol. 22, pp. 820–829, 12 2015.

[332] S. Hunziker, S. Gubler, J. Calle, I. Moreno, M. Andrade, F. Velarde, L. Ticona, G. Carrasco, Y. Castellón, C. Oria, M. Croci-Maspoli, T. Konzelmann, M. Rohrer, and S. Brönnimann, "Identifying, attributing, and overcoming common data quality issues of manned station observations," *International Journal of Climatology*, vol. 37, pp. 4131–4145, 9 2017.

[333] F. Vignola, Z. Derocher, J. Peterson, L. Vuilleumier, C. Félix, J. Gröbner, and N. Kouremeti, "Effects of changing spectral radiation distribution on the performance of photodiode pyranometers," *Solar Energy*, vol. 129, pp. 224–235, 2016.

[334] C. Voyant, F. Motte, G. Notton, A. Fouilloy, M. L. Nivet, and J. L. Duchaud, "Prediction intervals for global solar irradiation forecasting using regression trees methods," *Renewable Energy*, vol. 126, pp. 332–340, 2018.

[335] M. Journée and C. Bertrand, "Improving the spatio-temporal distribution of surface solar radiation data by merging ground and satellite measurements," *Remote Sensing of Environment*, vol. 114, pp. 2692–2704, 11 2010.

[336] J. Wallace and P. Hobbs, "Front Matter," in *Atmospheric Science* (J. Wallace and P. Hobbs, eds.), pp. ii–iii, San Diego: Elsevier, second ed., 2006.

[337] M. Suri and T. Cebecauer, "Satellite-based solar resource data: Model validation statistics versus user's uncertainty," *43rd ASES National Solar Conference 2014, SOLAR 2014, Including the 39th National Passive Solar Conference and the 2nd Meeting of Young and Emerging Professionals in Renewable Energy*, vol. 2, no. July, pp. 956–963, 2014.

[338] L. Mazorra Aguiar, J. Polo, J. Vindel, and A. Oliver, "Analysis of satellite derived solar irradiance in islands with site adaptation techniques for improving the uncertainty," *Renewable Energy*, vol. 135, pp. 98–107, 5 2019.

[339] E. W. Harmsen, P. T. Cruz, and J. R. Mecikalski, "Calibration of selected pyranometers and satellite derived solar radiation in Puerto Rico," *International Journal of Renewable Energy Technology*, vol. 5, no. 1, p. 43, 2014.

[340] G. B. Francesca, D. Scott, and C. A. Gueymard, "The road to bankability: Improving assessments for more accurate financial planning," *40th ASES National Solar Conference 2011, SOLAR 2011*, vol. 1, no. January 2011, pp. 733–738, 2011.

[341] J. Polo, C. Fernández-Peruchena, V. Salamalikis, L. Mazorra-Aguiar, M. Turpin, L. Martín-Pomares, A. Kazantzidis, P. Blanc, and J. Remund, "Benchmarking on improvement and site-adaptation techniques for modeled solar radiation datasets," *Solar Energy*, vol. 201, no. October 2019, pp. 469–479, 2020.

[342] G. Reikard, "Predicting solar radiation at high resolutions: A comparison of time series forecasts," *Solar Energy*, vol. 83, no. 3, pp. 342–349, 2009.

[343] L. Prokop, S. Mišák, V. Snášel, J. Platoš, and P. Krömer, "Supervised learning of photovoltaic power plant output prediction models," *Neural Network World*, vol. 23, no. 4, pp. 321–338, 2013.

[344] I. A. Ibrahim, M. J. Hossain, and B. C. Duck, "An Optimized Offline Random Forests-Based Model for Ultra-Short-Term Prediction of PV Characteristics," *IEEE Transactions on Industrial Informatics*, vol. 16, pp. 202–214, 1 2020.

[345] A. F. Zambrano and L. F. Giraldo, "Solar irradiance forecasting models without on-site training measurements," *Renewable Energy*, vol. 152, pp. 557–566, 8 2020.

[346] H. Wang, Y. Liu, B. Zhou, C. Li, G. Cao, N. Voropai, and E. Barakhtenko, "Taxonomy research of artificial intelligence for deterministic solar power forecasting," *Energy Conversion and Management*, vol. 214, p. 112909, 8 2020.

[347] R. H. Inman, H. T. Pedro, and C. F. Coimbra, "Solar forecasting methods for renewable energy integration," *Progress in Energy and Combustion Science*, vol. 39, pp. 535–576, 12 2013.

[348] R. Urraca, T. Huld, A. Gracia-Amillo, F. J. Martinez-de Pison, F. Kaspar, and A. Sanz-Garcia, "Evaluation of global horizontal irradiance estimates from ERA5 and COSMO-REA6 reanalyses using ground and satellite-based data," *Solar Energy*, vol. 164, no. February, pp. 339–354, 2018.

[349] J. M. Bright, "Solcast: Validation of a satellite-derived solar irradiance dataset," *Solar Energy*, vol. 189, pp. 435–449, 9 2019.

[350] D. Yang, "A correct validation of the National Solar Radiation Data Base (NSRDB)," *Renewable and Sustainable Energy Reviews*, vol. 97, no. August, pp. 152–155, 2018.

[351] A. Géron, *Hands-on machine learning with Scikit-Learn, Keras, and TensorFlow.* " O'Reilly Media, Inc.", 2022.

[352] C. M. Bishop, *Pattern recognition and machine learning.* New York: Springer, first ed., 2006.

[353] L. Breiman, "Random forests," *Random Forests*, p. 28, 2001.

[354] S. Kumar, L. Hussain, S. Banarjee, and M. Reza, "Energy Load Forecasting using Deep Learning Approach-LSTM and GRU in Spark Cluster," in *2018 Fifth International Conference on Emerging Applications of Information Technology (EAIT)*, pp. 1–4, IEEE, 1 2018.

[355] Y. Liu, Z. Su, H. Li, and Y. Zhang, "An LSTM based classification method for time series trend forecasting," in *2019 14th IEEE Conference on Industrial Electronics and Applications (ICIEA)*, pp. 402–406, IEEE, 6 2019.

[356] X. Qing and Y. Niu, "Hourly day-ahead solar irradiance prediction using weather forecasts by LSTM," *Energy*, vol. 148, pp. 461–468, 2018.

[357] J. Zhang, J. Yan, D. Infield, Y. Liu, and F. s. Lien, "Short-term forecasting and uncertainty analysis of wind turbine power based on long short-term memory network and Gaussian mixture model," *Applied Energy*, vol. 241, no. January, pp. 229–244, 2019.

[358] Y. Wang, Y. Shen, S. Mao, X. Chen, and H. Zou, "LASSO and LSTM Integrated Temporal Model for Short-Term Solar Intensity Forecasting," *IEEE Internet of Things Journal*, vol. 6, pp. 2933–2944, 8 2019.

[359] S. Ghimire, R. C. Deo, N. Raj, and J. Mi, "Deep solar radiation forecasting with convolutional neural network and long short-term memory network algorithms," *Applied Energy*, vol. 253, p. 113541, 11 2019.

[360] I. Goodfellow, Y. Bengio, and A. Courville, *Deep Learning.* MIT Press, 2016.

[361] R. Laubscher, "Time-series forecasting of coal-fired power plant reheater metal temperatures using encoder-decoder recurrent neural networks," *Energy*, vol. 189, p. 116187, 12 2019.

[362] J. Brownlee, *Introduction to Time Series Forecasting With Python: How to Prepare Data and Develop Models to Predict the Future.* Machine Learning Mastery, first ed., 2017.

[363] K. Cho, B. van Merrienboer, C. Gulcehre, D. Bahdanau, F. Bougares, H. Schwenk, and Y. Bengio, "Learning Phrase Representations using RNN Encoder–Decoder for Statistical Machine Translation," in *Proceedings of the 2014 Conference on Empirical Methods in Natural Language Processing (EMNLP)*, (Stroudsburg, PA, USA), pp. 1724–1734, Association for Computational Linguistics, 2014.

[364] XM S.A. E.S.P, "Reporte integral de sostenibilidad, operación y mercado 2018," tech. rep., XM S.A. E.S.P, 2018.

[365] UPME, "Plan Indicativo de Expansión de Cobertura de Energía Eléctrica 2013 - 2017," tech. rep., Colombian Energy and Mining Planning Unit, 2014.

[366] A. J. Cannon, S. R. Sobie, and T. Q. Murdock, "Bias Correction of GCM Precipitation by Quantile Mapping: How Well Do Methods Preserve Changes in Quantiles and Extremes?," *Journal of Climate*, vol. 28, pp. 6938–6959, 9 2015.

[367] P. E. Bett and H. E. Thornton, "The climatological relationships between wind and solar energy supply in Britain," *Renewable Energy*, vol. 87, pp. 96–110, 3 2016.

[368] M. El-Nouby Adam and E. A. Ahmed, "Comparative analysis of cloud effects on ultraviolet-B and broadband solar radiation: Dependence on cloud amount and solar zenith angle," *Atmospheric Research*, vol. 168, pp. 149–157, 2 2016.

[369] Y. Feng, D. Gong, Q. Zhang, S. Jiang, L. Zhao, and N. Cui, "Evaluation of temperature-based machine learning and empirical models for predicting daily global solar radiation," *Energy Conversion and Management*, vol. 198, p. 111780, 10 2019.

[370] O. Kisi, S. Heddam, and Z. M. Yaseen, "The implementation of univariable scheme-based air temperature for solar radiation prediction: New development of dynamic evolving neural-fuzzy inference system model," *Applied Energy*, vol. 241, pp. 184–195, 5 2019.

[371] L. Benali, G. Notton, A. Fouilloy, C. Voyant, and R. Dizene, "Solar radiation forecasting using artificial neural network and random forest methods: Application to normal beam, horizontal diffuse and global components," *Renewable Energy*, vol. 132, pp. 871–884, 3 2019.

[372] H. Jiang, N. Lu, J. Qin, W. Tang, and L. Yao, "A deep learning algorithm to estimate hourly global solar radiation from geostationary satellite data," *Renewable and Sustainable Energy Reviews*, vol. 114, no. 11, p. 109327, 2019.

[373] W. Lee, M. Chae, and D. Won, "Optimal Scheduling of Energy Storage System Considering Life-Cycle Degradation Cost Using Reinforcement Learning," *Energies*, vol. 15, no. 8, 2022.

[374] A. Sobu and G. Wu, "Dynamic optimal schedule management method for microgrid system considering forecast errors of renewable power generations," in *2012 IEEE International Conference on Power System Technology (POWERCON)*, pp. 1–6, 2012.

[375] T. M. Layadi, G. Champenois, M. Mostefai, and D. Abbes, "Lifetime estimation tool of lead–acid batteries for hybrid power sources design," *Simulation Modelling Practice and Theory*, vol. 54, pp. 36–48, 2015.

[376] J. Ma and X. Ma, "A review of forecasting algorithms and energy management strategies for microgrids," *Systems Science & Control Engineering*, vol. 6, pp. 237–248, 1 2018.

[377] S. Vinothine, L. N. Widanagama Arachchige, A. D. Rajapakse, and R. Kaluthanthrige, "Microgrid Energy Management and Methods for Managing Forecast Uncertainties," *Energies*, vol. 15, p. 8525, 11 2022.

[378] M. Mazidi, A. Zakariazadeh, S. Jadid, and P. Siano, "Integrated scheduling of renewable generation and demand response programs in a microgrid," *Energy Conversion and Management*, vol. 86, pp. 1118–1127, 10 2014.

[379] S. Mohseni, A. C. Brent, S. Kelly, and W. N. Browne, "Demand response-integrated investment and operational planning of renewable and sustainable energy systems considering forecast uncertainties: A systematic review," *Renewable and Sustainable Energy Reviews*, vol. 158, p. 112095, 4 2022.

[380] D. M. Rosewater, D. A. Copp, T. A. Nguyen, R. H. Byrne, and S. Santoso, "Battery Energy Storage Models for Optimal Control," *IEEE Access*, vol. 7, pp. 178357–178391, 2019.

[381] R. Chenni, M. Makhlouf, T. Kerbache, and A. Bouzid, "A detailed modeling method for photovoltaic cells," *Energy*, vol. 32, pp. 1724–1730, 9 2007.

[382] M. Sechilariu, B. C. Wang, F. Locment, and A. Jouglet, "DC microgrid power flow optimization by multi-layer supervision control. Design and experimental validation," *Energy Conversion and Management*, vol. 82, pp. 1–10, 6 2014.

[383] M. F. Zia, E. Elbouchikhi, and M. Benbouzid, "Optimal operational planning of scalable DC microgrid with demand response, islanding, and battery degradation cost considerations," *Applied Energy*, vol. 237, pp. 695–707, 3 2019.

[384] J. Silvente, G. M. Kopanos, E. N. Pistikopoulos, and A. Espuña, "A rolling horizon optimization framework for the simultaneous energy supply and demand planning in microgrids," *Applied Energy*, vol. 155, pp. 485–501, 10 2015.

[385] Y. Zhang, R. Wang, T. Zhang, Y. Liu, and B. Guo, "Model predictive control-based operation management for a residential microgrid with considering forecast uncertainties and demand response strategies," *IET Generation, Transmission & Distribution*, vol. 10, pp. 2367–2378, 7 2016.

[386] D. Trigkas, G. Gravanis, K. Diamantaras, S. Voutetakis, and S. Papadopoulou, "Energy Management in Microgrids Using Model Predictive Control Empowered with Artificial Intelligence," *Chemical Engineering Transactions*, vol. 94, pp. 961–966, 9 2022.

[387] P. Kumari and D. Toshniwal, "Deep learning models for solar irradiance forecasting: A comprehensive review," *Journal of Cleaner Production*, vol. 318, p. 128566, 2021.

[388] S. Cantillo-Luna, R. Moreno-Chuquen, D. Celeita, and G. Anders, "Deep and Machine Learning Models to Forecast Photovoltaic Power Generation," *Energies*, vol. 16, no. 10, 2023.

[389] E. A. Bakirtzis, C. K. Simoglou, P. N. Biskas, and A. G. Bakirtzis, "Storage management by rolling stochastic unit commitment for high renewable energy penetration," *Electric Power Systems Research*, vol. 158, pp. 240–249, 2018.

[390] M. Gaetani-Liseo, C. Alonso, and B. Jammes, "Identification of ESS Degradations Related to their Uses in Micro-Grids: application to a building lighting network with VRLA batteries," *European Journal of Electrical Engineering*, vol. 23, no. 6, pp. 455–466, 2021.

[391] Z. Chang, Y. Zhang, and W. Chen, "Electricity price prediction based on hybrid model of adam optimized LSTM neural network and wavelet transform," *Energy*, vol. 187, p. 115804, 11 2019.

[392] J. W. Stevens and G. P. Corey, "A study of lead-acid battery efficiency near top-of-charge and the impact on PV system design," in *Conference Record of the Twenty Fifth IEEE Photovoltaic Specialists Conference - 1996*, pp. 1485–1488, 1996.

[393] P. G. V. Sampaio and M. O. A. González, "Photovoltaic solar energy: Conceptual framework," *Renewable and Sustainable Energy Reviews*, vol. 74, pp. 590–601, 8 2017.

[394] K. Wang and R. E. Dickinson, "Contribution of solar radiation to decadal temperature variability over land," *Proceedings of the National Academy of Sciences*, vol. 110, no. 37, pp. 14877–14882, 2013.

[395] A. Hanslmeier, *The sun and space weather*, vol. 347 of *ASTROPHYSICS AND SPACE SCIENCE LIBRARY*. Dordrecht: Springer Netherlands, 2007.

[396] V. R. Barros, J. A. Boninsegna, I. A. Camilloni, M. Chidiak, G. O. Magrín, and M. Rusticucci, "Climate change in Argentina: trends, projections, impacts and adaptation," *Wiley Interdisciplinary Reviews: Climate Change*, vol. 6, pp. 151–169, 3 2015.

[397] C. Seiler, R. W. A. Hutjes, and P. Kabat, "Likely ranges of climate change in Bolivia," *Journal of Applied Meteorology and Climatology*, vol. 52, no. 6, pp. 1303–1317, 2013.

[398] A. F. P. de Lucena, A. S. Szklo, R. Schaeffer, R. R. de Souza, B. S. M. C. Borba, I. V. L. da Costa, A. O. P. Júnior, and S. H. F. da Cunha, "The vulnerability of renewable energy to climate change in Brazil," *Energy Policy*, vol. 37, pp. 879–889, 3 2009.

[399] F. Silvero, F. Rodrigues, and S. Montelpare, "Energy Efficiency Policies to Face Buildings' Climate Change Effects in Paraguay," *Applied Sciences*, vol. 10, no. 11, p. 3979, 2020.

Appendix

.1 Photovoltaic generation models

This section describes the basic generation model and the advanced generation model. These models are based on [303–307]

Inclined radiation

Both models calculate the power generation of the panel array for each day of a given year or a given RCP scenario, depending on the selected map. The first variable defined is the declination angle δ, which is the angle between the equator and a line drawn from the center of the Earth to the center of the sun. δ varies depending on the position of the Earth relative to the sun and is calculated using the number of the day d and the latitude ϕ as

$$\delta = 23.45^{\circ} \sin\left(\frac{360}{365}(284 + d)\right). \tag{1}$$

The next variable is the solar angle α, which measures the angle between the sun's rays and a horizontal plane, defined as

$$\alpha = 90 - \phi + \delta. \tag{2}$$

The daily averages of GHI for the specific coordinate and year or RCP scenario selected by the user are then used to obtain the inclined radiation R_i as

$$Ri = GHI\frac{sin(\alpha + \beta)}{sin(\alpha)}, \tag{3}$$

where β represents the panel array inclination.

Solar cell temperature

The solar cell temperature T_c is calculated using the panel temperature T_p and the inclined radiation calculated earlier. Initially, T_p is calculated as

$$T_p = Ri \exp^{(a+b*WS)} + \Delta T, \tag{4}$$

where WS represents wind speed daily average, T the ambient temperature average, and the constants a, b, and ΔT depend on the type of setup of the array. Both models support two types of setup, isolated (in this case, $a = -3.47$, $b = -0.0594$, and $\Delta T = 3$), or over the roof (where $a = -2.98$, $b = -0.0471$, and $\Delta T = 1$). Therefore, with the panel temperature T_p, the solar cell temperature T_c is calculated as

$$T_c = T_p + \frac{Ri}{1000}\Delta T. \tag{5}$$

Nominal power of the system

The nominal power P_{DCnom}, in kW, refers to the power produced by the panel array in standard conditions, that is, with global radiation of 1000W/m^2 and a solar cell temperature of 25°C. P_{DCnom} is calculated as

$$P_{DCnom} = \frac{P_{mp}N}{1000}, \tag{6}$$

where P_{mp}, in Watts, refers to the maximum panel power, and N refers to the number of panels in the array. These variables are defined by the user.

Output power - Basic generation model

The power produced by the array of panels with the basic generation model P_{DC} is calculated as

$$P_{DC} = \frac{Ri}{Rref} P_{DCnom}(1 + \gamma(T_c - T_0)), \tag{7}$$

where γ represents the maximum temperature coefficient of the solar cell. This constant is defined by the user. A value of -0.5%/°C is commonly used for monocrystalline solar panel cells. The nominal temperature T_0 is 25°C, and the reference radiation R_{ref} is 1000W/m^2.

Advanced generation model

The advanced generation model is defined based on the I-V curve that describes the behavior of a photovoltaic cell. First, the short circuit current I_{sc} is calculated as

$$I_{sc} = I_{sc,ref}\frac{Ri}{1000}(1 + \alpha I_{sc}(T_c - T_0)), \tag{8}$$

where the reference short circuit current $I_{sc,ref}$, and the short circuit current temperature coefficient αI_{sc}, are given by the user depending on the type of solar panel. The short circuit current is then used to calculate the current at maximum power of the panel I_{mp} as

$$I_{mp} = I_{mp,ref}\frac{I_{sc}}{I_{sc,ref}}, \tag{9}$$

where $I_{mp,ref}$ represents the reference current at maximum power given by the user.

The open circuit voltage V_{oc} is calculated as

$$V_{oc} = V_{oc,ref}s\delta(T_c)ln(E_e) + \beta_{Voc}(T_c - T_0), \tag{10}$$

where the reference open circuit voltage $V_{oc,ref}$, the number of solar cells in series s, and the open circuit voltage temperature coefficient β_{Voc} are defined by the user. The constant $\delta(T_c)$ is defined as 26 mV per solar cell.

The open circuit voltage V_{oc}, and the reference voltage at maximum power $V_{mp,ref}$, are then used to calculate the voltage at maximum power of the panel V_{mp} as

$$V_{mp} = V_{mp,ref}\frac{V_{oc}}{V_{oc,ref}}. \tag{11}$$

Finally, the DC power P_{DC} produced by the solar panel array is calculated using the voltage V_{mp} and current at maximum power I_{mp} as

$$P_{DC} = V_{mp}I_{mp}. \tag{12}$$

DC/AC Inverter and system loss

The DC power P_{DC} calculated using the basic or advanced generation models is converted into AC power as

$$P_{AC} = \eta P_{DC}, \tag{13}$$

where η represents the efficiency of the DC/AC inverter. The default value for this constant is 96%, but the user can change it depending on the solar panel.

The calculator takes into account losses produced by dust (2%), shadows (3%), manufacturing defects (2%), wiring (2%), connectors (0.5%), degradation of the cells caused by incident light (1.5%), down time (3%), and discrepancies between theoretical values and the actual performance of the panel (1%), resulting in a total loss PT of 15%. Therefore, the AC power $\hat{P}_{AC}$ is defined as

$$\hat{P}_{AC} = P_{AC}\left(1 - \frac{PT}{100}\right). \tag{14}$$

Capacity Factor

The capacity factor is the ratio of the annual average energy production and the theoretical maximum annual energy production of a plant assuming it operates at its peak rated capacity every hour of the year [284]. The system rated capacity SRC is calculated as

$$SRC = \frac{P_{DCnom}}{DC\_AC\_ratio}, \tag{15}$$

where P_{DCnom} is the nominal power of the system, and DC_AC_ratio is the relationship between the amount of DC power sent to the AC power inverters, this value is typically 1.25.

With the system rated capacity SRC and the annual energy production $\hat{P}_{AC}$, the capacity factor CF is obtained as

$$CF = \frac{\hat{P}_{AC}[\frac{kWh}{year}]}{SRC[kW] \times 24[\frac{hours}{day}] \times 365[\frac{days}{year}]}. \tag{16}$$

The resulting array of data, consisting of the power produced by the solar panel array for each day in a specific year or RCP scenario, is then used to calculate the average power generation per month, as well as the minimum and maximum power values.

Historical graphs

We present the historical data in five different graphs depending on the average selected. Each graph can be generated for GHI, DHI, DNI, temperature, and wind speed. Initially,

in the general view of the map with historical data (Figure 1), a graph with the global solar irradiance (the sum of the diffuse and direct solar irradiance) for each month of the current year is shown. In the Graphs tab, the user can generate the following graphs:

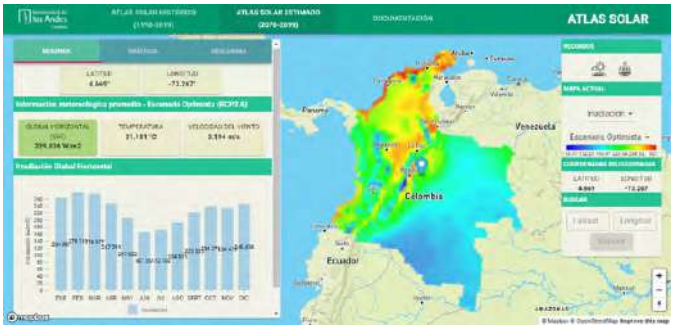

FIGURE 1: General view of the map with historical data.

- *Monthly averages*: This graph shows the averages per month calculated for a single year. An example can be seen in Figure 2.

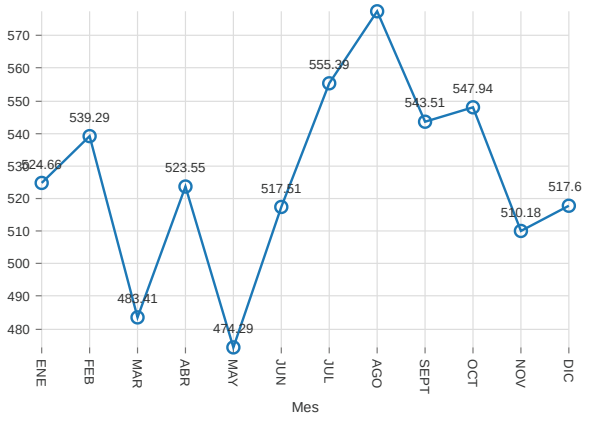

FIGURE 2: Monthly Averages plot.

- *Hourly averages*: In this case, the graph shows the averages for each hour calculated using the data of a single year. As illustrated in Figure 3, the averages take into account data from every hour, so low values are still shown to the user.

- *Historical yearly averages*: The yearly averages in the period 1998–2019 are shown for a single variable (see Figure 4).

- *Historical monthly averages*: This graph shows the historical data calculated for each month of all years. A heat map with a color gradient is used, where the highest value is shown in dark blue and the lowest in white, as is presented in Figure 5.

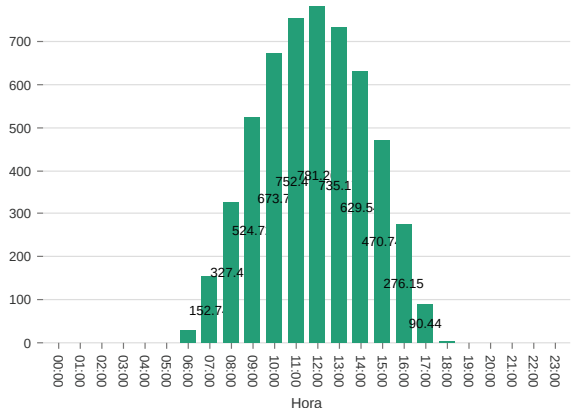

FIGURE 3: Hourly Averages plot.

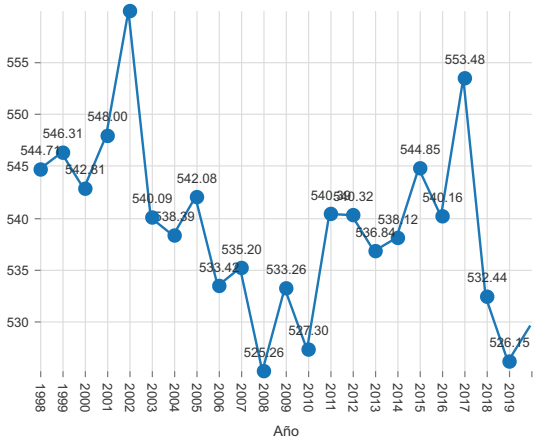

FIGURE 4: Historical Yearly Averages plot.

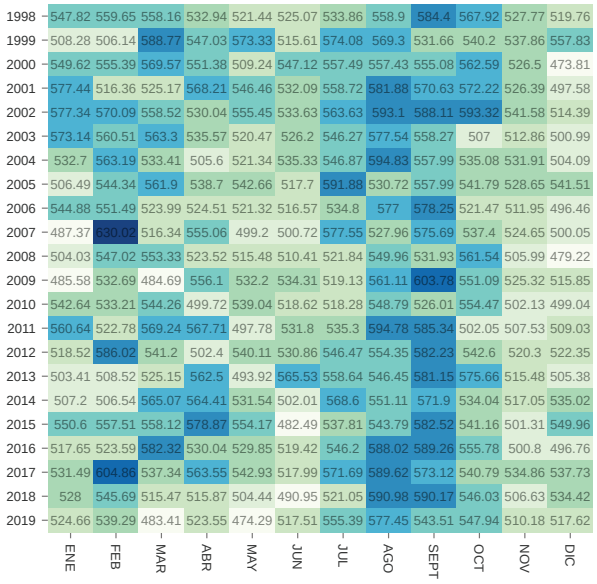

FIGURE 5: Historical Monthly Averages plot.

- *Historical hourly averages*: The final graph shows the historical hourly averages per year, using a heat map with a green scale where the shade is assigned depending on the average value, like in Figure 6.

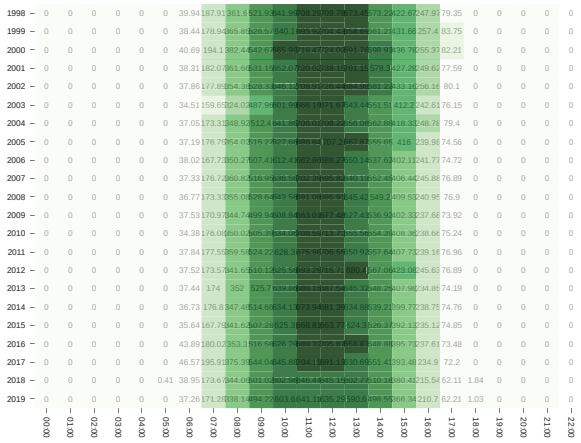

FIGURE 6: Historical Hourly Average plot.

.2 Map with climate change scenarios

For Colombia, the CORDEX database provides 2,484 coordinates. We downloaded data from 2070–2099 for solar irradiance, temperature, and wind speed, for the two RCP scenarios. We worked with this period (2070–2099), intending to have an estimate of the possible PV power potential by the end of the century, and compare this potential with current conditions.

Data visualization

In the same way, the map with historical data was constructed. The map with climate change scenarios contains three main components: interactive maps, graphs of the meteorological variables, and the PV generation calculator. Depending on the two possible RCP, a user can select a single point on the map (a coordinate) to explore, visualizing a summary of the meteorological variables and different plots describing their estimated behavior in 2070–2099. Also, the user can estimate the PV generation depending on the RCP scenario. The photovoltaic generation calculator is explained in Section 3.3.3.

Interactive maps

We developed a map for the meteorological variables (solar irradiance, wind speed, and temperature) available for each proposed scenario, best-case and worst-case. Each map displays the average of the estimated variables between 2070–2099 for all points. The available maps are shown in Figure 7.

FIGURE 7: Available maps (from left to right): solar irradiance, temperature, and wind speed.

The left side of the map shows a summary with the latitude, longitude, and averages of the variables mentioned above. In the same panel, the user can access the behavior graphs of the variables and download the averages of the variables for a selected coordinate. On the right side of the map, the user can change the current map and access the photovoltaic generation calculator.

Data visualization

The estimated data are presented in two different plots depending on the selected average. Initially, in the general view of the map with estimated data (Figure 8), a graph with the solar irradiance for each month of the selected coordinate is presented.

The first graph is the *Monthly Behavior*, which shows the monthly behavior of the averages of any variable for the selected RCP scenario. Each month is assumed to have 30 days. An example can be seen in Figure 9. The second graph is the *Daily Behavior*, which shows the daily behavior of the averages of any variable for the selected RCP scenario. The days in the graph are divided into intervals of 10 days, as presented in Figure 10.

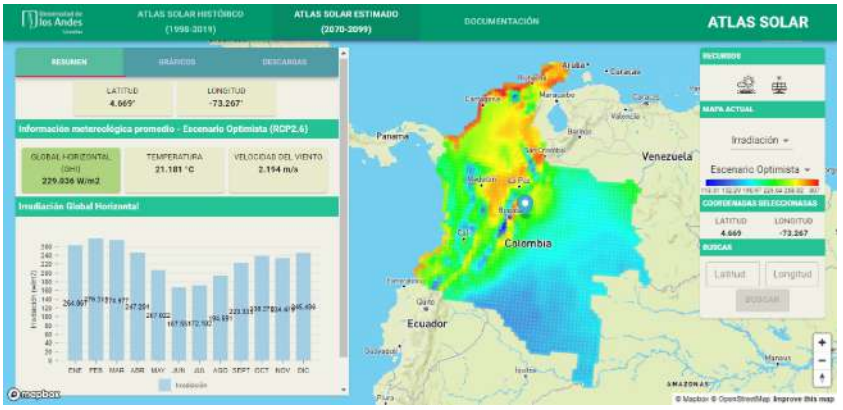

FIGURE 8: General view of the map with estimated data.

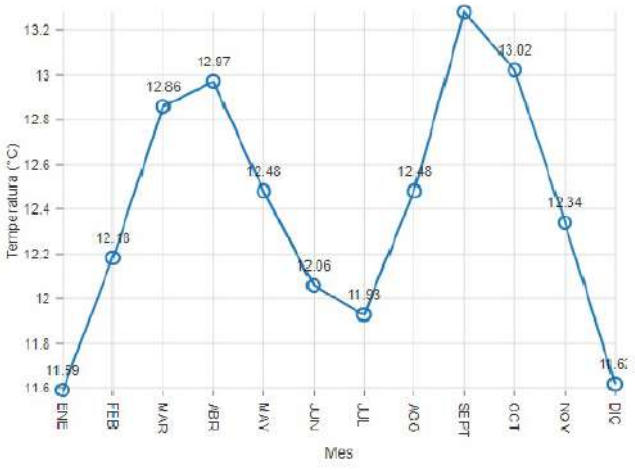

FIGURE 9: Monthly behavior graph.

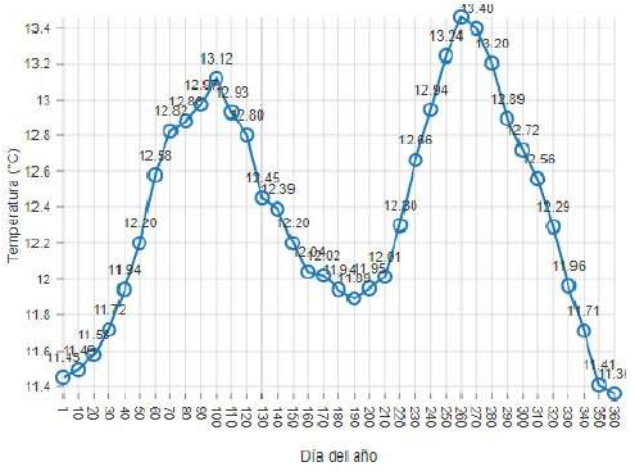

FIGURE 10: Daily behavior graph.

.3 PV power potential formulation

The PV power potential is represented as a dimensionless quantity, indicating the performance of PV cells concerning ambient conditions and their rated power capacity. It is influenced by surface-downwelling shortwave radiation (RSDS), surface air temperature (TAS), and surface wind speed (WS) [381]. Higher irradiance results in increased output current, enhancing the PV panel's performance. Conversely, elevated PV cell temperature reduces the output voltage, thereby decreasing the PV panel's efficiency. In this study, we utilized monocrystalline silicon panels due to their well-established efficiency and extensive industrial use [393]. According to [201], the expression for PV power potential (PV_{pot}) is as follows:

$$PV_{pot} = PR\frac{RSDS}{RSDS_{STC}}, \tag{17}$$

where $RSDS$ at the boundary of the atmosphere has a maximum of 1359 W/m^2, STC represents standard test conditions ($RSDS_{STC} = 1000\ W/m^2$), and PR is the Performance Ratio, which takes into account changes in the efficiency of the PV cells due to changes in their temperature. The definition of this ratio is as follows:

$$PR = 1 + \gamma(T_{cell} - T_{STC}), \tag{18}$$

where $\gamma = -0.005°C^{-1}$ is a variable quantity that depends on physical parameters of PV cells [381], and $T_{STC} = 25°C$. The cell temperature T_{cell} is formulated as

$$T_{cell} = c_1 + c_2 TAS + c_3 RSDS + c_4 WS, \tag{19}$$

with $c_1 = 4.3°C$, $c_2 = 0.943$, and $c_3 = 0.028°Cm^2/W, c_4 = -1.528°Cs/m$ being variable quantities depending on the physical characteristics of the PV cells [381]. According to Equations (17) and (18), under standard conditions, the PV power output attains its nominal value ($PV_{pot} = 1$). If the air temperature is higher than the nominal temperature ($T_{cell} > 25°C$) or the solar irradiance is lower than the nominal one ($RSDS < 1000W/m^2$), the PV power output will be less than the rated power of the module ($PV_{pot} < 1$). On the other hand, if the temperature is lower than the nominal temperature ($T_{cell} < 25°C$), or if the irradiance is higher than the nominal irradiance ($RSDS > 1000W/m^2$), the nominal generation of the PV panel will improve ($PV_{pot} > 1$).

By utilizing Equations (17) - (19), it is possible to express PV_{pot} as:

$$PVpot = RSDS(a + bRSDS + cTAS + dWS), \tag{20}$$

where

$$\begin{aligned} a &= \tfrac{1+\gamma(c_1 - T_{STC})}{RSDS_{STC}}, \\ b &= \tfrac{\gamma c_3}{RSDS_{STC}}, \\ c &= \tfrac{\gamma c_2}{RSDS_{STC}}, \\ d &= \tfrac{\gamma c_4}{RSDS_{STC}}. \end{aligned}$$

Equation 20 provides a way to calculate the changes in PV_{pot}, represented as ΔPV_{pot}:

$$\begin{aligned} \Delta PV_{pot} = \quad & \Delta RSDS\,(a + b\Delta RSDS + 2bRSDS + cTAS + dWS) \\ & + cRSDS \cdot \Delta TAS \\ & + dRSDS \cdot \Delta WS \\ & + c\Delta RSDS \cdot \Delta TAS \\ & + d\Delta RSDS \cdot \Delta WS \end{aligned} \tag{21}$$

Changes in PV_{pot} attributed to the individual effects of $\Delta RSDS$, ΔTAS, and ΔWS can be computed using Equation (21). For instance, to determine the impact of $RSDS$ variations, we set $\Delta TAS = \Delta WS = 0$, while keeping the remaining variables (TAS, WS) constant at their annual mean during the reference period (1970-1999). We adopt the same methodology as previously presented in [46, 201, 309]. However, it is essential to acknowledge that isolating the exact contribution of each variable is not entirely feasible due to the presence of cross-products in the last two terms of Equation (21). It is important to note that both temperature and wind speed depend on solar irradiance. The amount of solar irradiance received at a particular location is influenced by various factors such as latitude, time of day, season, cloud cover, and atmospheric conditions. The absorbed solar energy contributes to the heating of the Earth's surface, affecting temperature. Regions with higher solar irradiance experience increased heating and higher temperatures, while areas with lower solar irradiance have cooler temperatures due to reduced energy input. Solar irradiance also creates temperature gradients, leading to pressure systems that drive air movement, resulting in variations in wind speed across different regions [394, 395].

.4 Changes in PV_{pot} by country

The following is an analysis of the impact of climate change in the most populated South American countries based on the RCP8.5 scenario. We decided to focus on the RCP8.5 scenario to analyze the worst-case scenario and evaluate how much this scenario could affect the PV power potential.

Argentina

The results suggest that the northern part of the country will have an overall increase in air temperature between 3° and 4°, with the most significant increase near the border with Chile and Bolivia (9°). Argentina is projected to have an average temperature increase of 3° throughout the country. These results are consistent with those presented in [396]. This increase in air temperature will have a negative impact on the country's PV potential, resulting in a general reduction of 0.3% and a maximum reduction of 1.4% in the warmer regions. Changes in solar irradiance vary between $-23W/m^2$ and $25W/m^2$, leading to changes in PV potential of -2.6% and 2.5%, respectively.

Bolivia

The overall temperature increase in the country would be 5.1° with a maximum increase of 11.3° in the southwest. These changes could result in reductions in PV potential by 0.6% and 1.8%, respectively. However, a general increase of $10.7W/m^2$ in solar irradiance is expected. These air temperature and solar irradiance projections align with those presented in [397]. This increase in solar irradiance would result in a 1% increase in PV potential, compensating to some extent for losses due to temperature increase.

Brazil

The minimum temperature increase in the coastal zone of Brazil would be 0.4°, while the northern zone could experience increases of up to 8.2°. The average temperature increase for the entire country is 5.1°, resulting in a 0.5% to 1% decrease in PV potential. Changes in solar irradiance range from $-29W/m^2$ on the coast and $42W/m^2$ in the northwest, resulting in a decrease in PV potential of up to 2.5%, and an increase of up to 3.5%. These climate change projections for Brazil could also impact other energy sectors, such as hydropower generation and liquid biofuel production, as shown in [398].

Chile

Southern Chile shows a decrease in temperature of up to 2°, as well as a decrease in solar irradiance of up to $22W/m^2$. These changes in solar irradiance could cause a decrease in the PV potential of up to 2.6%. However, the decrease in temperature could increase the PV potential by up to 0.2%. On the other hand, northern Chile exhibits an increase in both temperature (with a maximum of 8.5°) and solar irradiance (with a maximum of $17W/m^2$), causing the PV potential to decrease by 1.3%, and to increase by 1.7%, respectively.

Colombia

Solar irradiance levels show a generalized increase, with a mean increase of $25W/m^2$, and a maximum increase of $74W/m^2$. While a maximum decrease of $27W/m^2$ is observed in the southwest. The southwest of Colombia presents the smallest increase in temperature; however, this increase is considerable, with values of around 3°. These changes could cause decreases in PV potential varying from 0.5% to 2.4%. These results are consistent with those presented in [46]. The southeast and northwest would experience increases in solar irradiance (with a maximum of $74W/m^2$), resulting in an increase in PV potential of up to 6.6%. However, these regions could also experience a decrease in PV potential of up to 1% due to temperature increase (with a maximum of 7.4°). On average, the entire Colombian territory would experience an increase in solar irradiance of about $25W/m^2$, resulting in a 2% increase in PV potential. The temperature will increase by 4.7°, leading to a decrease in PV potential of 0.5%.

Ecuador

The coast would present decreases in solar irradiance levels (maximum $38W/m^2$), leading to drops in PV potential of up to 3.1%. This zone shows temperature increases ranging from 2° to 3°, affecting the PV potential between 0.2% and 0.4%. On the other hand, the eastern side of the country would exhibit increases in solar irradiance ($31W/m^2$), but also higher temperature increases (4.4°). These changes would have a positive effect on PV potential, increasing it by up to 2.7% due to irradiance increases, but would also have a negative impact, reducing it by up to 0.6% due to higher temperatures. On average, solar irradiance would decrease by $1.6W/m^2$, and temperature would increase by 3.6°. These changes would decrease the PV potential by 0.2% and 0.4%.

Paraguay

Paraguay could experience temperature increases of between 4° and 5.6°, which would cause reductions in PV potential of about 0.5%. These changes are similar to those presented in [399]. Solar irradiance would not undergo significant changes, with variations between $-5.7W/m^2$ and $9.1W/m^2$, affecting the PV potential between -0.5% and 0.8%.

Peru

The results show that a small region in southern Peru would drastically decrease solar irradiance levels by $-130W/m^2$, leading to a decrease in PV potential of up to 14.6%. It would be worthwhile to examine the accuracy of the irradiance data for this particular region, as these changes differ significantly from those observed in the rest of the country and the sub-continent. The maximum increase in solar irradiance is up to $38W/m^2$, which can boost the PV potential by up to 3%. This increase is most notable in the northeast of the country. The average temperature across the entire Peruvian territory presents an increase of 4.3°, leading to a decrease in PV potential by up to 1.2%. However, the models show a decrease in temperature in the northwest of up to 1.4°, which could have a positive effect on PV potential by up to 0.2%.

Uruguay

Uruguay is the country with the least drastic changes. The temperature would vary between 1.4° and 3.7°, while irradiance would vary between $-15W/m^2$ and $1.2W/m^2$. These variations affect the PV potential, which can decrease by up to -1.4% or increase by up to 0.1%.

Venezuela

Solar irradiance would vary from $-34W/m^2$ to $58W/m^2$. Increases in irradiance are mainly observed in the east and west, while decreases are observed in the northern part of the country. These changes in irradiance would affect the PV potential by -3% to 4.7%. The temperature across the country would increase on average by 5.7°, with a maximum of 7.7° in the center and west, affecting the PV potential by up to 0.8%.

.5 Optimal Scheduling

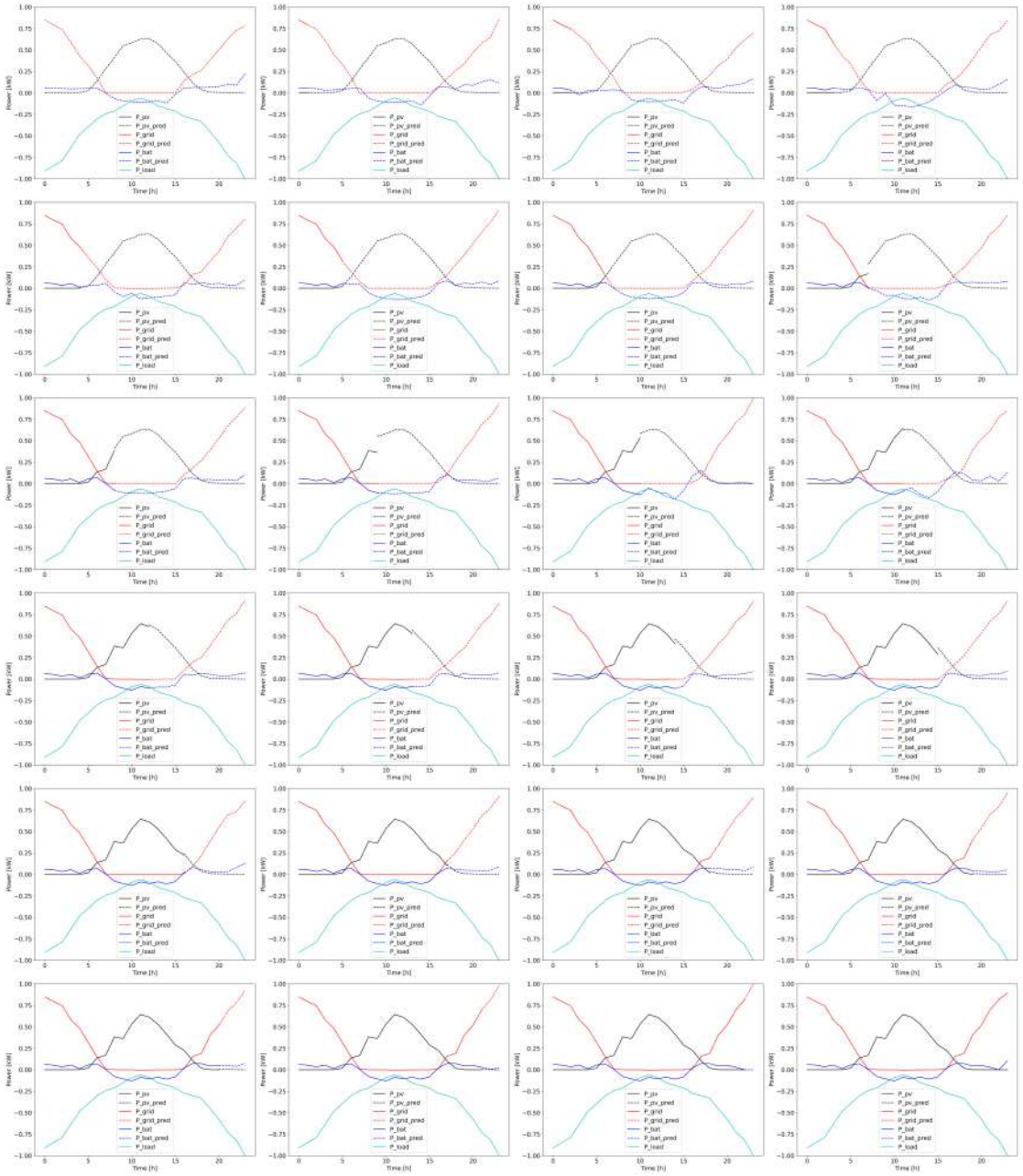

FIGURE 11: BESS scheduling results with the proposed formulation.

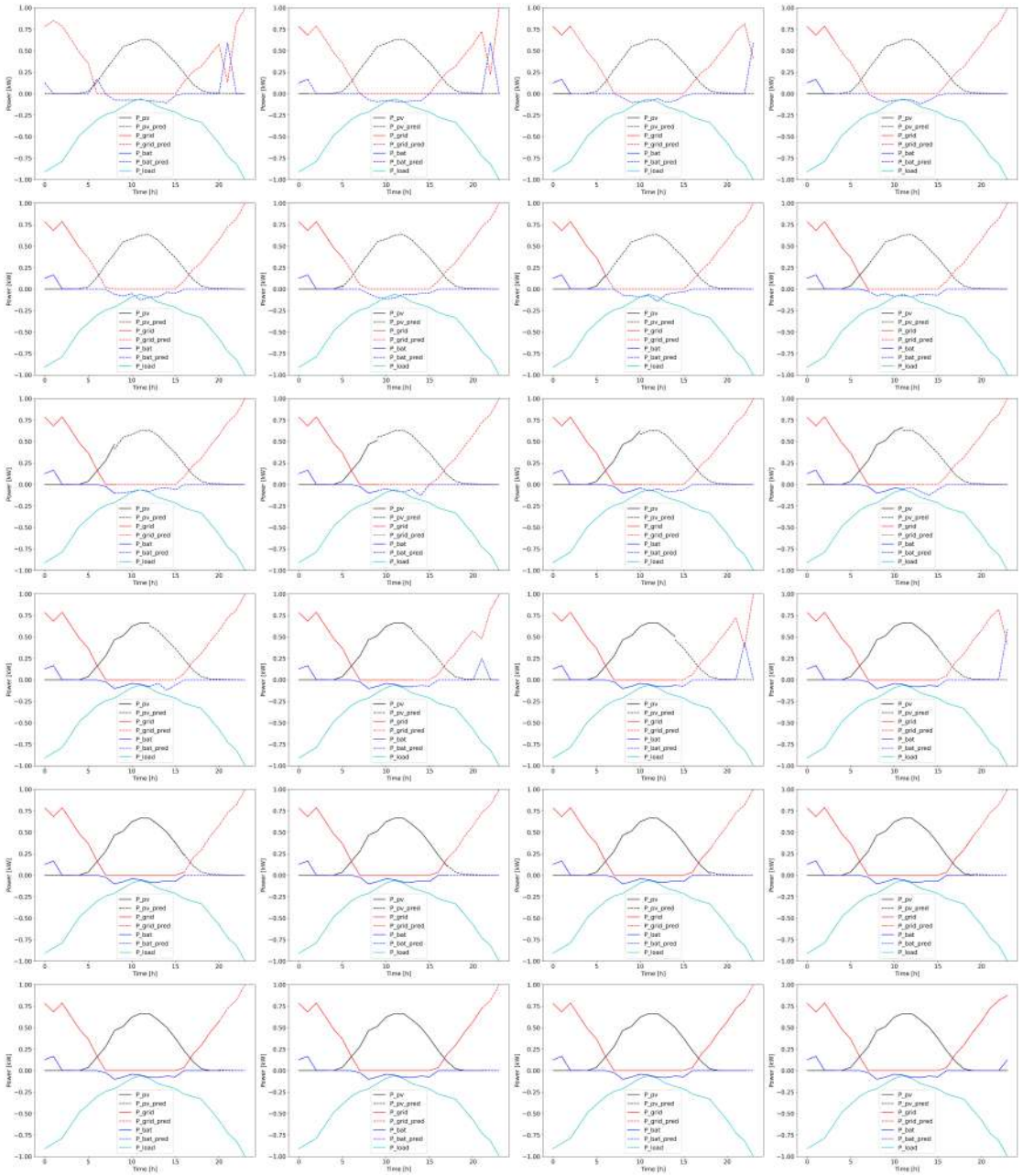

FIGURE 12: BESS scheduling results with Lee formulation.